BB-3.1.3-15-MO1
TN-AP-67-239

contract NAS8-4016 schedule II, vehicle systems integration

SA-204/LM-1 LAUNCH VEHICLE DYNAMICS ANALYSES

PART II
REVISION I

SPACE DIVISION ◆ **CHRYSLER** CORPORATION

BB-3.1.3-15-M01

TN-AP-67-239

SA-204/LM-1 LAUNCH VEHICLE DYNAMICS ANALYSES
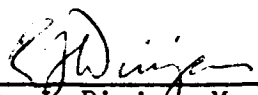Revision I

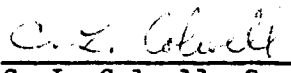
January 8, 1968

Prepared By
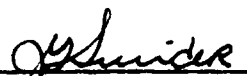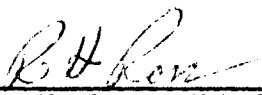

.Vehicle Controllability Unit

of the

AEROSPACE PHYSICS BRANCH

CHRYSLER CORPORATION SPACE DIVISION

Approved By:

R. J. Dinjan, Managing Engineer
Rigid Body Control Group

C. L. Colwell, Supervisor
Vehicle Controllability Unit

J. G. Swider, Manager
Flight Mechanics Section

R. H. Ross, Chief Engineer
Aerospace Physics Branch

FOREWORD

This report provides a comprehensive summary of detailed trajectory analyses data which are applicable to the Saturn IB launch vehicle for the SA-204/LM-1 mission. All analyses documented herein were generated in the Aerospace Physics Branch, Chrysler Corporation Space Division, by authorization of Marshall Space Flight Center, National Aeronautics and Space Administration, under contract NAS8-4016, Schedule II Mod. MSFC-1, Amendment 23, MCRR-101, BB Item 3.1.3-15-M01.

ABSTRACT

Contained in the report are the summary of results and des-
cription of detailed (six degree of freedom) trajectory analyses which
are applicable to the Saturn IB launch vehicle for the Apollo-Saturn
204/IM-1 mission. The documentation is divided into two sections.
Section 1, SUMMARY OF RESULTS, is an integrated summary of conclusions
obtained from each analysis. Section 2, ANALYSES, is a collection
of technical presentations in each of which are described the study
assumptions, mathematical models, analytical approaches and the results
obtained. The specific analyses which are included pertain to:

1) Liftoff Motion

2) Rigid Body Boost Flight Wind Limits

3) Engine Out Controllability

4) Separation Motion

The data results for the nominal and off nominal vehicle flights
are presented in the form of time histories and envelopes of extreme
values for significant detailed trajectory parameters. For flights in
which the vehicle is subjected to extreme winds or system malfunctions,
there are additional displays in the form of flight limitations imposed
by launch pad obstructions, vehicle controllability requirements,
vehicle structural integrity, and stage separation clearance distance.

INTRODUCTION

The primary mission for the SA-204/LM-1 Saturn IB launch vehicle is to inject a complete, fully loaded Lunar Module (LM) payload into an elliptical near earth orbit having an 85 nautical mile perigee and a 120 nautical mile apogee. The primary objective of this mission is to test a complete LM for verification of LM subsystems in orbital operations and LM staging fire-in-the hole capability. A test to determine the feasibility of S-IVB stage passivation is also planned.

There is no preplanned alternate mission for the SA-204/LM-1 Saturn IB. The inflight SA-204/LM-1 Saturn IB alternate mission is to abort to orbit as flight time effectivity of engine failures permit. Approximately 805 kilograms mass of S-IVB stage propellant can be allocated for an inflight alternate mission. The SA-204/LM-1 Saturn IB inflight alternate mission capability during S-IB stage powered flight is for one engine out. The alternate mission is, then, seven engine S-IB stage burn, S-IVB stage burn, and LM DPS burn to orbit. The inflight alternate mission during S-IVB stage powered flight is for loss of thrust. The alternate mission is then LM DPS burn to orbit (see Reference 1).

The SA-204/LM-1 Saturn IB, which is comprised of an S-IB first stage, an S-IVB second stage, an Instrument Unit, and a payload consisting of a Lunar Module (LM), Spacecraft LM Adapter (SLA), and a 25° Nose Cone, is to be launched from Cape Kennedy Launch Facility 37B. After rising vertically for 10 seconds, the booster initiates a roll maneuver from the 90 degree launch azimuth to the 72 degree flight azimuth simultaneously with a time dependent pitch program. The S-IB stage propels the vehicle essentially in a gravity turn flight path until an approximate outboard engine cutoff (OECO) time of 143.89 seconds after liftoff. At S-IB stage OECO, the predicted range, altitude, inertial velocity, and inertial flight path angle are approximately 61 kilometers, 62 kilometers, 2361 meters per second, and 63.1 degrees, respectively. After S-IB/S-IVB stage separation, the S-IVB stage is roll stabilized by the Auxiliary Propulsion System while steering signals are provided to the S-IVB stage pitch and yaw control channels by the Iterative Guidance Mode. The S-IVB stage propels the payload until an approximate J-2 engine cutoff time of 582.26 seconds after liftoff. At S-IVB stage J-2 engine cutoff, the predicted range, altitude, inertial velocity, and inertial flight path angle are approximately 1762 kilometers, 163 kilometers, 7821 meters per second, and 90 degrees, respectively. The nominal SA-204/LM-1 mission trajectory which is used as the basis for the analyses reported herein, is documented in Reference 1.

TABLE OF CONTENTS

TABLE OF CONTENTS (continued)

LIST OF FIGURES

LIST OF FIGURES (continued)

LIST OF FIGURES (continued)

LIST OF FIGURES (continued)

LIST OF FIGURES (continued)

LIST OF TABLES

SECTION 1

SUMMARY

of

RESULTS

1.1   LIFTOFF MOTION

The clearance distance between the SA-204/LM-1 launch vehicle drift envelope during liftoff motion and the Cape Kennedy Launch Facility 37B umbilical tower is conveniently expressed as percent of initially available clearance. The minimum percentage value occurs at the top of the handrail on the Swing Arm No. 4 Platform. At this level, there is a 3σ probability that the launch vehicle drift envelope will not consume more than 81.9 percent of the initially available clearance distance during a January launch. Close ground support equipment constitutes less of a collision hazard than the umbilical tower. The worst case wind speed limits which will insure a 3σ conditional probability of tower clearance occurs for a wind azimuth of 30° east of north. The maximum allowable wind speed for that azimuth is 10.7 meters per second (steady-state, i.e., 11.3 meters per second peak wind speed) at the 60 ft. reference level. If the SA-204/LM-1 vehicle is subjected to 95% QSS design surface winds with a concurrent loss of thrust in Engine No. 1 prior to 2.55 seconds, collision with Swing Arm No. 4 Platform will result. The same result applies to the occurrence of yaw control single actuator hardover on Engine No. 1 prior to .61 seconds.

1.2 BOOST FLIGHT WIND RESTRICTION

Boost flight wind speed limits based upon the control system limitations and structural integrity of the SA-204/LM-1 launch vehicle have been determined for the altitude interval between 5 and 15 kilometers. The associated nominal flight time interval is between 52 seconds and 82 seconds. Wind speed limits are most restrictive at an altitude of 11 kilometers for tailwinds. At that altitude, the tailwind limit is 79 meters per second. Thus, the SA-204/LM-1 launch vehicle can be flown through design tailwinds. Disturbances other than wind speed used to establish this wind speed limit are 99 percent shears and gusts and three sigma C_1, and C_2 variations. These disturbances are combined by the root sum square technique to establish the peak wind limit. The 95 percent envelopes of predicted wind speeds for the months of January through March do not exceed the 5 to 15 kilometer wind speed restrictions. Therefore, the probability that the launch will be restricted by inflight winds is less than five percent for a January through March launch window.

1.3 ENGINE OUT CONTROLLABILITY

There are no structural integrity or controllability problems associated with the occurrence of a single engine failure during SA-204/LM-1 Saturn IB first stage boost flight with the AS-204 Saturn IB engine out steering compensation utilized. The controllability and structural loads estimates are based upon worst case (95% QSS deterministic design) wind profiles superimposed upon worst case engine failures. (Neither system nor environmental tolerances are considered in conjunction with engine failures.) It is therefore verified that the AS-204 Saturn IB engine out steering compensation is acceptable for the SA-204/LM-1 mission.

1.4 SEPARATION MOTION

No S-IB/S-IVB stage separation problems exist provided there is no retro rocket ignition failure just prior to S-IB/S-IVB stage separation relative motion. Potential problems considered are lateral relative motion of the J-2 bell with respect to the S-IB interstage wall during physical separation, and S-IVB post separation controllability. In the event of a single retro rocket failure, the probability of the J-2 bell clearing the S-IB interstage wall is estimated to be 93% provided the residual S-IB propellants are fully seated in the bottom of the tanks. If an estimated 732 kgm. of the residual S-IB propellants are unseated during retro action, however, the probability of clearing is then estimated to be 96%.

SECTION 2

ANALYSES

2.1 LIFTOFF MOTION

2.1.1 Objective

The drift envelope and active malfunction mode studies are conducted in order to establish criteria for safe liftoff conditions as determined by Cape Kennedy Launch Facility 37B umbilical tower proximity to the SA-204/LM-1 launch vehicle during liftoff motion. A ground wind restriction is established for conditional probability levels ranging from zero sigma to three sigma. A ground wind restriction is also established for a 3σ conditional probability level of tower clearance in conjunction with the measured control deflection error. Also determined are the launch time intervals during which the occurrence of selected active malfunction modes can result in an SA-204/LM-1 launch vehicle collision with a launch pad obstruction when subjected to concurrent 95% QSS design surface winds.

2.1.2 Discussion

The primary concern during the liftoff motion of the SA-204/LM-1 vehicle is the clearance of the Cape Kennedy Launch Facility 37B umbilical tower as shown in profile on Figure 1. The top of the handrail on the Swing Arm No. 4 Platform, the Tower Top, and the top of the Lightning Mast are the three points in closest proximity to the SA-204/LM-1 Launch Vehicle. These proximities are tabulated in Table 1 and are determined from the dimensions obtained from References 2 and 3.

At holddown arm release, the SA-204/LM-1 vehicle orientation on LC-37B is shown on Figure 2 (see Reference 4). The vehicle is situated on the launch pedestal with the vehicle pitch plane oriented in the 90 degree azimuth plane and the inertial platform pitch plane oriented in the 72 degree azimuth plane. The sequence of events after holddown arm release entails a vertical rise for 10 seconds and subsequent simultaneous initiation of the pitch and roll maneuvers as defined in Reference 1. Inasmuch as these maneuvers are a factor in determining vehicle clearance with the umbilical tower during launch, the clearance of each vehicle fin adjacent to an umbilical tower obstruction is considered.

All trajectories calculated for this study are generated with a digital flight mechanics computer routine which simulates rigid body vehicle motion in three dimensional space with six degrees of freedom. The simulation includes variable mass characteristics, angle of attack dependent aerodynamics, multiple thrust vectors variable in both magnitude and direction, and an idealized control system which has proven adequate for tower clearance in previous analyses. Included, however, are hardware control signal limits and control gimbal deflection limits which are significant during active malfunction modes. The computer imput data which define launch vehicle physical characteristics and the data which describes the tilt maneuver and sequence of events conform to Reference 1. For the

liftoff motion studies, angle of attack dependent liftoff aerodynamics of Reference 5 are substituted for those of Reference 1.

Synthetic surface wind profiles (see Figure 3) are generated from the power law:

$$V = V_1 \left(\frac{Z}{Z_1} \right)^P$$

where: V is the wind speed at any altitude Z; V_1 is the wind speed at the reference altitude Z_1; and P is the power law exponent as determined by the wind speed value at the reference altitude Z_1. The value of the wind speed in the azimuth of the umbilical tower direction is obtained from the wind rose of Reference 6. The power law exponent which is a function of V_1 is also obtained from Reference 6. The superimposed surface wind gust is a saw-tooth function which peaks at a wind speed value of 1.4 times the corresponding surface wind speed value as illustrated in Figure 4. The gust is initiated at holddown arm release, ramps up to the peak value at 2 seconds after holddown arm release, and ramps back down to the surface wind profile at 4 seconds after holddown arm release. A composite aerodynamic tolerance consisting of a 10% increase in normal force coefficient and a simultaneous .35 caliber forward CP shift is used to simulate distributed aerodynamics.

In order to determine the vehicle launch surface wind restriction, the partial derivatives of vehicle drift, with respect to each tolerance and wind magnitude, are obtained at the levels of closest proximity to each umbilical tower obstruction. The drift contribution due to a tolerance or wind is then generated by multiplying the appropriate partial by its corresponding parameter magnitude. The drift contributions are then root-sum-squared to yield a composite drift. Computation of the composite drift as a function of azimuth yields the desired envelope for each level of closest vehicle proximity to the respective umbilical tower obstruction. The SA-204/LM-1 drift envelopes are developed for January steady state surface winds and those tolerances which are the primary drift contributors (see Reference 7). These tolerances include: a 2 inch lateral CG offset (see Reference 8), a .338 degree composite H-1 thrust misalignment (see Reference 9), and a .306 degree composite control deflection error (see Table 2). Comparison of the drift envelopes for each vehicle fin with the respective umbilical tower obstruction perimeters will furnish the resultant clearance distance for each obstruction. The obstruction having the least percentage of initially available clearance distance is then the obstruction for which the wind restriction is determined. The wind is found

which results in reducing the obstruction clearance to zero when the drift
contribution due to the wind is added to the root-sum-squared drift con-
tribution due to a zero to three sigma range of primary drift contributors.
A wind magnitude limit corresponding to a range of zero to three sigma
conditional probability of umbilical tower clearance during liftoff motion
is thus generated as a function of wind azimuth.

The SA-204/LM-1 launch vehicle is surface wind speed limited with
respect to launch pad obstruction in conjunction with control deflection
error levels. These limits are established by determining the surface wind
speed for which the worst case obstruction clearance distance is reduced
to zero. The limit is determined by adding the drift contributions of
surface wind, a superimposed surface wind gust, distributed aerodynamics,
and control deflection error to the root-sum-squared drift contributions
of the 3σ values of the remaining primary drift contributors. The re-
sulting surface wind speed limit for a 3σ conditional probability of tower
clearance is specified as a function of wind azimuth.

In order to determine the time intervals during which an active mal-
function mode results in an umbilical tower collision, the appropriate
malfunctions are simulated for a spect.rum of flight times of occurrence.
Active malfunction mode umbilical tower collision is analyzed for the top
of the handrail on the Swing Arm No. 4 Platform. All active malfunctions
are assumed to occur in the presence of 95% QSS design surface winds.
The effects of surface winds on the active malfunction mode of single
engine thrust failure (significant change in thrust to weight ratio) are
determined by including the surface winds in the engine failure computer
simulation. However, for malfunctions which do not significantly change
the thrust to weight ratio, the effects of surface winds can be determined
from the Swing Arm No. 4 vehicle drift versus wind speed curve shown in
Figure 4 (no additional computer simulation of winds is necessary). This
curve was generated in the no malfunction liftoff analysis and is, there-
fore, based on a nominal thrust to weight ratio. The active malfunctions
considered, which do not significantly change the thrust to weight ratio,
are single control actuator hardover and loss of hydraulic power. The
time interval during which an active malfunction mode, with a concurrent
95% QSS design surface wind, results in umbilical tower collision is then
determined by interpolating for zero tower clearance from a graph of
clearance distance versus the time of malfunction.

2.1.3 Results

The parameterization of drift due to a tolerance or wind magnitude
shows that the drift versus tolerance magnitudes are linear and that the
drift versus wind magnitude is non-linear. The drift versus wind magnitude
at the critical obstruction levels of the umbilical tower are depicted in
Figure 5. The root-sum-squared drift envelopes of the trailing edge of
fins No. 1, No. 2 and No. 3 are illustrated in Figures 6, 7, and 8. The

clearance distance resulting from the root-sum-squared drift envelopes is presented in Table 1. The minimum percent of initial clearance is found to be at the top of the handrail on the Swing Arm No. 4 Platform. The wind speed limits which will insure a zero sigma to three sigma range of conditional probability of tower clearance is shown in Figure 9. The worst case wind speed limit which will insure a 3σ conditional probability of tower clearance occurs for a wind azimuth of 30° east of north. The minimum allowable wind speed for that azimuth is 10.7 meters per second (steady state, i.e., 11.3 meters per second peak wind speed) at the 60 ft. reference level. The wind speed limit in conjunction with measured control deflection errors are shown in Figure 10 for a 3σ conditional probability of tower clearance.

Engines No. 1, 5 and 6 constitute a potential thrust loss collision hazard as determined from previous analyses (see Reference 7). The drift envelopes of fins No. one, two, and three for concurrent 95% QSS design winds and spectra of engines 1, 5, and 6 thrust loss times are shown in Figures 11, 12, and 13, respectively. The launch time interval during which the occurrence of engine thrust losses can result in collision with the Swing Arm No. 4 Platform when the vehicle is subjected to concurrent 95% QSS design surface winds is depicted in Figure 14. The SA-204/LM-1 is wind limited for engine thrust loss occurrences as shown in Figure 15. The time required for the SA-204/LM-1 launch vehicle to clear the LC 37B obstructions is shown in Figure 16 as a function of time of thrust loss occurrence.

Yaw control single actuator hardover constitutes the worst single actuator hardover collision hazard as determined from previous analyses (see Reference 7). Consequently, only yaw control single actuator hardover data is presented herein. The drift envelopes of fins No. 1, 2, and 3 for concurrent 95% QSS design surface winds and spectra of yaw control single actuator hardover times of engines No. 1, 2, 3, and 4 are presented in Figures 17, 18, 19, and 20 respectively. The launch time interval during which the occurrence of single yaw actuator hardovers can result in collision with the Swing Arm No. 4 Platform when the vehicle is subjected to concurrent 95% QSS design surface winds is depicted in Figure 21. The SA-204/LM-1 is wind limited for single yaw actuator hardovers as shown in Figure 22.

2.2 BOOST FLIGHT WIND RESTRICTION

2.2.1 Objective

The objective of the boost flight wind limits analysis is to establish the wind speed at which restrictions must be placed upon the launch to assure a successful flight from a vehicle controllability and structural integrity point of view. Particular emphasis is placed upon the vehicle flight segment characterized by possible high wind speeds and concurrent high dynamic pressure. If a wind limit is exceeded by pre-launch measured winds, it is recommended that a controllability and structural loads trajectory analysis be conducted prior to launch. A final objective of the boost flight wind limits analysis is to provide an estimate of launch probability by comparing the computed wind limits with the probable wind speeds during the scheduled vehicle launch.

2.2.2 Discussion

All calculated trajectories for this study are generated using a digital flight mechanics computer routine which simulates rigid body vehicle motion in three dimensional space with six degrees of freedom. Those features included in the mathematical model, which are of particular importance to rigid body boost flight wind limit determination, are simulation of the aerodynamic forces and moments, and the simulation of the vehicle attitude control system of the S-IB stage. Features of the study which are paramount, however, are the methods used for computing vehicle structural loads indicators and the assumptions concerning the super-position of wind shear and gust disturbances upon normal boost flight. The analysis described herein is based upon the predicted flight of the SA-204/LM-1 first stage as provided in Reference 1. The sequence of events pertinent to the predicted trajectory is presented in Table 3. Nominal flight vehicle parameters directly related to the launch vehicle dynamic response characteristics are shown in Figures 23 - 25. The parameter C_1 is the derivative, with respect to angle of attack, of angular acceleration due to aerodynamic moment. The parameter C_2 is the derivative, with respect to control engine gimbal deflection, of angular acceleration due to control moment. The parameters CG and CP are the longitudinal center of mass and center of aerodynamic pressure locations, respectively, measured from the engine gimbal station plane. The parameter Y_{am} is the negative static margin (i.e., the difference, CP - CG). The CG, CP, and Y_{am} time histories show the vehicle to be aerodynamically unstable, i.e., the CG is aft of the CP, except at staging. The negative static margin, Y_{am} varies from 1.8 meters at 58 seconds to a maximum of 14.3 meters at 95 seconds, and reduces to -0.47 meters at staging. The $-C_1/C_2$ ratio reaches a local peak instability

of .19 at approximately 52 seconds, a local peak in stability of .60 at approximately 67 seconds, and a local peak instability of 0.8 at approximately 86 seconds. Displayed in Figure 26 are the nominal flight time histories of commanded pitch attitude and the resulting pitch attitude response. Figure 27 presents the nominal flight dynamic pressure and pitch angle of attack. Two other time histories exhibited for the first stage powered flight are pitch moment of inertia (Figure 28) and the gradient of the normal force coefficient, C_z (Figure 29). A vehicle mass breakdown is provided in Table 4.

The aerodynamic center of pressure location, and the normal and axial force coefficients are computed as bivariate functions of both angle of attack and Mach number. Consideration of the nonlinearity with respect to angle of attack of these aerodynamic parameters is desirable for wind limit trajectory studies because the angle of attack can become excessively large during the flight time in which the vehicle is subjected to a wind shear and gust disturbance. The vehicle aerodynamic data used in this study are applicable to the SA-204/LM-1 vehicle and are extracted from References 10, 11, and 12.

The attitude of the Saturn IB Launch Vehicle, S-IB stage, is maintained by a control system which utilizes: computed values for attitude error (i.e., deviations from commanded Euler angle values) in the pitch, yaw, and roll ordered rotations; the pitch, yaw, and roll body angular rates; and the accelerations normal to the vehicle pitch and yaw planes. The attitude error signals are obtained from the LVDC. The rate and acceleration signals are obtained from the body mounted rate gyro packages and accelerometers, respectively. These sensed signals are multiplied by their respective gains, modified by electrical shaping networks (filters), and combined to provide commanded values for pitch, yaw, and roll signals that in turn become mixed for pitch and yaw actuator commands to each of the four gimballed control engines. The logic, equations, and numerical data which are used in this study to simulate the overall control system are representative, within the limitations of digital simulation, of the actual control system aboard the SA-204/LM-1 Launch Vehicle. Filter networks, internal limits, and engine actuator dynamics, with the exception of the engine actuator rate limits, are included in the mathematical model. In Figures 30 and 31 may be found block diagrams displaying the logic and data flow of the pitch-roll and yaw-roll channels for the digital simulation used in this study. The time histories of the control system gains (a_0, a_1, g_2) used are shown in Figure 32. In Table 5 may be found the form and the numerical values for each of the individual component transfer functions. These diagrams and data are extracted from References 13, 14, and 15.

The structural limits criteria used are those presented in Reference 16. These limiting criteria indicate structural integrity limits in terms of control engine gimbal deflection and angle of attack for a specified

Mach number, dynamic pressure, and time of flight. Given that for a specified Mach number the dynamic pressure is the same for all wind limit trajectories, angle of attack can be multiplied by the specified dynamic pressure and this product cross-plotted against Mach number and control engine gimbal deflection as illustrated in Figure 33. This product of angle of attack and dynamic pressure is the structural integrity limiting parameter and is designated as the $q\alpha$ limit. The trajectory flight mechanics computer routine simulation calculates the pitch and yaw $q\alpha$ limits as a bivariate table versus Mach number and pitch and yaw control engine gimbal deflection, respectively. (The data for the bivariate table is obtained from Figure 33.) The critical $q\alpha$ ratios for the pitch and yaw planes are computed by dividing the pitch and yaw trajectory simulated $q\alpha$ products by the $q\alpha$ limits.

Synthetic wind profiles are used to establish the boost flight wind limits. These synthetic wind profiles are comprised of a steady-state wind envelope, a wind shear buildup, and a superimposed gust. Steady-state wind envelopes are members of the family, "Scalar Wind Speed Profile Envelopes (Quasi-Steady-State) for Eastern Test Range" found in Reference 6. The 75% QSS, and 95% QSS steady-state wind envelopes are used in this analysis in the 5 to 15 kilometer altitude region. Wind shears are defined by a linear wind speed buildup from zero speed at the surface of the earth to a point of tangency on a 99 percentile shear build-up envelope. The shear buildup envelope is followed to the intersection with the steady-state envelope. The 99 percentile shear envelopes for reference wind speeds (the reference wind speed is the value on the steady-state envelope at the altitude of intersection) are also provided in Reference 6. The superimposed gust is an extension of the shear buildup envelope to a peak value of 9 meters per second (99 percentile gust magnitude) above the steady-state wind speed. This peak value of the gust is held constant for a short interval of altitude and then the wind speed returns, in a linear fashion, to the steady-state value. These synthetic wind profiles used in the wind limit analysis are found in Figures 34 and 35.

In order to establish the rigid body boost flight wind limits, the vehicle is subjected to a spectrum of synthetic headwind, tailwind and crosswind profiles as defined in the preceding paragraph. Gust altitudes are specified at one kilometer intervals between 5 and 15 kilometers. For each wind direction and for each gust altitude in the flight region of interest, vehicle flight is simulated for four different wind conditions. Those conditions are 1) QSS design wind profile only, 2) 99% shear to QSS design wind profile, 3) 99% shear to QSS design wind profile with a superimposed 99% gust, and 4) 99% shear to QSS design wind profile and a superimposed 99% gust with concurrent vehicle tolerance.

2.2.3 Results

Displayed in Figure 36 are sample time histories of critical $q\alpha$ ratios for the four simulated wind conditions corresponding to the 95%

QSS tailwinds at 11 kilometers. These time histories correspond to the worst case altitude and wind direction. The composite critical $q\alpha$ ratio for tailwinds at 11 kilometers is shown in Figure 37. The tailwind limit at 11 kilometers is 79 meters per second which is in excess of the Saturn IB design wind magnitude of 75 meters per second. It can be seen that the vehicle can be flown through tailwinds equalling the design wind speed.

Figures 38 and 39 depict the wind limit versus altitude determination for each wind direction. The inner curves on the wind limit figures obtained for Reference 17, depict the 95 percentile envelopes of predicted winds for the months of January, February and March. The wind limit as a function of azimuth is shown in Figure 40 for the worst gust altitude. From Figure 40, it is apparent that the 95 percentile envelopes of wind speeds for the months of January, February and March do not exceed the wind limit for any wind direction. The vehicle tolerance included is that which approximates a 3σ composite (C_1, C_2) variation. Trajectory and vehicle dynamic response data which corresponds to a specific wind speed profile are generated. The monitored trajectory and vehicle dynamic response variables are control engine gimbal deflection, angle of attack and critical $q\alpha$ ratio. The time histories of control system sensor parameters are examined to determine if they have exceeded their limits. The trajectories that do not exceed these limits are used to determine the wind limits. The incremental variations in critical $q\alpha$ ratio for successive simulated conditions are root-sum-squared and added to the critical $q\alpha$ ratio due to the QSS design wind only. This composite critical $q\alpha$ ratio time history peak value for the 75% QSS and 95% QSS winds having the same direction and gust altitude are plotted against the corresponding steady-state wind magnitudes. The steady-state wind magnitudes at which the critical $q\alpha$ ratio equals one is the wind limit for that direction and altitude. The incremental variations in angle of attack and control gimbal deflection for the four simulated wind conditions are summarized in Table 6.

2.3 ENGINE OUT CONTROLLABILITY

2.3.1 Objective

The objective of the Engine Out Controllability Analysis is to verify the acceptability of the AS-204 Saturn IB engine out steering compensation for a single engine failure (see Reference 19) during the SA-204/LM-1 Saturn IB first stage boost flight. The criteria used to verify the acceptability of the predetermined engine out steering compensation are first stage boost flight controllability and structural integrity, as well as second stage post separation controllability.

2.3.2 Discussion

Deviations from the SA-204/LM-1 mission trajectory due to single engine failures during first stage boost flight result in more severe environmental conditions, primarily large trim angles of attack. Control engine failures tend to result in more severe environmental conditions than fixed engine failures due to control channel cross coupling and reduced control authority. The large trim angles of attack, control channel cross coupling and reduced control authority can lead to structural and controllability problems during S-IB boost flight and controllability problems during post stage separation S-IVB flight if no steering compensation for engine failures is provided.

In a preliminary engine out study (Reference 19) for the Saturn IB/Apollo configuration, it was found that the large aerodynamic moments and loads which accompany early engine failure may be effectively reduced to within tolerable limits by adopting a "chi-freeze" adjustment to the time history of the pitch attitude commands. In the chi-freeze steering mode, upon engine failure, the commanded pitch attitude value is frozen for an incremental duration and then the nominal (albeit, displaced in time) pitch program is resumed until S-IB outboard engine cutoff (see Figure 41). The duration of the chi-freeze is chosen to be a variable function of the time of engine failure. The satisfactory value for the freeze interval is one approximately equal to the extended S-IB burning time (corresponding to outboard engine failure) which results from seven engine burning for the remainder of flight. Because chi-freeze is not required for late engine failure, at a flight time of 40 seconds the chi-freeze duration is ramped down from the extended burning time value to zero at 65 seconds; thereafter chi-freeze steering is not utilized. A further modification to the above described policy is related to very early failures. Because extended periods of vertical or near-vertical flight are objectionable near the launch complex, the chi-freeze mode is inhibited during the first 30 seconds of flight. During inhibited chi-freeze, the pitch attitude is not frozen until 30 seconds; the duration of the chi-freeze is, however, equivalent to the extended burn time for the time of engine failure (see Figure 42).

The nominal vehicle SA-204/LM-1 trajectory, sequence of events, vehicle weight breakdown, control system, superposition of wind shear and gust disturbances (reduced by 15% for engine out controllability), and bivariate aerodynamic characteristics used for this engine out analysis are the same as that discussed in Section 2.2.2. Consideration of bivariate aerodynamics is desirable for engine out trajectory simulation because the angle of attack can become excessively large following an engine failure, particularly, with a superimposed wind shear and gust disturbance.

The nominal vehicle propulsion and propellant consumption used in this analysis are those specified in Reference 1. Two primary assumptions are made in order to readily facilitate simulation of the propulsion (vacuum thrust) and propellants consumption (mass loss) characteristics subsequent to single H-1 engine failures during first stage boost flight. The first assumption is that vacuum thrust levels on the individual H-1 engine are essentially independent of the difference in the vehicle acceleration profiles between an eight engine burn and a seven engine burn. The second assumption is that post engine out propellant consumption is uniformly distributed between the respective fuel and oxidizer tank clusters via the respective propellant tank cluster manifolds. The total seven engine propellant consumption rate is further assumed to be 7/8 of the nominal eight engine propellant consumption rate, and the total usable propellant is also assumed to be independent of the number of engines consuming the propellant.

The following equations are used to predict the times of inboard engines cutoff signal and outboard engines cutoff signal subsequent to single inboard H-1 engine failures and single outboard H-1 engine failures, respectively.

$$1) \quad t_{OECO} = t_{IEO} + \frac{8}{7} (t_{PSLU} - t_{IEO}) + 3.1 + \frac{4 \times 3 + 3.1}{4}$$

$$2) \quad t_{OECO} = t_{OEO} + \frac{8}{7} (t_{PSLU} - t_{OEO}) + 3.1 + \frac{4 \times 3 + 3.1}{3}$$

where: t_{OECO} = flight time of outboard engine cutoff signal

t_{IEO} = flight time of single inboard engine failure

t_{OEO} = flight time of single outboard engine failure

t_{PSLU} = nominal flight time of propellant sensor level uncover

These equations are derivable by employing the second assumption. The sum of the first two terms in each equation is the predicted flight time of propellant sensor level uncover subsequent to a single engine failure.

The sum of the first three terms in each equation is the predicted time of inboard engine cutoff signal subsequent to a single engine failure. Table 7 presents predicted engine shutdown times for a spectrum of early engine failure times.

The vacuum thrust time histories of H-1 engine for a spectrum of single engine failure times are shown in Figure 43 As shown in the figure, the first assumption culminates in merely dilating the time scale of the nominal vacuum thrust time histories subsequent to the single H-1 engine failure time. The scale factors for the time dilation are appropriately selected in order to duplicate the nominal engine cutoff vacuum thrust values at the predicted termination of extended burn time (t_{OECO}) due to the single H-1 engine failure.

The propellant consumption time histories for a spectrum of single H-1 engine failure times are shown in Figure 44. As shown in the figure, the second assumption culminates in merely dilating the time scale of the nominal propellant consumption time history subsequent to the single H-1 engine failure time. The scale factors for the time dilation are appropriately selected in order to achieve the main burn propellant consumption mass at both the predicted propellant sensor level uncover and predicted outboard engine cutoff signal subsequent to a single H-1 engine failure.

The Saturn IB Vehicle, S-IVB stage, during powered flight utilizes the same type of sensed signals as the S-IB stage except for the accelerometer signals. These signals are manipulated the same way as in the S-IB stage except the commanded pitch, yaw, and roll signals are not mixed. Instead, the pitch and yaw commanded signals are sent to the J-2 actuators as their commanded deflections, and the roll signal is sent to the Auxiliary Propulsion System. In Figure 45 may be found the block diagram displaying the logic and data flow of the S-IVB stage pitch and yaw channels for the digital simulation used in this study. The Auxiliary Propulsion System was not simulated. Consequently, a moment balance about the S-IVB stage roll axis is assumed. The time history curves of the S-IVB stage control system gains (a_0, a_1) are presented in Figure 46. In Table 8 the form and the numerical values for each of the individual S-IVB component transfer functions may be found. These diagrams and data are extracted from References 13, 15, and 20.

A structural loads indicator well suited for malfunctioning vehicle trajectory analysis is the "bending moment critical ratio". Time histories of bending moment critical ratios are obtained by computing the bending moments and axial loads at several vehicle stations. The axial load values are used to compute the critical bending moment value. The critical bending moment at each station corresponds to that value for which a structural limit is violated. The bending moment critical ratio

for each station is the quotient of the bending moment at that station
and the corresponding critical bending moment for that station. Hence,
a bending moment critical ratio equal to unity represents the limiting
constraint for structural integrity. Bending moment critical ratios are
used in this engine out controllability analysis rather than the critical
$q\alpha$ ratios discussed in Section 2.2.2. The critical $q\alpha$ ratios can not
be used since the α-β structural limits data employed to compute these
ratios is based upon eight engine flight. See Reference 21 for further
details.

Design winds specified in Reference 6 are used with modifications
established in Reference 22 to conform to the MSFC practice. Basically,
this practice is to use wind shear values which will not be exceeded 99
percent of the time (reduced by 15 percent) to establish a wind speed
build up to a quasi-steady-state, scalar wind speed envelope at a pre-
scribed altitude. At the prescribed altitude, a trapezoidal gust, which
will not be exceeded 99 percent of the time (reduced by 15 percent), is
superimposed upon the wind profile. The percentile quasi-steady-state
envelope is chosen to be compatible with January, February, and March winds
in each direction referenced to the flight plane (Figure 47). The
January, February, and March wind envelopes are found in Reference 17.
Tables 9 - 12 present monthly 95 percentile wind envelope comparisons with
QSS design wind envelopes for a 75 degree flight azimuth.

In order to compare engine failure effects, it is first necessary
to generate envelopes for loads and controllability parameters associated
with eight engine flight. This objective is accomplished by subjecting an
otherwise nominal flight to a spectrum of superimposed design winds. The
eight engine flight data then are used to provide the basis for comparison
with engine out flight. This comparative rather than absolute approach is
convenient because the analysis is essentially a trajectory comparison.
The structural loads indicators are calculated internally within the digital
trajectory simulation by approximate loads computation formulas. These
approximate loads computations, although more accurate than might be pre-
supposed, serve primarily as a means for indicating the flight conditions
and vehicle stations where possible structural problems are most likely to
occur.

The second step in the engine out analysis is the simulation of
vehicle flights which are otherwise normal but with an engine failed at
selected times during first stage boost flight. The trajectories are
computed with the AS-204 Saturn IB pitch attitude command engine out steering
compensation utilized subsequent to the engine failure. This trajectory
set provided the information useful for the preliminary verification of
the acceptability of the AS-204 Saturn IB engine out steering compensation
for the SA-204/LM-1 mission. Examination of the peak steady-state values
for control gimbal deflection and bending moment critical ratios are in-

dicative of the controllability and loads trends as a function of the
time of engine failure. The engine out trajectory set also provides
trend data of the post separation controllability of the second stage.
The variation of stage separation $q\alpha$ as a function of engine out time is
applicable toward verifying the acceptability of the AS-204 Saturn IB
engine out steering compensation for SA-204/LM-1 staging controllability
requirements.

The final step in the technical approach is the final verification
of the AS-204 Saturn IB engine out steering compensation for the SA-204/LM-1
mission. This objective is accomplished by means of a comprehensive wind
response and stage separation motion analyses. Envelopes of the peak
transient values for loads and controllability parameters corresponding to
each engine out time are generated by subjecting the vehicle to a spectrum
of superimposed design wind shear and gust disturbances over the range of
altitudes within the post engine out high $q\alpha$ flight region. Second stage
trajectories are also simulated for each engine out time in order to de-
termine peak dynamic response transients during the first few seconds
following stage separation. The envelopes of extreme values for all para-
meters are used compatibly to provide final verification of the accept-
ability of the AS-204 Saturn IB engine out steering compensation for the
SA-204/LM-1 mission.

2.3.3 Results

The most direct indicator for controllability during S-IB boost
flight is the maximum control engine gimbal deflection. In Figures 48
and 49 are shown the envelopes of peak control gimbal deflection without
engine failure for a spectra of superimposed 50 percent QSS headwinds and
crosswinds, and 95% QSS tailwinds. The maximum value shown for the spectrum
of headwind gusts and crosswind gusts is 3.4 degrees at an altitude of
14 kilometers. The maximum value shown for the spectrum of tailwind gusts
is 3.8 degrees at an altitude of 14 kilometers. Thus, 52.5 percent of the
total available control gimbal deflection remains for accommodating an
engine out malfunction.

Figures 50 and 51 present the envelopes of maximum bending moment
critical ratios as a result of spectra of 50% QSS headwinds and crosswinds,
and 95% QSS tailwinds superimposed during eight engine flights. Bending
moment critical ratio is an indicator for structural integrity. A critical
ratio value of unity or greater indicates that the vehicle structural
limits have been exceeded. The largest ratio which is shown in Figure 50
is approximately .70. All values presented in this figure are for the
worst case vehicle station and for a safety factor of 1.25.

In Figures 52 - 54 are plotted, versus time of engine failure, the envelopes of transient peak values (no wind conditions) for control gimbal deflection and bending moment critical ratio (S.F. = 1.25). The peak values are the extremes found during the high q time of flight subsequent to the engine failure time for which the associated time of chi-freeze is shown in Figure 42. It is inferred that the trend behavior of these transient peak values due only to engine failure and steering compensation is indicative of the trend behavior of extrema exhibited by bending moment ratio and control gimbal deflection with superimposed wind induced transient conditions.

A preliminary verification of the acceptability of the engine out steering compensation shown in Figure 42 is accomplished through examination of the data shown in Figures 55 and 56. The data presented in these figures is based upon control engine No. 3 or No. 4 being failed during boost with a no wind condition. Particular note should be taken of Figure 55 in which the aerodynamic moment on the S-IVB stage at physical separation is shown versus the time of engine failure. The S-IVB post separation dynamic response transient peaks are increasing functions of the aerodynamic moment on the S-IVB stage at physical separation. The data in Figure 55 indicates that the worst engine failure time for S-IVB post separation controllability occurs at approximately 65 seconds of flight time. A comparison of Figure 55 (staging aero moment) with Figure 56 (staging qα product) illustrates the fact that staging aero moment is proportional to the staging qα product.

Plotted against time of H-1 engine failure in Figures 57 - 59 are the envelopes of maximum magnitudes of post separation S-IVB pitch attitude error, pitch attitude rate, and J-2 engine pitch control gimbal deflection, respectively. The peak values represent extrema obtained from second stage flight simulation over a time interval which begins at stage separation and terminates at the Iterative Guidance Mode (second stage steering) initiation. The initial conditions of the second stage flight simulations reflect only the effects of H-1 engine failure with its corresponding engine out steering compensation. Furthermore, H-1 engine failure occurs in the presence of a no wind condition. All three variables in the above figures exhibit similar trends in the dynamic response transient peak envelopes. For all three variables the maximum magnitude occurs for an H-1 engine failure time of 65 seconds. The prescribed limits for post separation controllability are 15.3 degrees attitude error, 10 degrees per second attitude rate, and 7 degrees J-2 control gimbal deflection. The first two limits may be associated with the S-IVB control system internal limits and the last limit is to be identified with the J-2 engine gimbal stops. As shown in the figures the maximum parameter magnitudes for engine out failure are 2.8 degrees, 1.15 degrees per second, and 2.4 degrees, respectively. Thus, the chi-freeze policy as shown in Figure 42 requires no change in order to accommodate acceptable post separation S-IVB controllability.

Final verification of the acceptability of the engine out steering compensation as depicted in Figure 42 is obtained from a comprehensive wind response rigid body analysis for engine out flights. The rigid body wind response data are obtained by subjecting the vehicle to an engine out malfunction and spectra of superimposed 50% QSS headwinds and crosswinds, and 95% QSS tailwinds. In Figures 60 and 61 are shown the envelopes of peak control gimbal deflections in response to the above spectra of 50 percent QSS headwinds and crosswinds and 95% QSS tailwinds for different failure times of engines No. 3 and No. 4, respectively. Each of the points defining these envelopes is obtained by first selecting a particular wind direction, a particular engine out time, and a control engine to be failed (No. 3 and No. 4). Next, a series of trajectories are simulated for different wind gust initiation altitudes. Each of the series incorporates the same wind direction, engine failure time, and engine to be failed. For each trajectory (wind gust initiation altitude) the maximum value of control gimbal deflection is recorded. Finally, a plot is made of these recorded maximum control gimbal deflections versus gust initiation altitude. The peak value on this plot is the value presented in Figure 60 or Figure 61 depending on which control engine is failed (No. 3 or No. 4). From Figures 60 and 61 it can be seen that the maximum control gimbal deflection encountered in an engine out flight with superimposed 95 percent QSS tailwinds is 7.3 degrees. In comparison, the maximum gimbal deflection required for eight engine flight with the above winds is 3.8 degrees. Thus, the chi-freeze policy as shown in Figure 42 requires no compromise in order to insure adequate control capability for engine out flight.

In Figures 62 and 63 are shown the envelopes of peak bending moment critical ratios (S.F. = 1.25) in response to a spectrum of 50 percent QSS headwinds and crosswinds and 95% QSS tailwinds for different failure times of engines No. 3 and No. 4, respectively. Each of the points defining these envelopes is obtained by the same method to determine the peak control gimbal deflection envelopes in Figures 60 and 61. It can be seen from Figures 62 and 63 that engine out flight with superimposed 50 percent QSS headwinds results in a maximum bending moment critical ratio of .72. Eight engine flight with the above winds produces a maximum bending moment critical ratio of .63. Thus, there exists an apparently sufficient margin between the maximum ratio values and the limiting value of unity to preclude any possibility of vehicle loss by structural failure. Therefore, the chi-freeze policy as shown in Figure 42 requires no change in order to insure structural integrity for engine out flight.

In Figures 64 and 65 may be found the envelopes of peak roll attitude error responses to a spectrum of 50% QSS headwinds and crosswinds in combination with engine No. 3 and No. 4 failures, respectively. Roll attitude error is presented to provide a more complete picture of the effects of engine failure upon vehicle dynamic response. From Figures 64 and 65 it is seen that the maximum roll attitude error experienced in an engine out flight with superimposed 50 percent QSS crosswinds is 7.4 degrees. Implicit in the roll attitude error excursions are the appreciable effects of control channel cross coupling. Therefore, the chi-freeze policy as shown in Figure 42 is proven to be adequate for all control considerations.

2.4 SEPARATION MOTION

2.4.1 Objective

The objective of the stage separation analysis is to verify
S-IB/S-IVB staging capability for the SA-204/LM-1 primary mission. S-IB/
S-IVB stage separation capability is also investigated for single retro
rocket ignition failures. Staging capability is assured if, during
separation relative motion, lateral clearance of the J-2 engine bell with
the S-IB interstage is accomplished and S-IVB post staging controllability
is maintained.

2.4.2 Discussion

The first requirement for successful SA-204/LM-1 S-IB/S-IVB
stage separation is lateral clearance of the J-2 bell with the S-IB
interstage during the physical separation relative motion. Figure 66
depicts J-2 bell initial lateral clearance at the interstage exit plane
and is based upon References 23 and 24. The second requirement of success-
ful stage separation is retention of the S-IVB stage controllability
during and after its physical separation from the S-IB stage.

Both potential separation problems of J-2 bell interstage collision
and S-IVB stage controllability are mainly affected (assuming no retro
failures) by large aerodynamic moments or attitude rates existing at first
stage boost flight termination. These two problems can be minimized by
appropriate first stage boost trajectory shaping which reduced to acceptable
levels the dynamic pressure, angle of attack, and attitude rates at separ-
ation. Therefore, the SA-204/LM-1 first stage boost flight is terminated
by a nose down and subsequent chi-arrest maneuver such that the angle of
attack is small and the attitude rate is essentially zero at S-IB/S-IVB
first relative motion. The nose is initiated at 112 seconds and the chi-
arrest is initiated at 133.2 seconds as specified in Reference 1. Out-
board engine cutoff occurs at 143.89 seconds and the subsequent S-IB/S-IVB
stage separation sequence of events is as shown in Table 13 (see Reference 25).

The main contributor to the physical separation of the S-IB stage
from the S-IVB stage is the thrust of the four retro rockets. To a very
slight degree, the three ullage thrusts also contribute to the physical
separation. Proper phasing of the retro thrust with respect to the separation
signal and H-1 thrust decay is necessary for successful staging and is
shown in Figure 67 (see Reference 25). The time histories of the retro and
ullage thrusts are obtained from References 26 and 27, respectively.
Reference 28 provides the H-1 thrust decay profiles. Impingement of the
retro rocket plumes on the vehicle creates pressure distributions on the
surface of the S-IB/S-IVB interstage and lower S-IVB stage. If a retro
rocket fails to ignite, these pressure distributions then become asymmetrical

thereby causing imbalanced forces to act on the stages as shown in Figures 68 and 69. This imbalanced force condition constitutes a potential S-IB/ S-IVB collision hazard. Figure 67 indicates that the S-IVB stage is without effective J-2 control thrust for approximately 4.6 seconds after physical separation from the S-IB stage. It is during this time interval that S-IVB stage dynamic transients can become excessively large.

All trajectories for this analysis are generated with a digital flight mechanics computer routine which simulates rigid body vehicle motion in three dimensional space with six degrees of freedom. The computer input data which define launch vehicle physical characteristics and the data which describe the trajectory shape and sequence of events conform to Reference 1. Separation aerodynamic characteristics of the two launch vehicle stages correspond to those of Reference 29.

Figures 70, 71 and 72 are a summary of the SA-204/LM-1 S-IVB controllability during separation motion. These figures present a nominal time history with $\pm 3\sigma$ bands for each of eight S-IVB controllability parameters. The $\pm 3\sigma$ bands are determined from off nominal conditions. These off nominal conditions are simulated one at a time and include those which occur during first stage boost as well as those which occur during stage separation. For a given flight time and S-IVB controllability parameter, the $+3\sigma$ deviation about the nominal is determined by adding to the nominal the root-sum-square of the positive incremental excursions resulting from each off nominal condition considered independently. A similar method is used to obtain the -3σ deviation about the nominal. The tolerances which are the main contributors to S-IVB dynamic excursions during S-IB/S-IVB separation are those S-IB boost flight tolerances which have the greatest influence on $q\alpha$ product dispersions at staging, and S-IVB stage variations which increase the moments on the S-IVB stage. Table 14 shows the tolerance magnitudes considered for determining the S-IVB dynamic responses during separation motion (see Reference 30).

The S-IB/S-IVB potential collision problem subsequent to a single retro rocket failure is investigated with the latest available estimates of forces and their points of application which are representative of pressure distributions due to asymmetric plume impingements. The S-IB/S-IVB relative motion resulting from each of four retro rocket failures in combination with stage separation tolerances, subsequent to a nominal S-IB boost flight, is analyzed in order to ascertain retro out staging probability. The quoted probabilities are defined by the probability law:

$$P = \sum_{i=1}^{4} P_i \, P_i{}^*$$

where: P   ≡ probability of successful separation with one retro rocket
failed.

   P_i ≡ probability that retro rocket number "i" is the one which
failed.

   P_i* ≡ probability of successful separation with retro rocket
number "i" failed.

The P_i* probabilities quoted pertain to the cumulative distribution function.
Each $\bar{P}_i$* is determined by root-sum-squaring the incremental lateral travel
due to each tolerance with retro rocket number "i" failed. Those stage
separation tolerances which have the greatest influence on S-IB/S-IVB
relative lateral motion are those which create significant moments on the
S-IB stage. Aerodynamic moments resulting from aerodynamic tolerances
are not large enough on either stage to be significant contributors to
a potential S-IB/S-IVB collision. The stage separation tolerances consid-
ered in the retro out collision analysis are, therefore, retro rocket
thrust variation (not composite), retro rocket thrust misalignment (not
composite), and S-IB lateral CG deviation (no aerodynamic tolerances).
Values for these tolerances are given in Table 15 and are derived from
References 26, 31 and 32, respectively.

2.4.3   Results

Figures 70, 71, and 72 are a summary of the SA-204/LM-1 S-IVB
controllability during separation motion. These figures present a nominal
time history with ±3σ bands for each of eight S-IVB controllability para--
meters. The eight parameters shown are pitch, yaw, and roll attitude errors
and body rates, and J-2 pitch and yaw control gimbal deflections. Time
zero in these figures occurs at S-IB/S-IVB separation structure completely
severed (OECO +1.379 seconds). These parameters are influenced mainly by
the S-IB boost tolerances (primary contributors to qα product staging dis-
persions), misalignment of the J-2 thrust with the S-IVB stage, and S-IVB
CG lateral deviation. The widths of the 3σ envelopes for these eight para-
meters indicate that the SA-204/LM-1 mission success will not be impaired.

The single retro rocket failure results are presented in Figure 66,
Figure 73, and Table 16. Table 16 gives the lateral clearance of the un-
deflected J-2 bell bottom (at interstage exit plane) with the S-IB inter-
stage for each of the four single retro rocket failures possible. Clear-
ances are shown for each of two assumptions. The first assumption is that
the residual S-IB propellants are fully seated in the tank bottoms during
retro action. The second assumption is that 732 kgm of the residual S-IB
propellants become unseated during retro action. Table 16 and Figure 73
show results which are based upon all retro failures being simulated
during an otherwise nominal separation subsequent to a nominal S-IB boost

flight. For the fully seated case the smallest lateral clearance is
0.126 meters and for the unseated case the smallest lateral clearance is
0.158 meters. Figure 73 presents the undeflected J-2 bell lateral
drift in profile view for the cases of retro No. 1 out and retro No. 3
out (smallest and largest drift, respectively). These results assume
732 kgm of the residual S-IB propellants become unseated during retro
rocket thrusting. Also shown for each case is the required control
gimbal deflection to produce a collision between bell and interstage.
These required deflections are 5.4 degrees and 4.0 degrees for retro
No. 1 out and retro No. 3 out, respectively. In comparison with these
required deflections which would produce a collision, the maximum expected
J-2 bell gimbal deflection when the bell bottom is at the interstage exit plane
is 1.2 degrees. It is estimated that the probability (cumulative dis-
tribution) of the J-2 bell clearing the interstage for a single retro
failure in combination with stage separation tolerances is 93% (1.47σ)
assuming the residual S-IB propellants to be fully seated in the bottom
of the tanks. If an estimated 732 kgm of the residual S-IB propellants
are unseated during retro rocket thrusting, the probability of clearing
is then 96% (1.80σ).

FIGURE 1

PROFILE OF CAPE KENNEDY LAUNCH FACILITY 37B UMBILICAL TOWER

FITTED FOR THE SA-204/LM-1
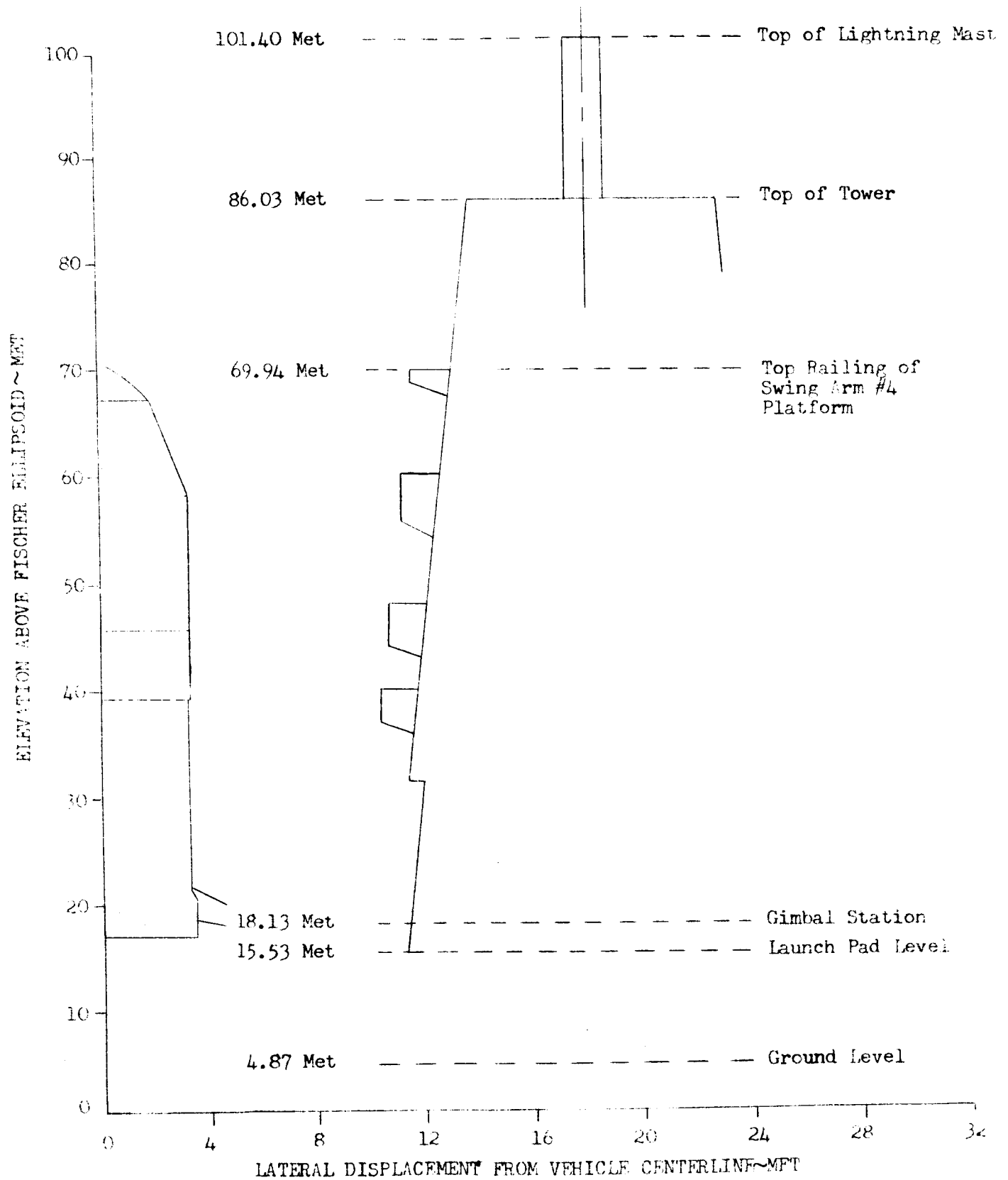
FIGURE 2

CAPE KENNEDY LAUNCH FACILITY 37B
LIFTOFF SCHEMATIC
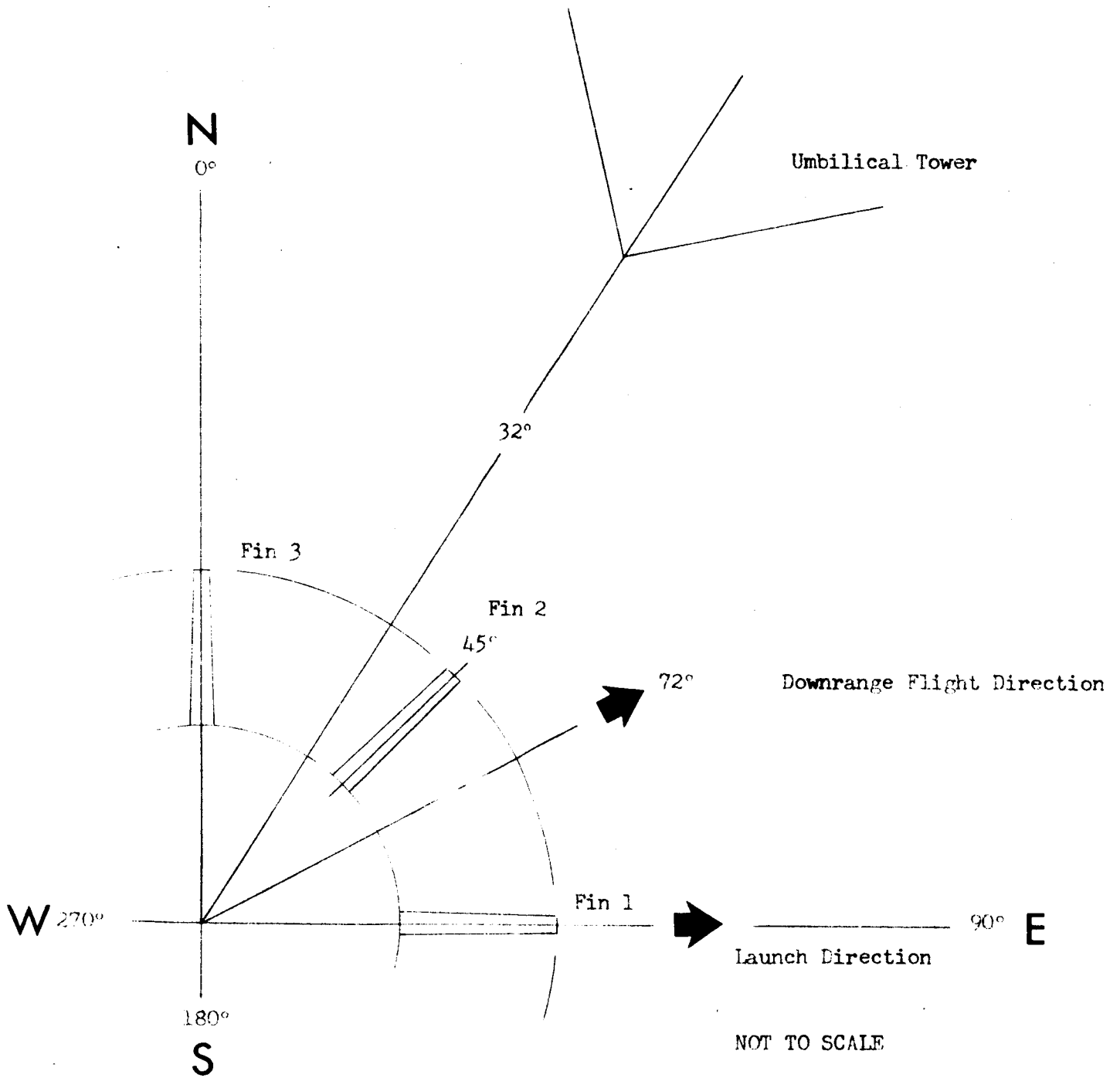
NOT TO SCALE

FIGURE 3

CAPE KENNEDY SURFACE WIND PROFILES
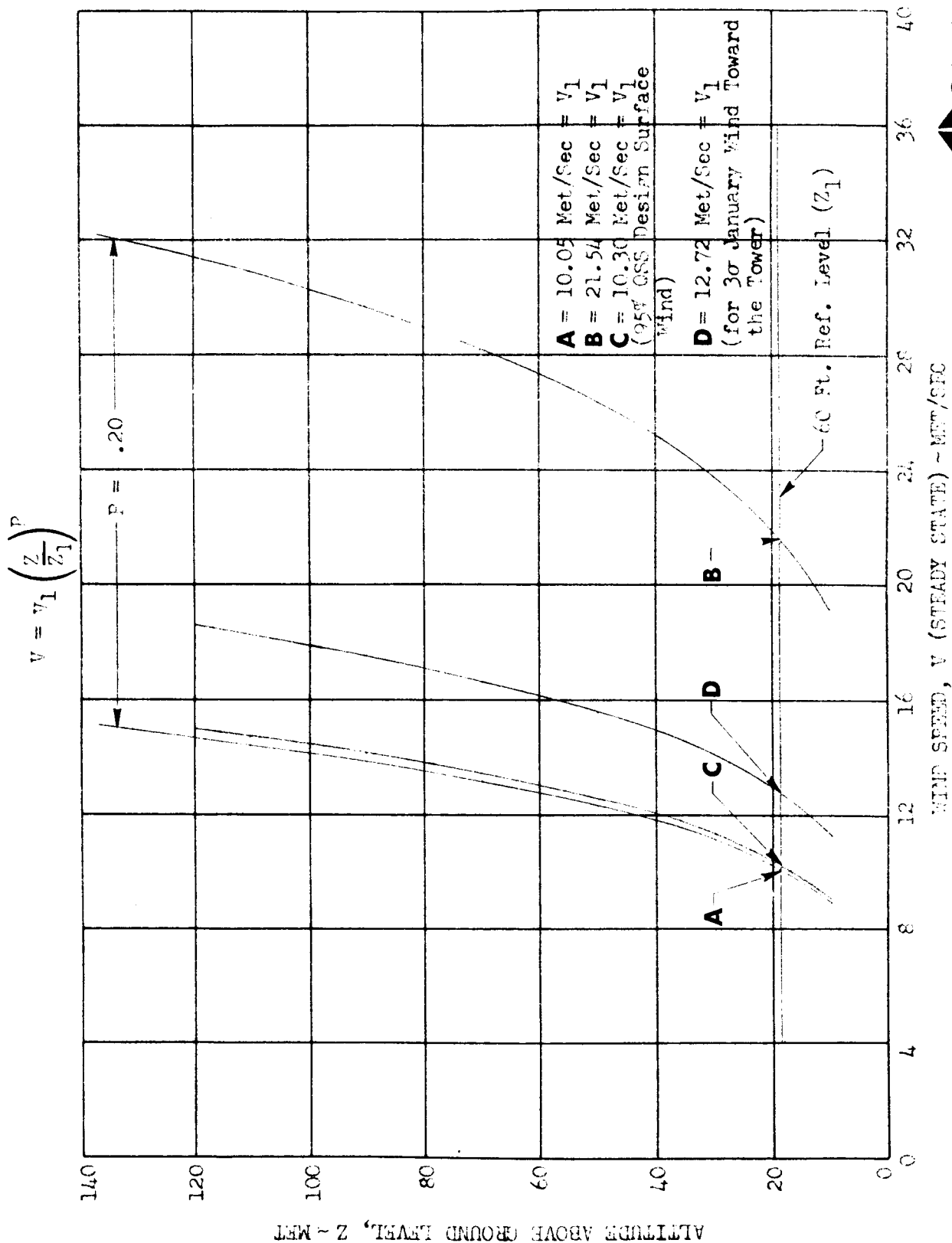
$$v = v_1 \left(\frac{z}{z_1} \right)^p$$

A = 10.05 Met/Sec = V_1
B = 21.54 Met/Sec = V_1
C = 10.30 Met/Sec = V_1
(95% QSS Design Surface Wind)

D = 12.72 Met/Sec = V_1
(for 3σ January Wind Toward the Tower)

60 Ft. Ref. Level (Z_1)

WIND SPEED, V (STEADY STATE) ~ MET/SEC

ALTITUDE ABOVE GROUND LEVEL, Z ~ MET

CHRYSLER
SPACE DIVISION

-28-

Peak

.95

.95

.95

t = 2 sec.

t = 1 sec.

t = 0 sec.

40 f.p.s. Ref. Level (C_i)

TIME SPEED (V) ~ METERS/SEC.

FLIGHT PATH ANGLE (Z) ~ METERS
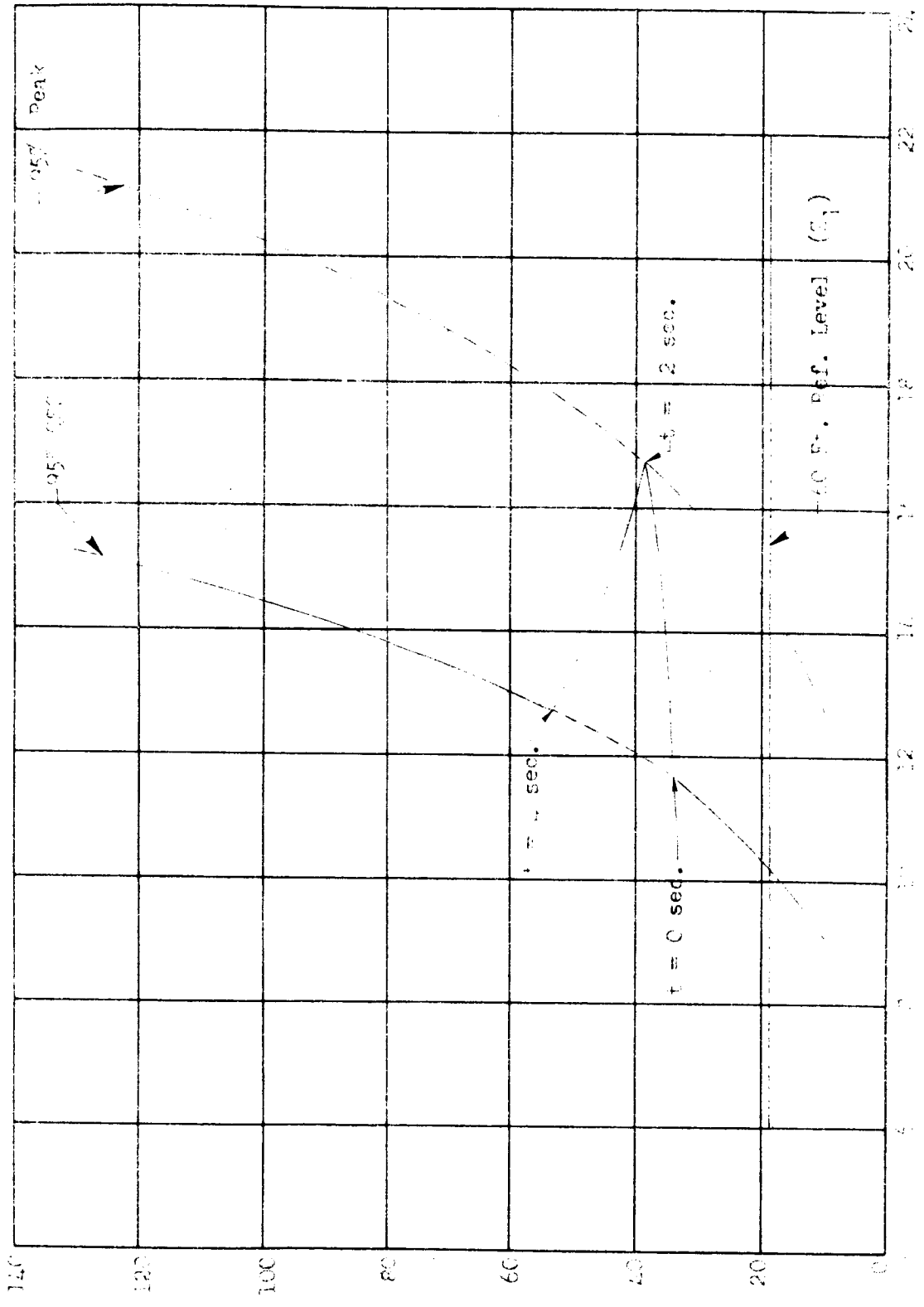
CHRYSLER CORPORATION

SPACE DIVISION

WIND SPEED, V_1 (60' STEADY STATE)
~METERS/SEC

SPACE DIVISION CHRYSLER CORPORATION

FIGURE 6

SA-204/LM-1 DRIFT ENVELOPES AT TOP RAILING

OF SWING ARM NO. 4 PLATFORM

99% QSS Design Wind

95% QSS Design Wind

Top Railing of Swing Arm #4 Platform

3σ January Monthly Winds

N

W

S

E Launch Direction

SCALE:

1 CM = 1 MFT
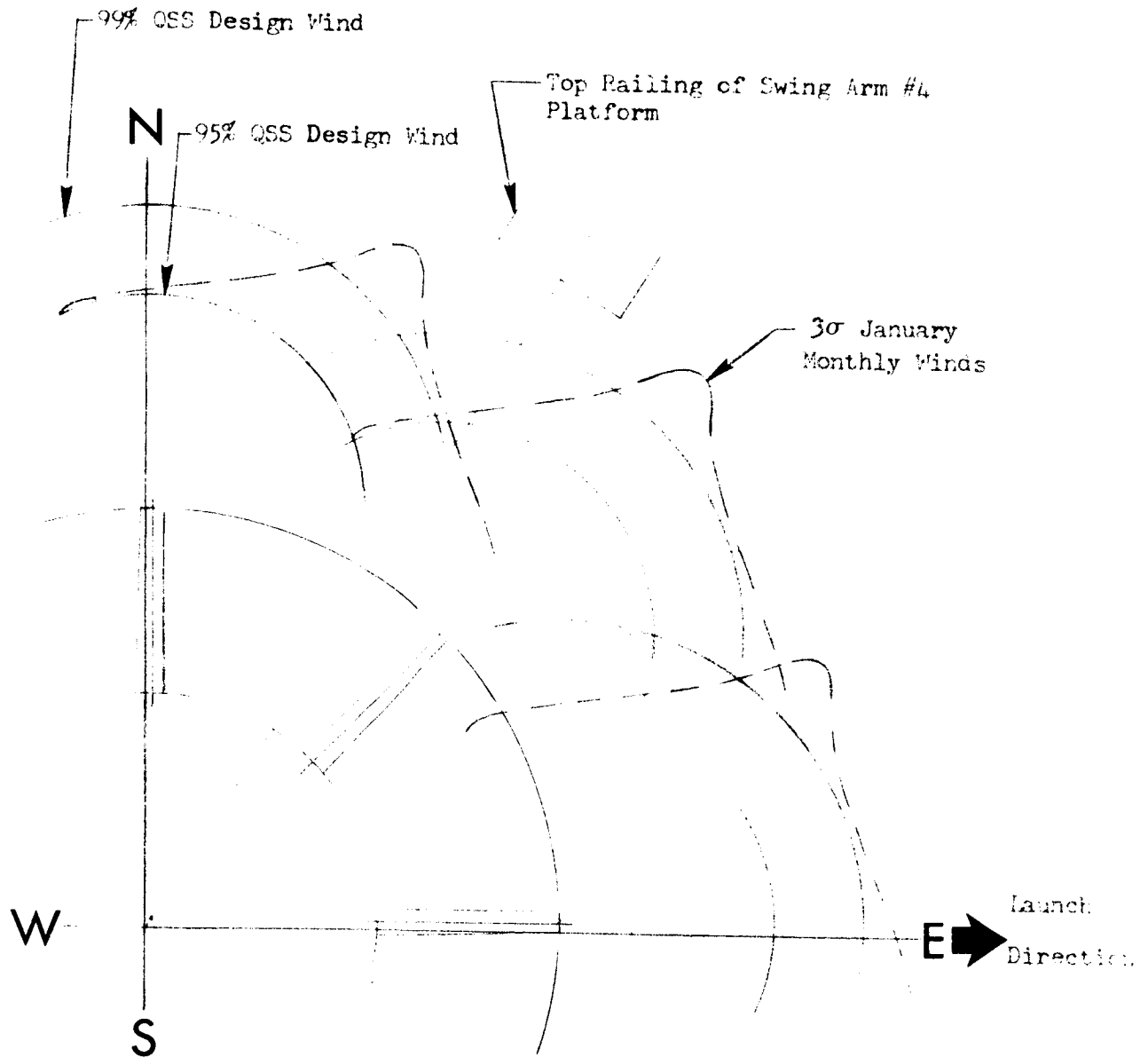
FIGURE 7

SA-204/LM-1 DRIFT ENVELOPES AT TOWER TOP

Tower Top Envelope

99% QSS Design Wind

95% QSS Design Wind

3σ January Monthly Winds

Launch
Direction

N

W

S

E

-32-
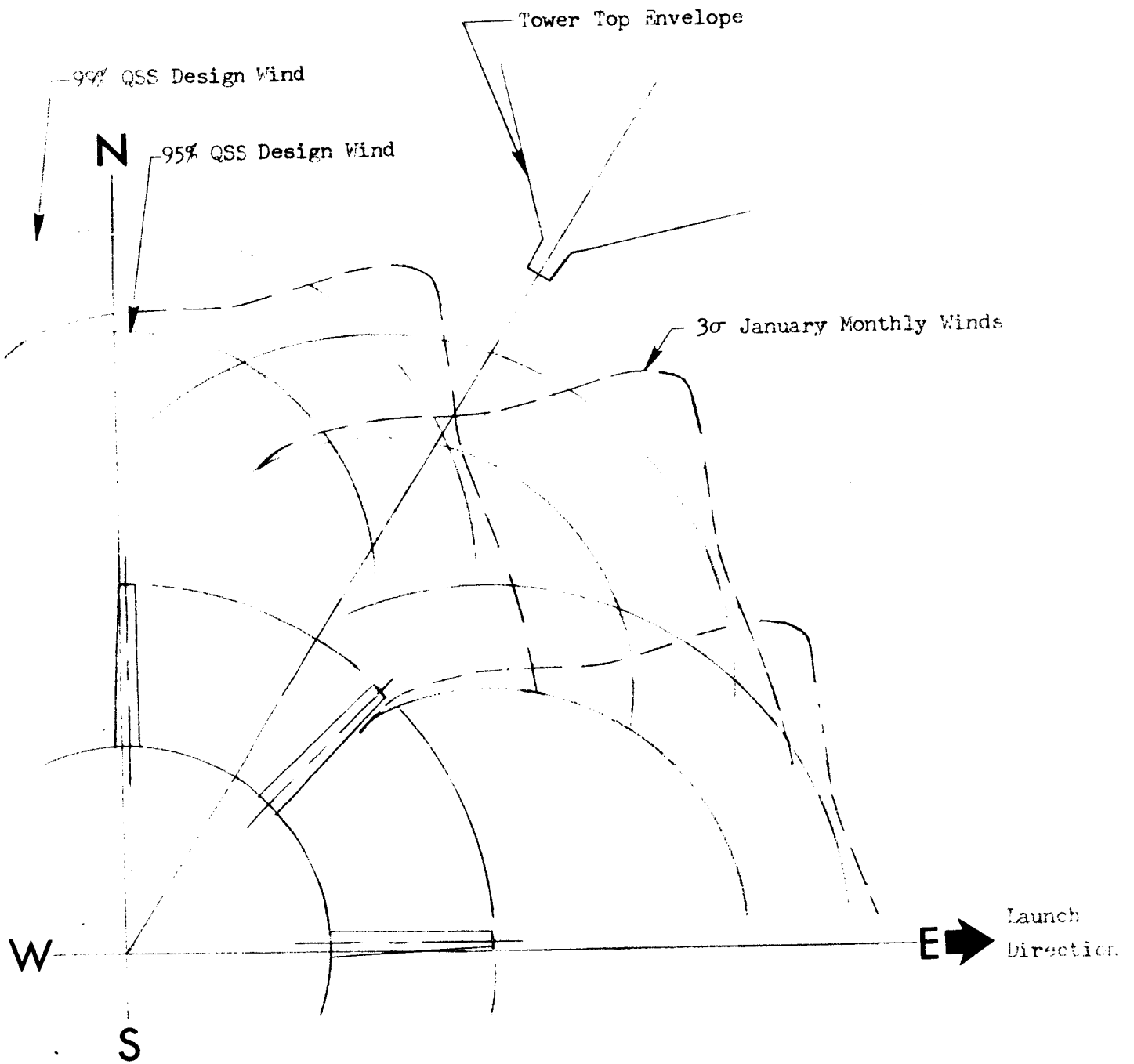
SCALE:

1 CM = 1 MET

FIGURE 8

SA-204/LM-1 DRIFT ENVELOPES AT LIGHTNING MAST TOP

SCALE:

1 CM = 1 MET

-33-
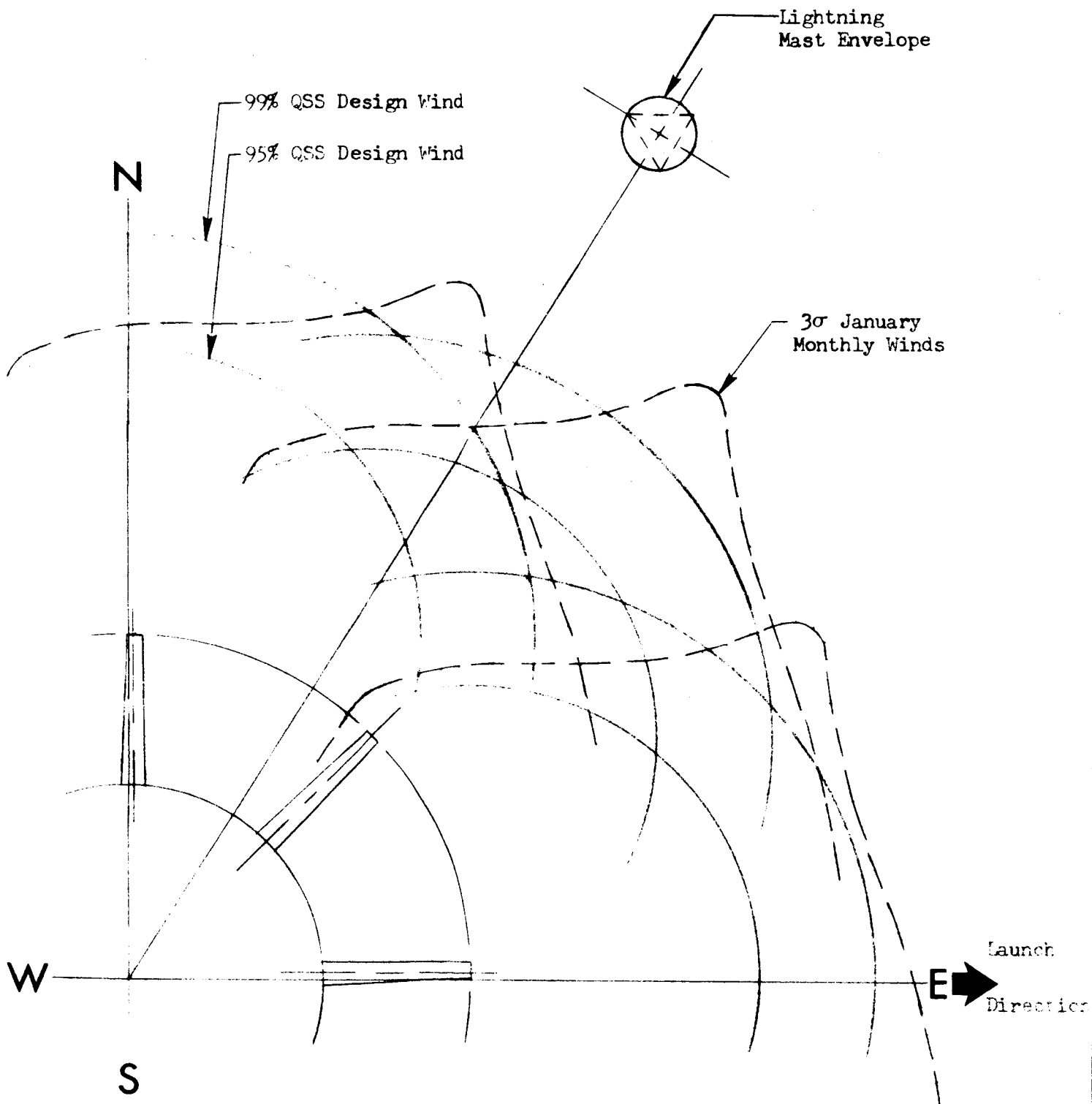
FIGURE 9

SA-204/LM-1 LIFTOFF UMBILICAL TOWER COLLISION
WIND LIMIT FOR SWING ARM #4 PLATFORM

NOTE: Steady State
Wind Speed at
60 Foot
Reference Level

SPACE DIVISION CHRYSLER CORPORATION
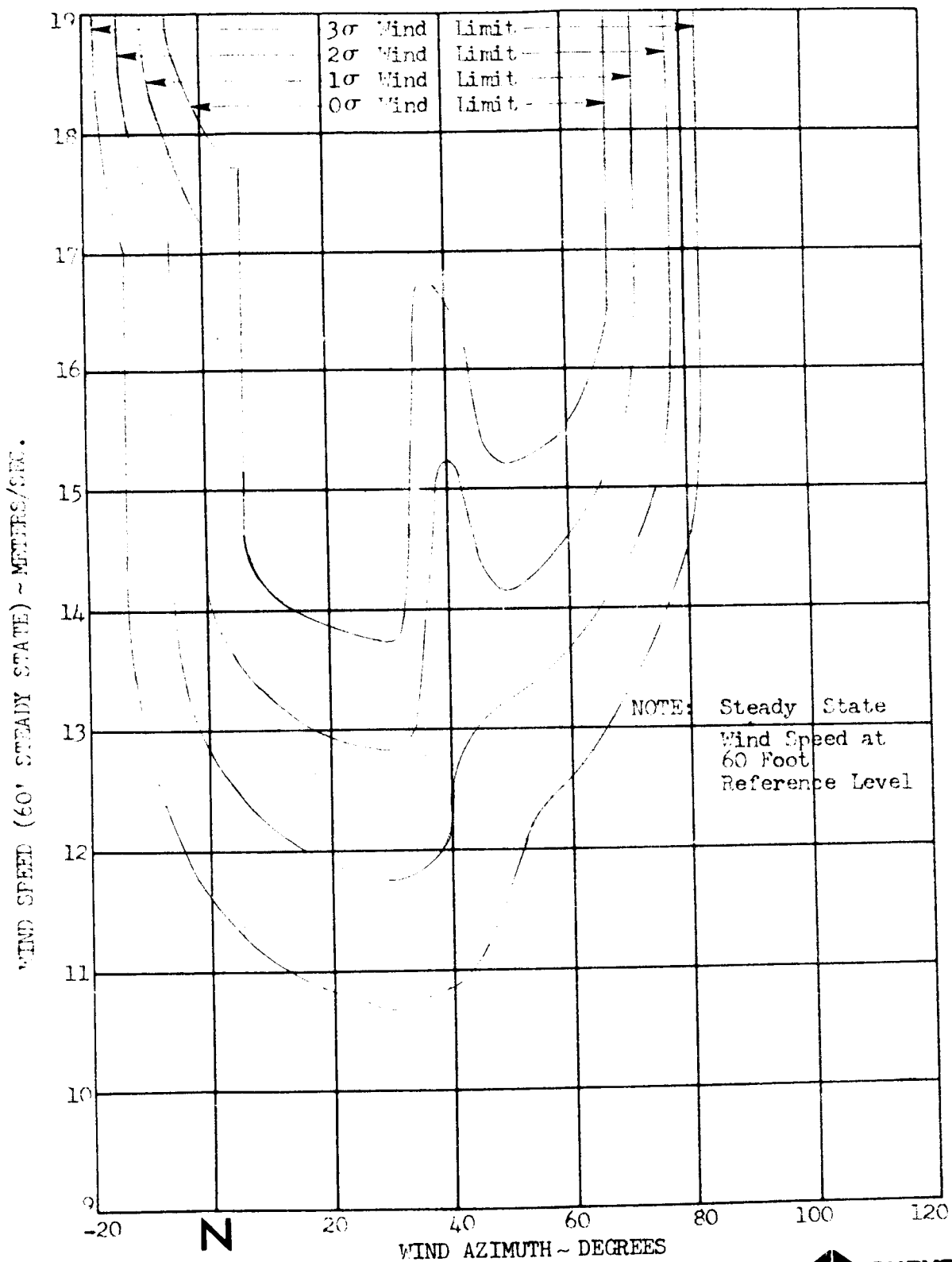
FIGURE 10

SA-204/LM-1 WIND SPEED AND COMPOSITE CONTROL

DEFLECTION COMBINATION LIMIT

WIND SPEED (60' STEADY STATE) ~ MET/SEC

WIND AZIMUTH ~ DEG. FROM NORTH

$\Delta\beta = 0$

$\Delta\beta = .2$

$\Delta\beta = .4$

$\Delta\beta = .6$

-35-

PLATE 11
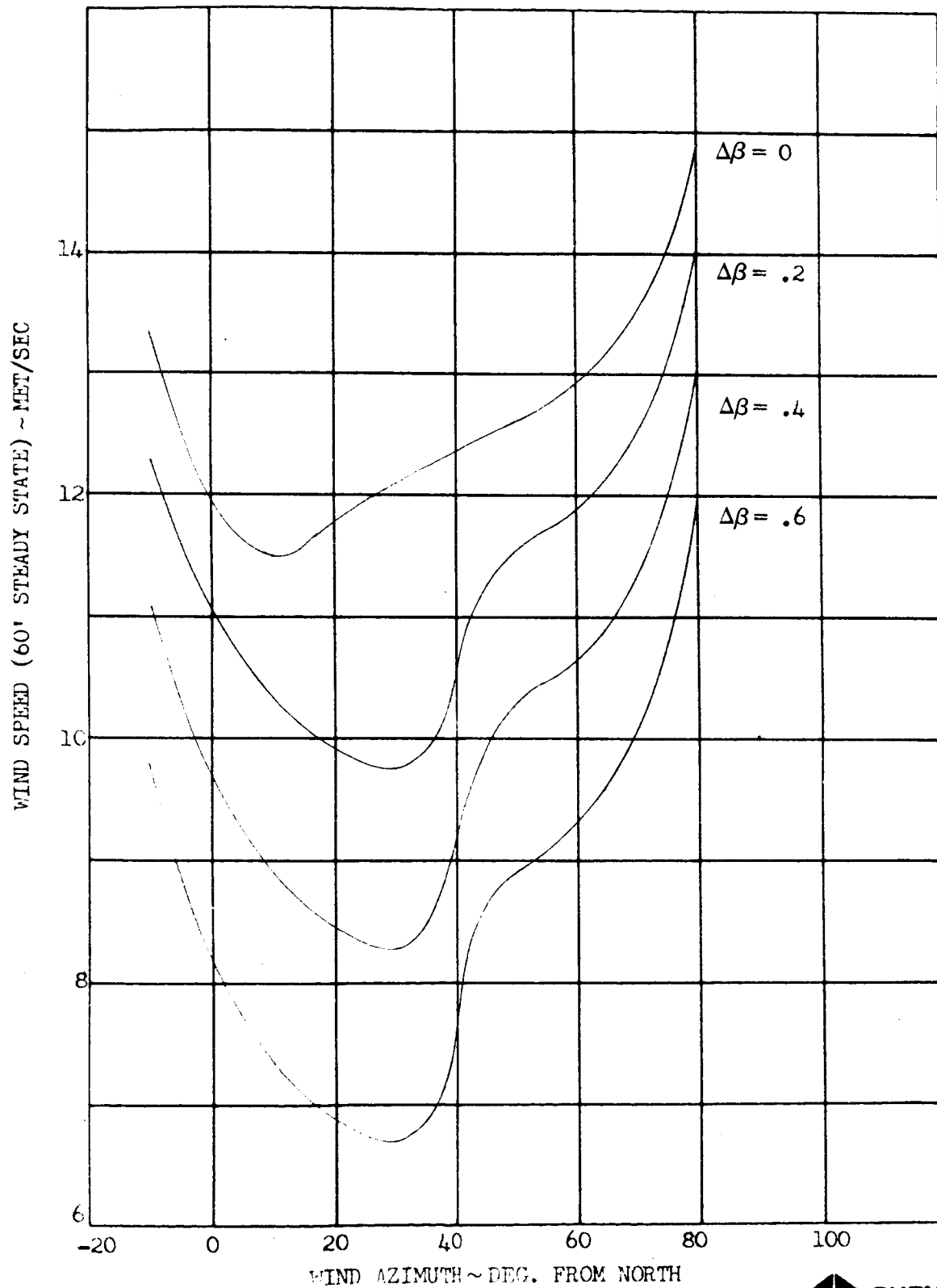
SA-204/LM-1 LIFTOFF MALFUNCTION DRIFT ENVELOPES

FOR ENGINE NO. 1 FAILURES

N

Drift of Fin Trailing Edge
(95% OSS Design Surface Winds Included)

Top of Swing Arm
No. 4 Platform

#1 E/O at 0.1 Sec.

#1 E/O at 2 Sec.

#1 E/O at 4 Sec.

E Launch
Direction

W

S
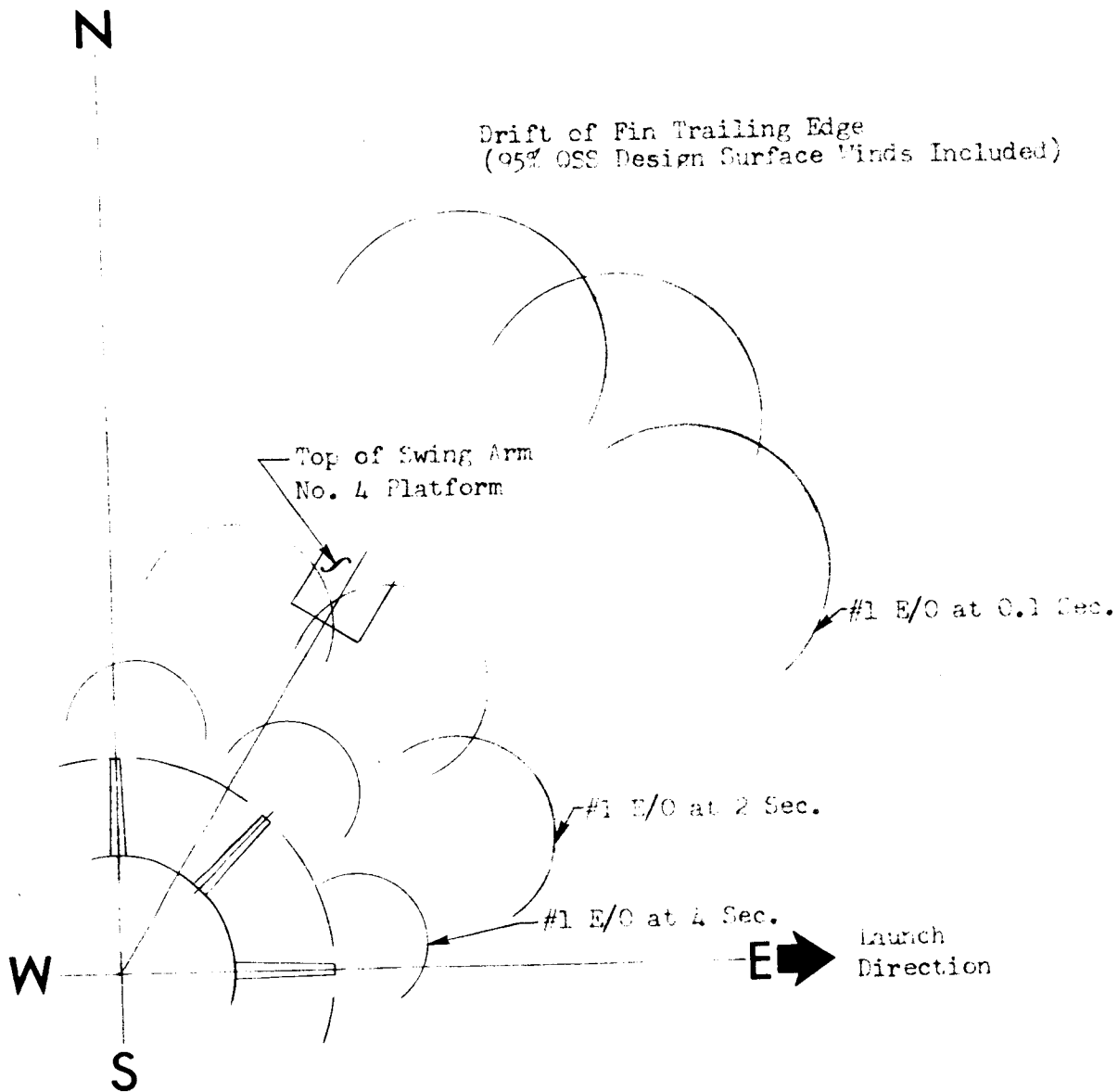
SCALE:
1 CM = 2 MET

FIGURE 12

SA-204/LM-1 LIFTOFF MALFUNCTION DRIFT ENVELOPES

FOR ENGINE NO. 5 FAILURES

N

Top of Swing Arm No. 4 Platform

Drift of Fin
Trailing Edge
(95% QSS Design Surface
Winds Included)

#5 E/O at 0.1 Sec.

#5 E/O at 2 Sec.

#5 E/O at 4 Sec.

W

E ➤ Launch
Direction

S
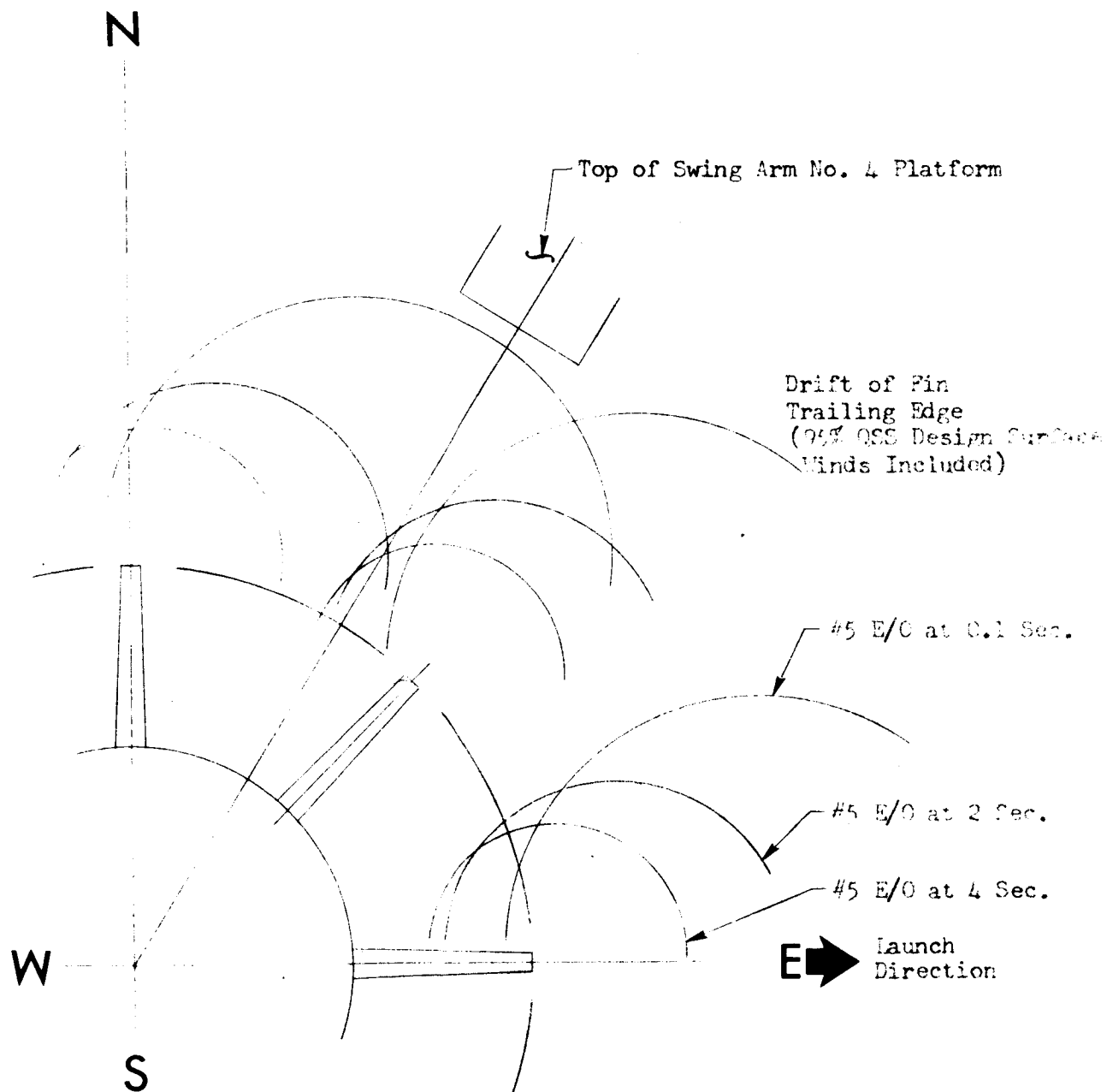
SCALE:
1 CM = 1 MET

FIGURE 13

SA-204/LM-1 LIFTOFF MALFUNCTION DRIFT ENVELOPES

FOR ENGINE NO. 6 FAILURES

Drift of Fin Trailing Edge
(95% QSS Design Surface Winds Included)

Top of Swing Arm No. 4 Platform

#6 E/O at 0.1 Sec.

#6 E/O at 2 Sec.

#6 E/O at 4 Sec.

Launch Direction

SCALE:
1 CM = 1 MET
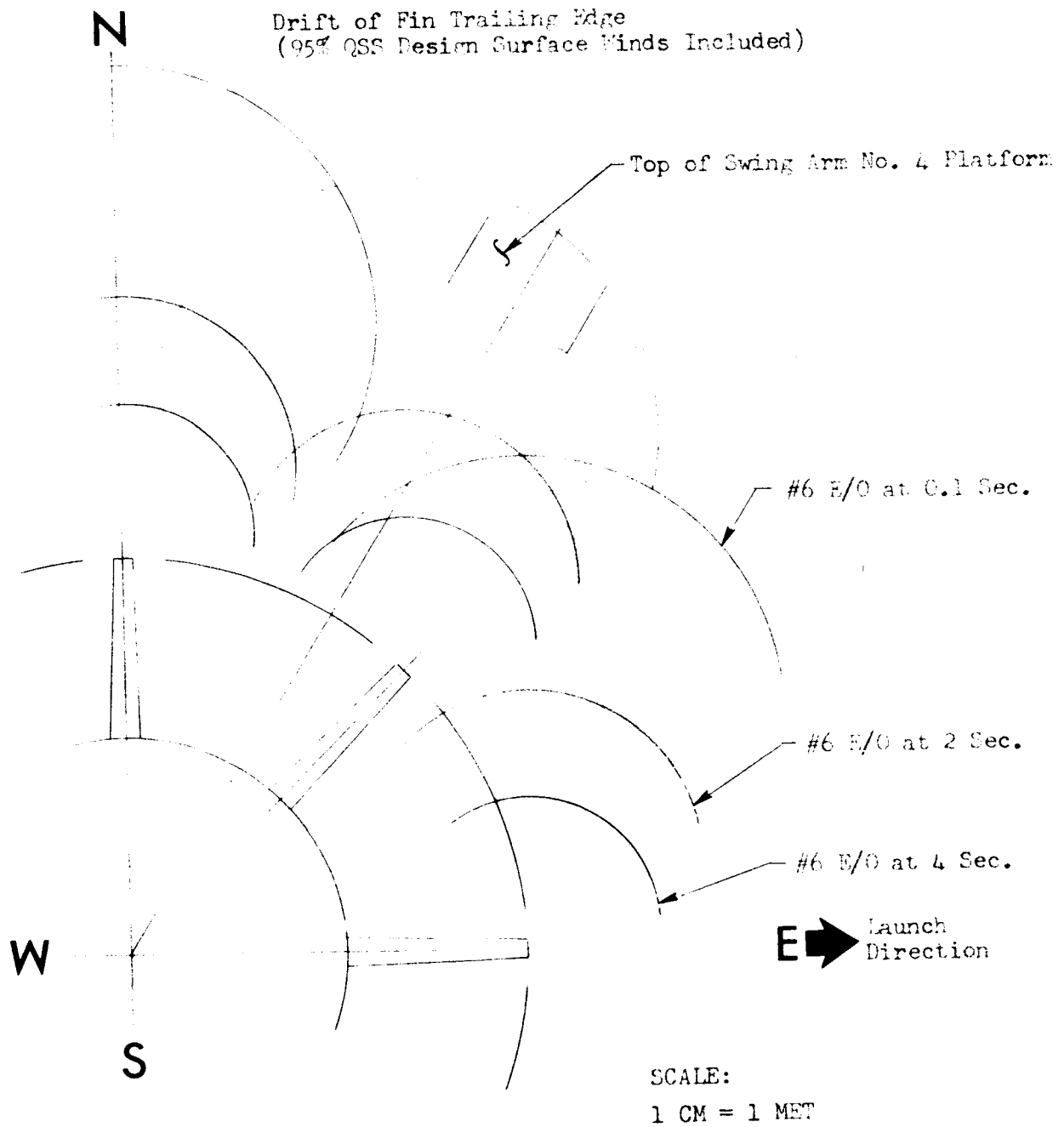
FIGURE 14

SA-204/LM-1 LIFTOFF ENGINE FAILURE CRITICAL TIMES

NOTE: 95% QSS Design
Surface Winds Included

2.55 Sec.

0.85 Sec.

Eng. No. 5

Eng. No. 6

Eng. No. 1

TIME OF MALFUNCTION OCCURRENCE ~ SEC

MINIMUM TOWER CLEARANCE DISTANCE ~ FT

CHRYSLER
CORPORATION

SPACE DIVISION

-39-
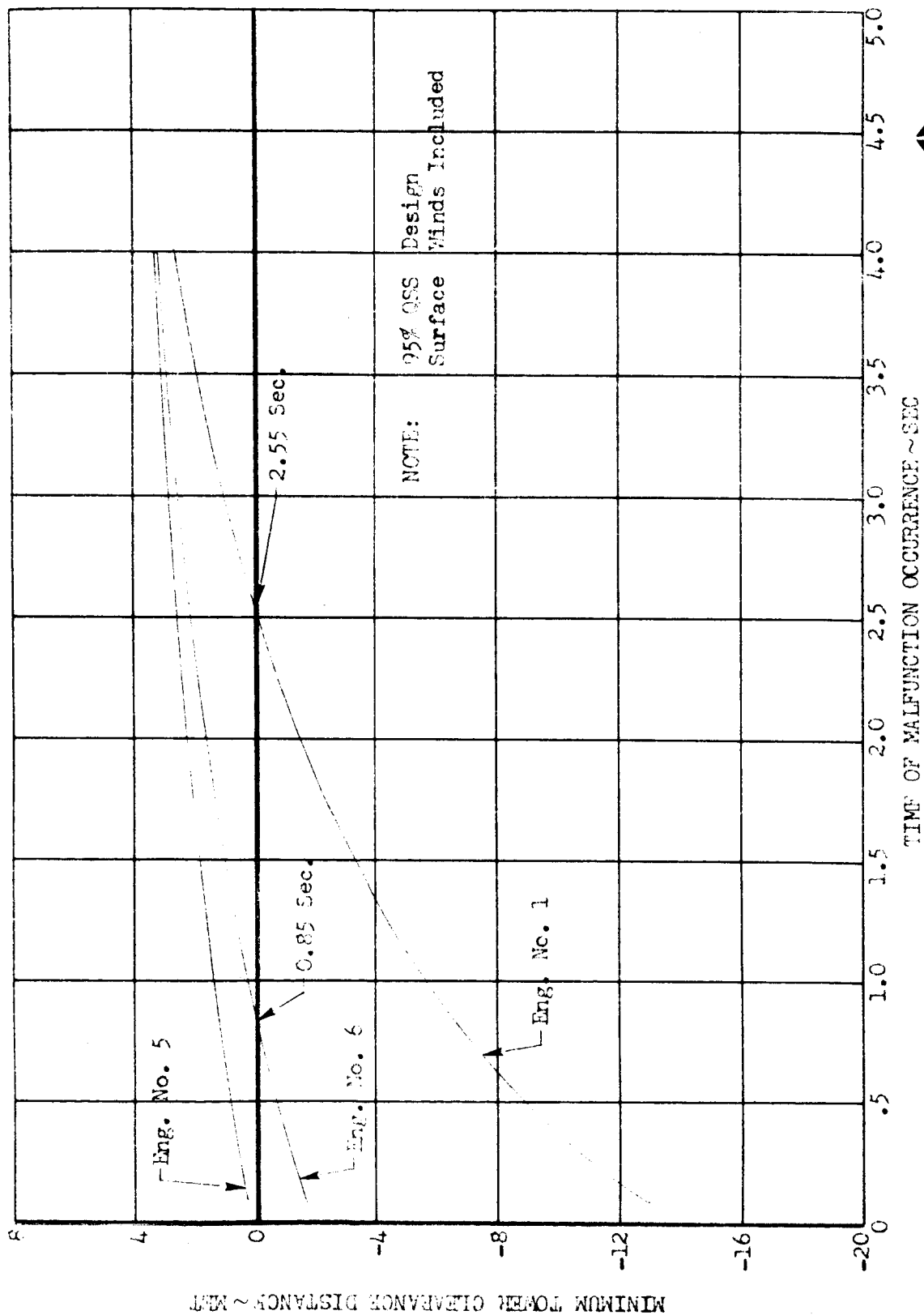
FIGURE 15

SA-204/LM-1 LIFTOFF ENGINE FAILURE WIND RESTRICTION

SPACE DIVISION   CHRYSLER CORPORATION
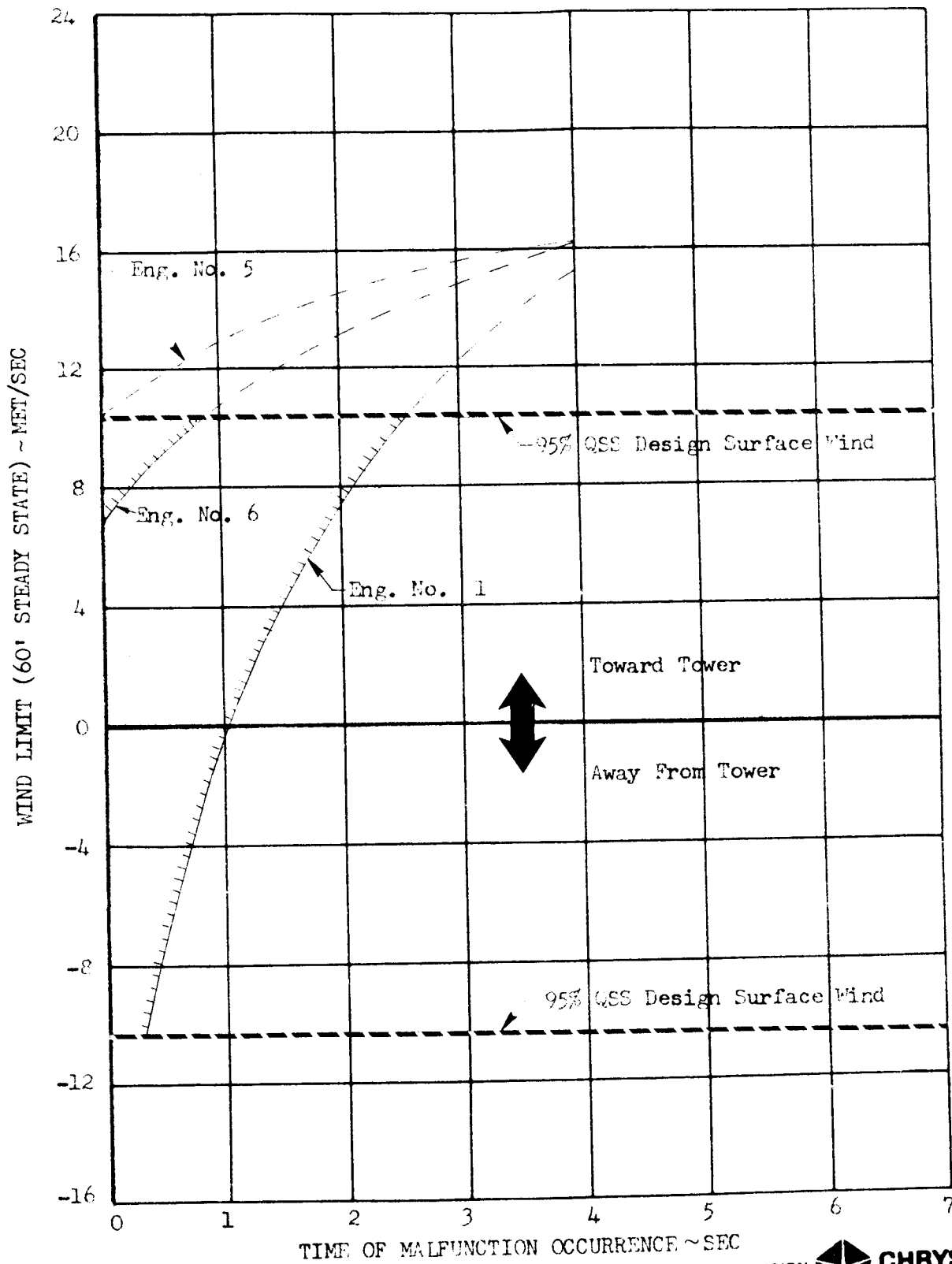
FIGURE 26

SA-204/LM-1 CLEARANCE TIME FOR ENGINE FAILURES
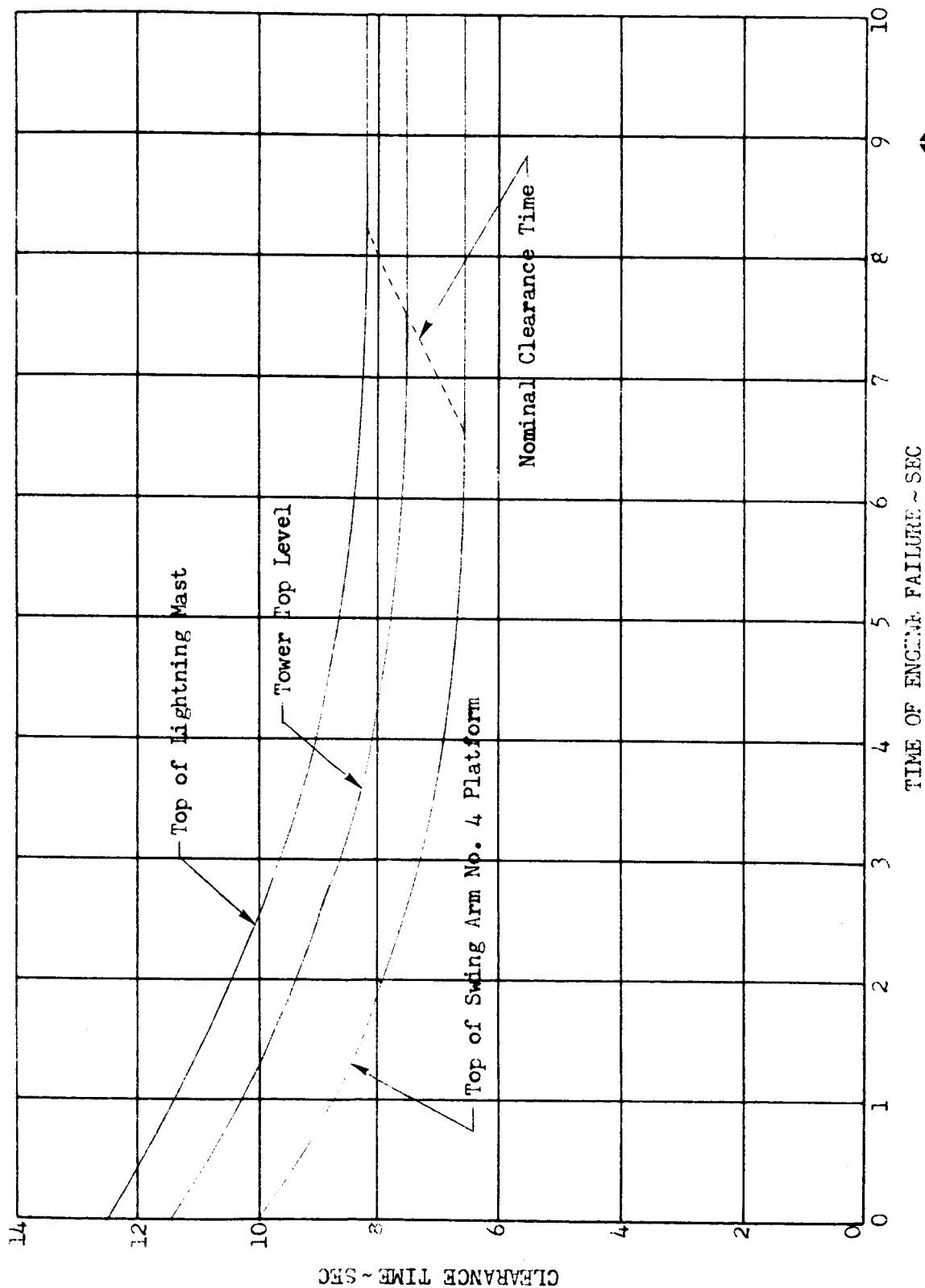
FIGURE 17

SA-204/LM-1 LIFTOFF MALFUNCTION DRIFT ENVELOPES
FOR ENGINE NO. 1 SINGLE ACTUATOR HARDOVERS

N

Drift of Fin Trailing Edge
(95% OSS Design Surface Winds Included)

Top of Swing Arm No. 4 Platform

#1E H/O at 0 Sec.

#1E H/O at 2 Sec.

#1E H/O at 4 Sec.

W

E ➡ Launch
Direction

S

SCALE:
1 CM = 1 MET

-42-
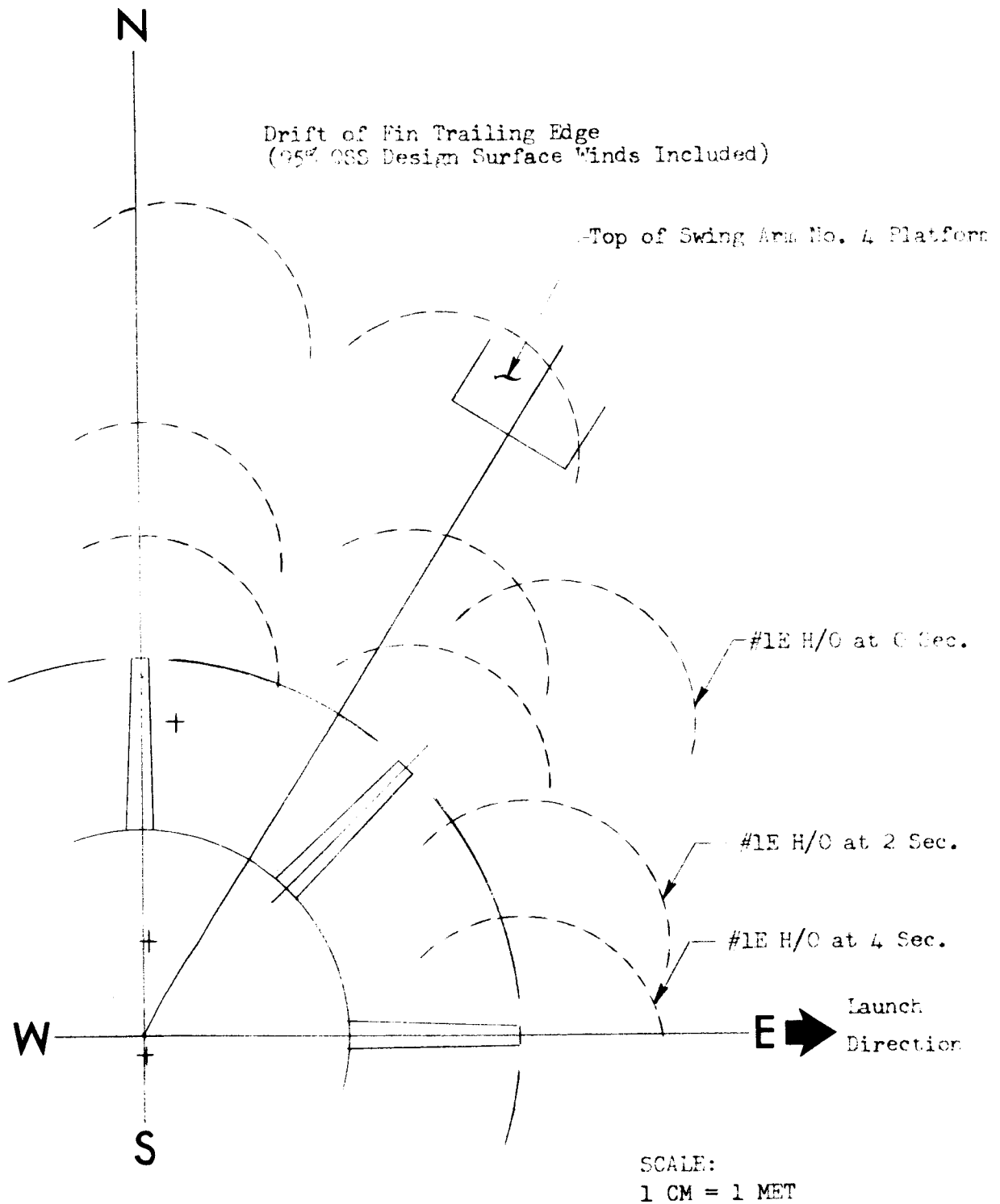
FIGURE 18

SA-204/LM-1 LIFTOFF MALFUNCTION DRIFT ENVELOPES
FOR ENGINE NO. 2 SINGLE ACTUATOR HARDOVERS

Drift of Fin Trailing Edge
(95% QSS Design Surface Winds Included)

Top of Swing Arm No. 4 Platform

#2E H/O at 0 Sec.

#2E H/O at 2 Sec.

#2E H/O at 4 Sec.

Launch
Direction

SCALE:
1 CM = 1 MET

FIGURE 19

SA-204/LM-1 LIFTOFF MALFUNCTION DRIFT ENVELOPES
FOR ENGINE NO. 3 SINGLE ACTUATOR HARDOVERS

Drift of Fin Trailing Edge
(95% GSS Design Surface Winds Included)

Top of Swing Arm No. 4 Platform

#3E H/O at 0 Sec.

#3E H/O at 2 Sec.

#3E H/O at 4 Sec.

Launch
Direction

SCALE:
1 CM = 1 MET

-44-
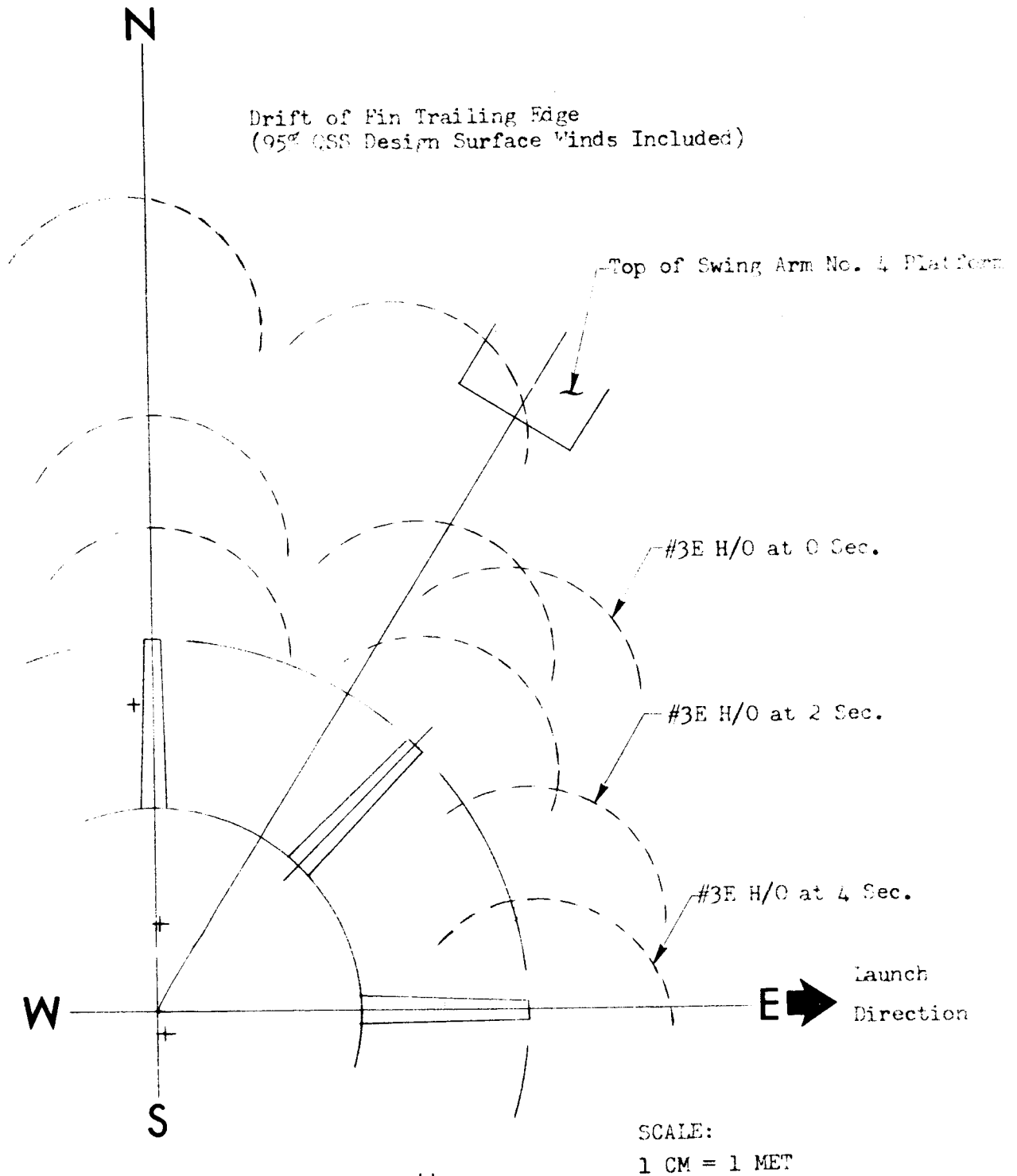
FIGURE 20

SA-204/LM-1 LIFTOFF MALFUNCTION DRIFT ENVELOPES
FOR ENGINE NO. 4 SINGLE ACTUATOR HARDOVERS

Drift of Fin Trailing Edge
(95% QSS Design Surface Winds Included)

SCALE:

1 CM = 1 MET
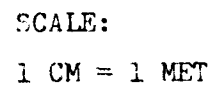
FIGURE 21

SA-204/LM-1 LIFTOFF SINGLE ACTUATOR HARDOVER CRITICAL TIME

NOTE: 95% QSS Design Surface Winds Included

CHRYSLER CORPORATION

SPACE DIVISION
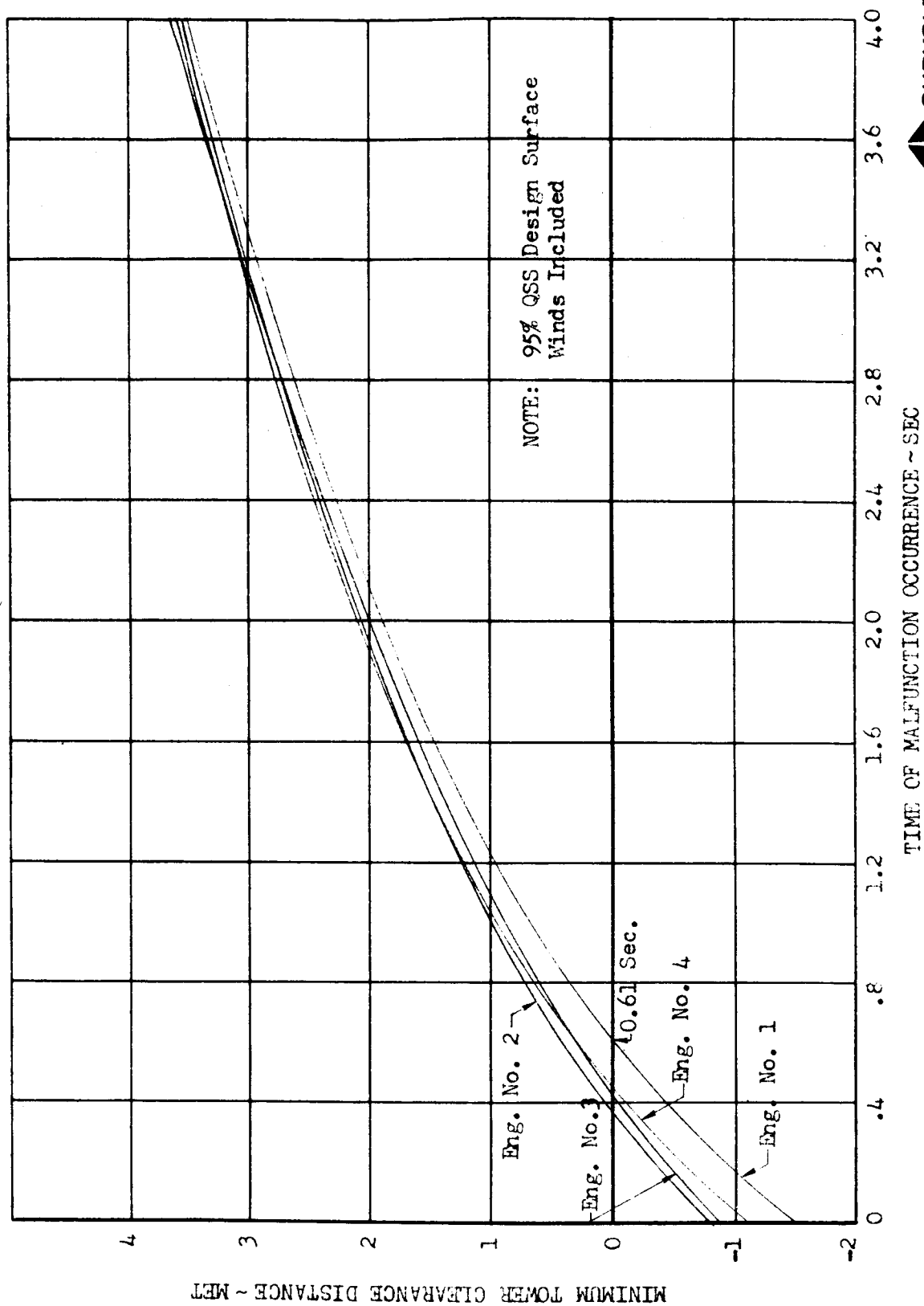
FIGURE 22

SA-204/LM-1 LIFTOFF SINGLE ENGINE ACTUATOR HARDOVER WIND LIMITS
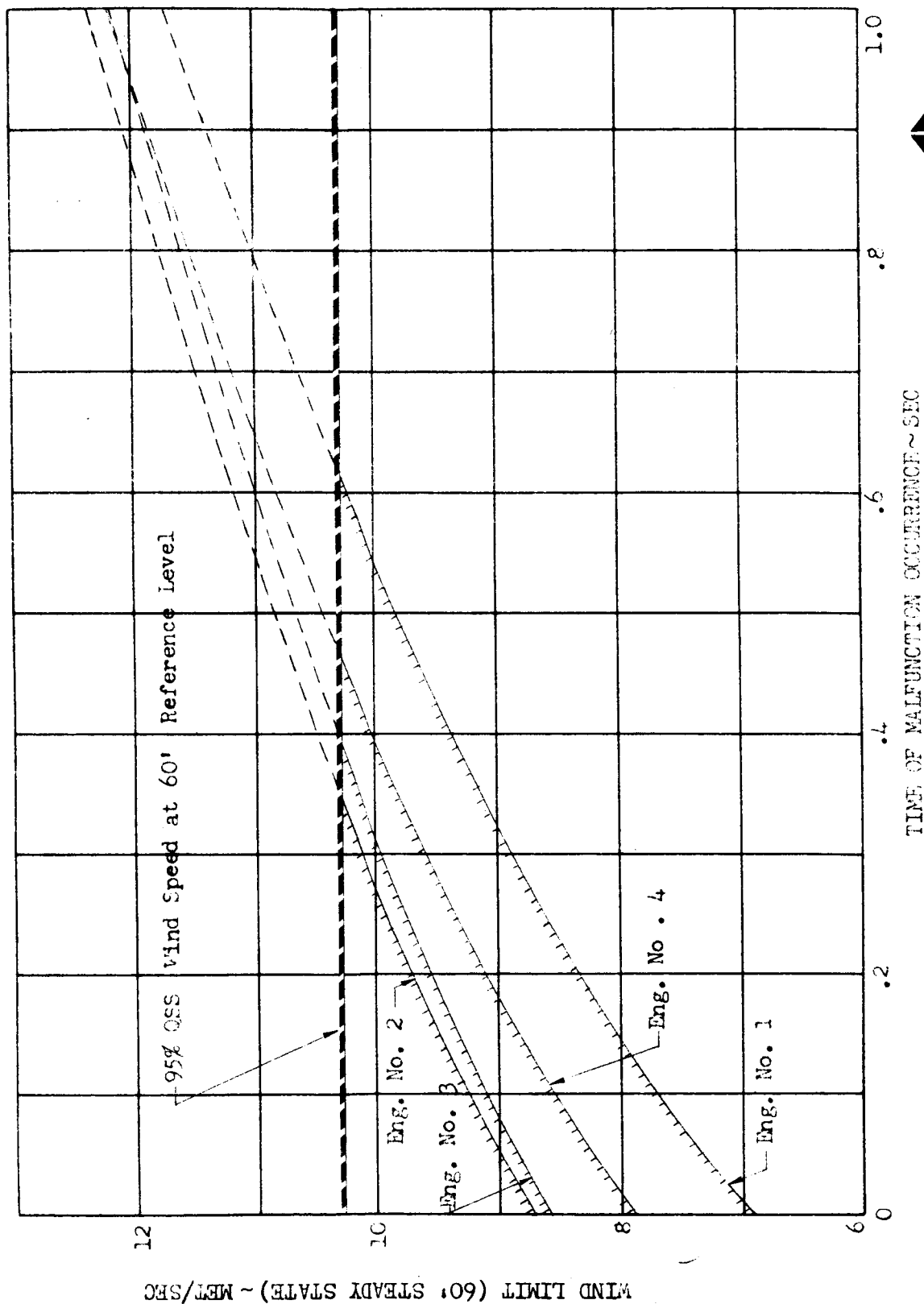
FIGURE 23

SA-204/LM-1 NOMINAL FLIGHT ANGULAR-ACCELERATIONS

PER UNIT ANGLE OF ATTACK AND UNIT CONTROL GIMBAL DEFLECTION

SPACE DIVISION **CHRYSLER CORPORATION**

-48-
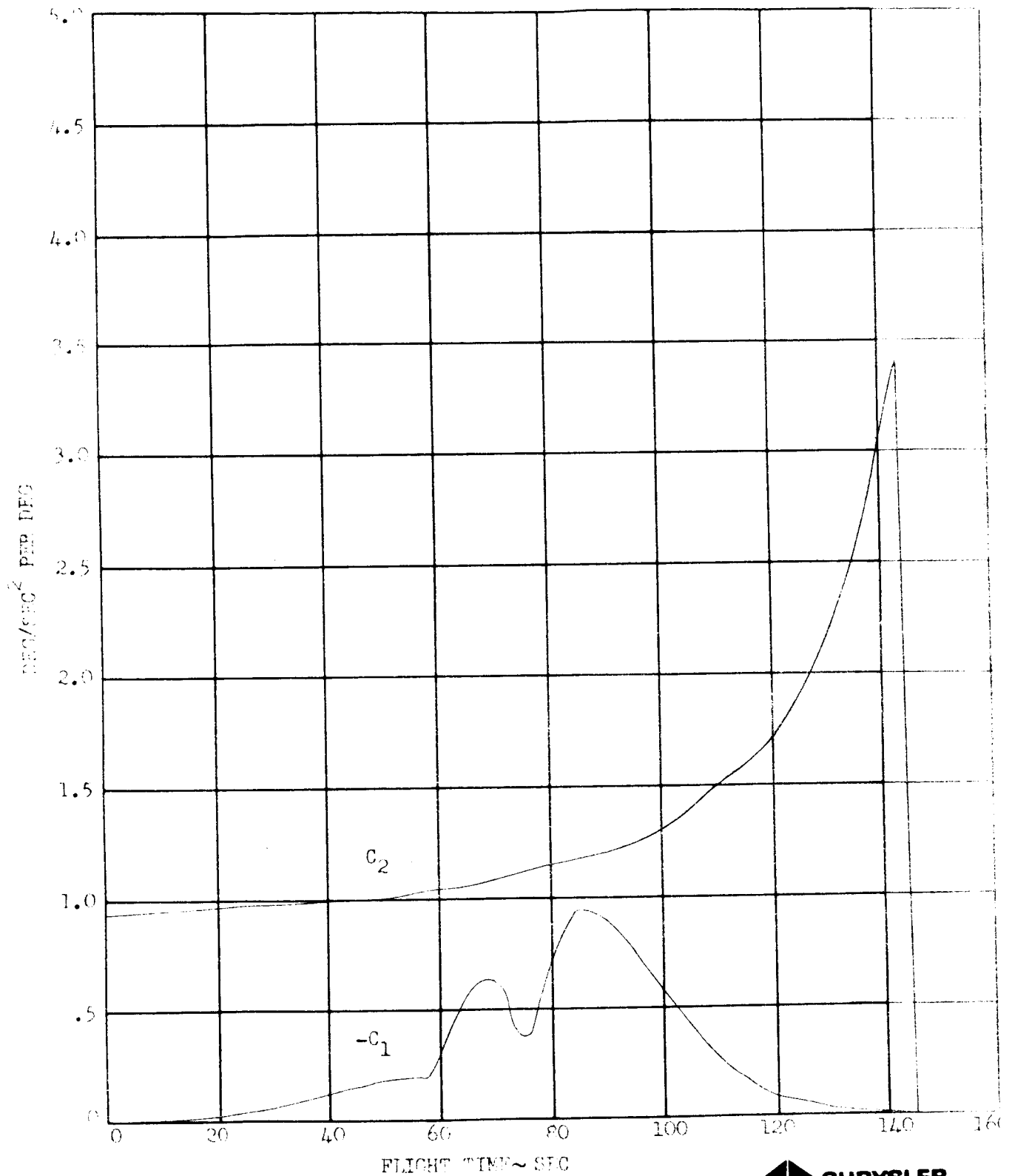
FIGURE 24

SA-204/LM-1 NOMINAL FLIGHT

RATIO OF CONTROL GIMBAL DEFLECTION TO ANGLE OF ATTACK

(STEADY STATE)

$-c_1/c_2$

FLIGHT TIME ~ SEC

SPACE DIVISION · CHRYSLER CORPORATION

-49-
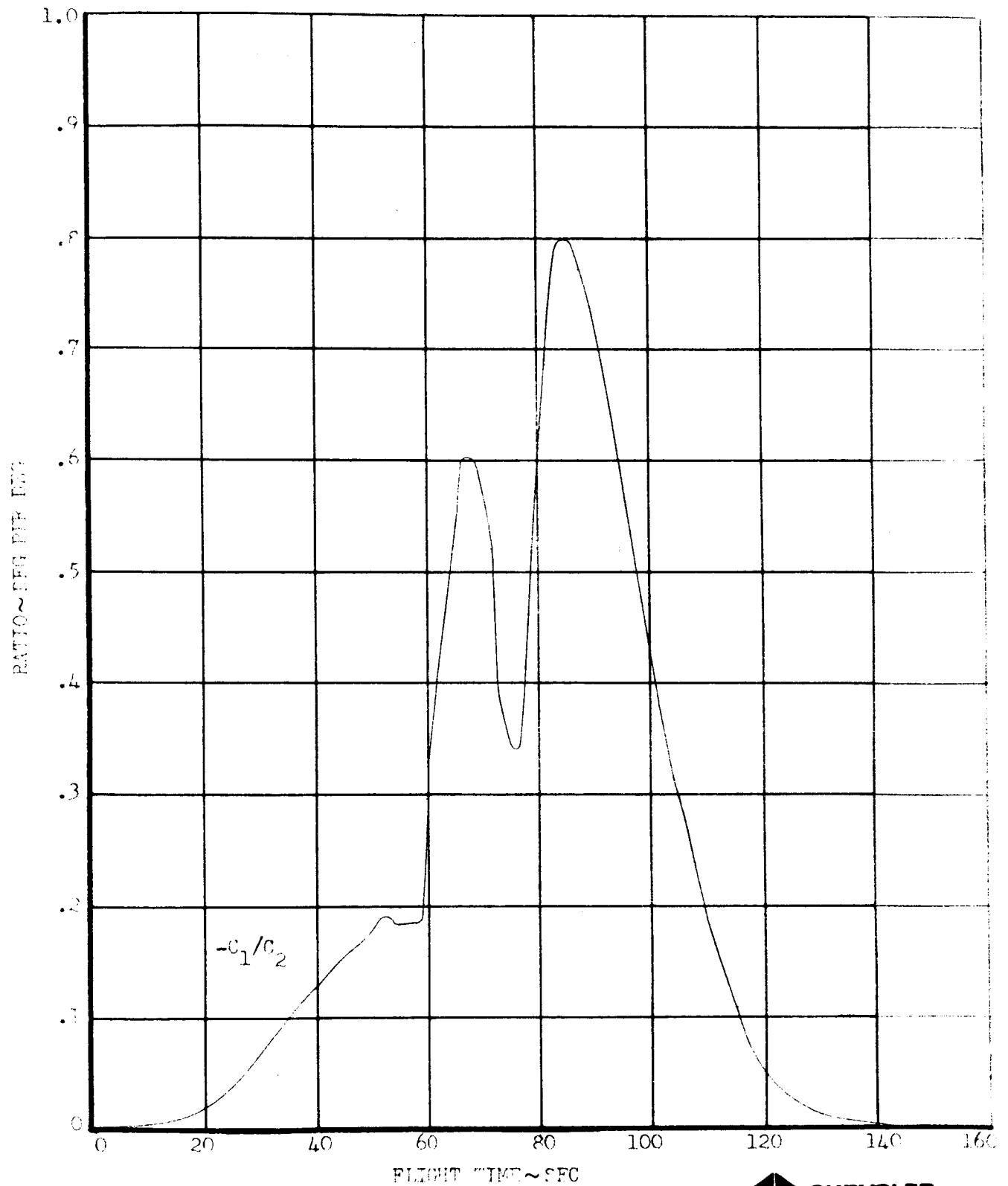
FIGURE 25

SA-204/LM-1 NOMINAL FLIGHT CENTER OF PRESSURE
CENTER OF GRAVITY AND NEGATIVE STATIC MARGIN

FLIGHT TIME ~ SEC

SPACE DIVISION CHRYSLER CORPORATION

-50-
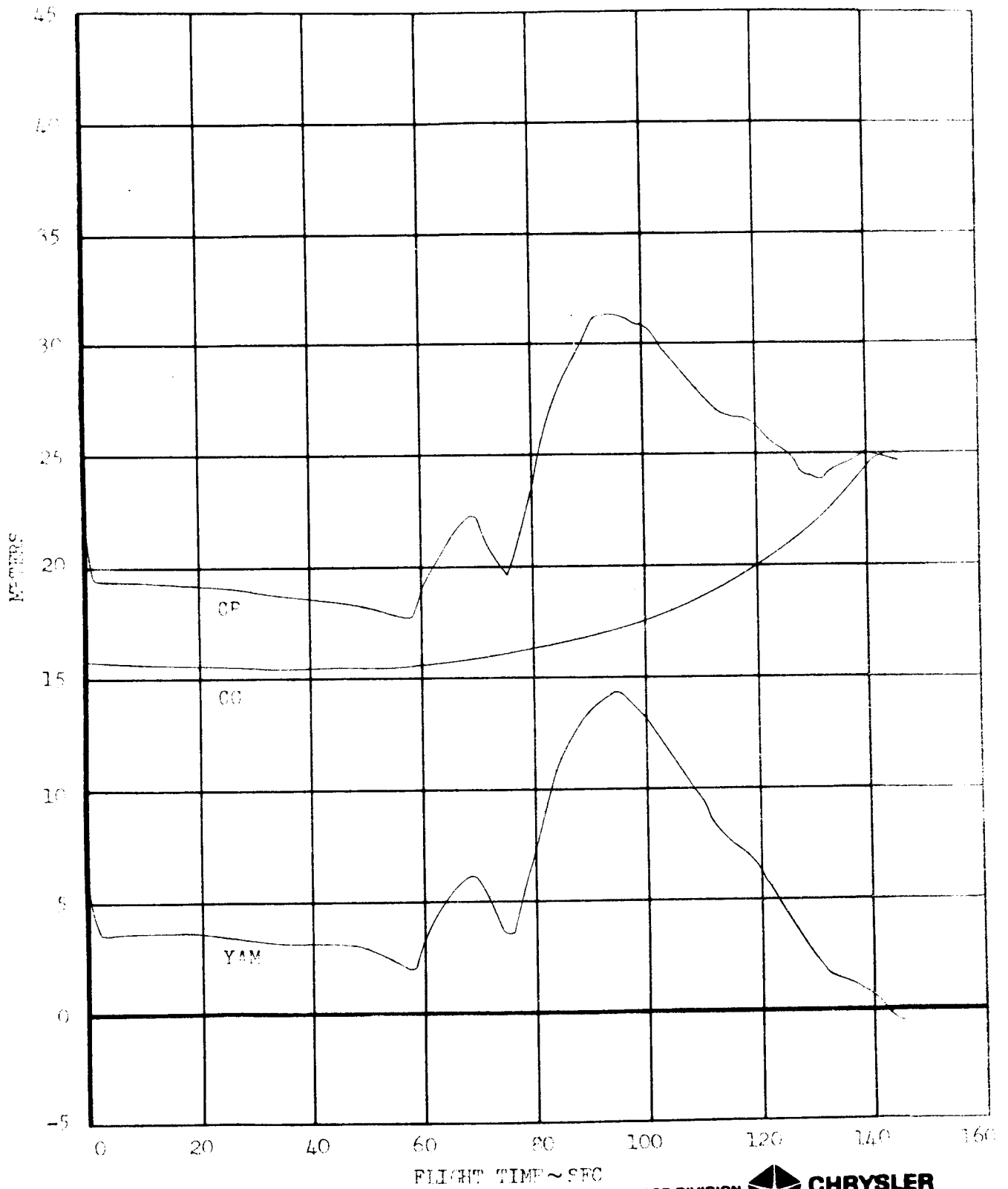
FIGURE 26

SA-204/LM-1 NOMINAL FLIGHT PITCH ATTITUDE COMMAND

84 431 62618 C
JAN 66
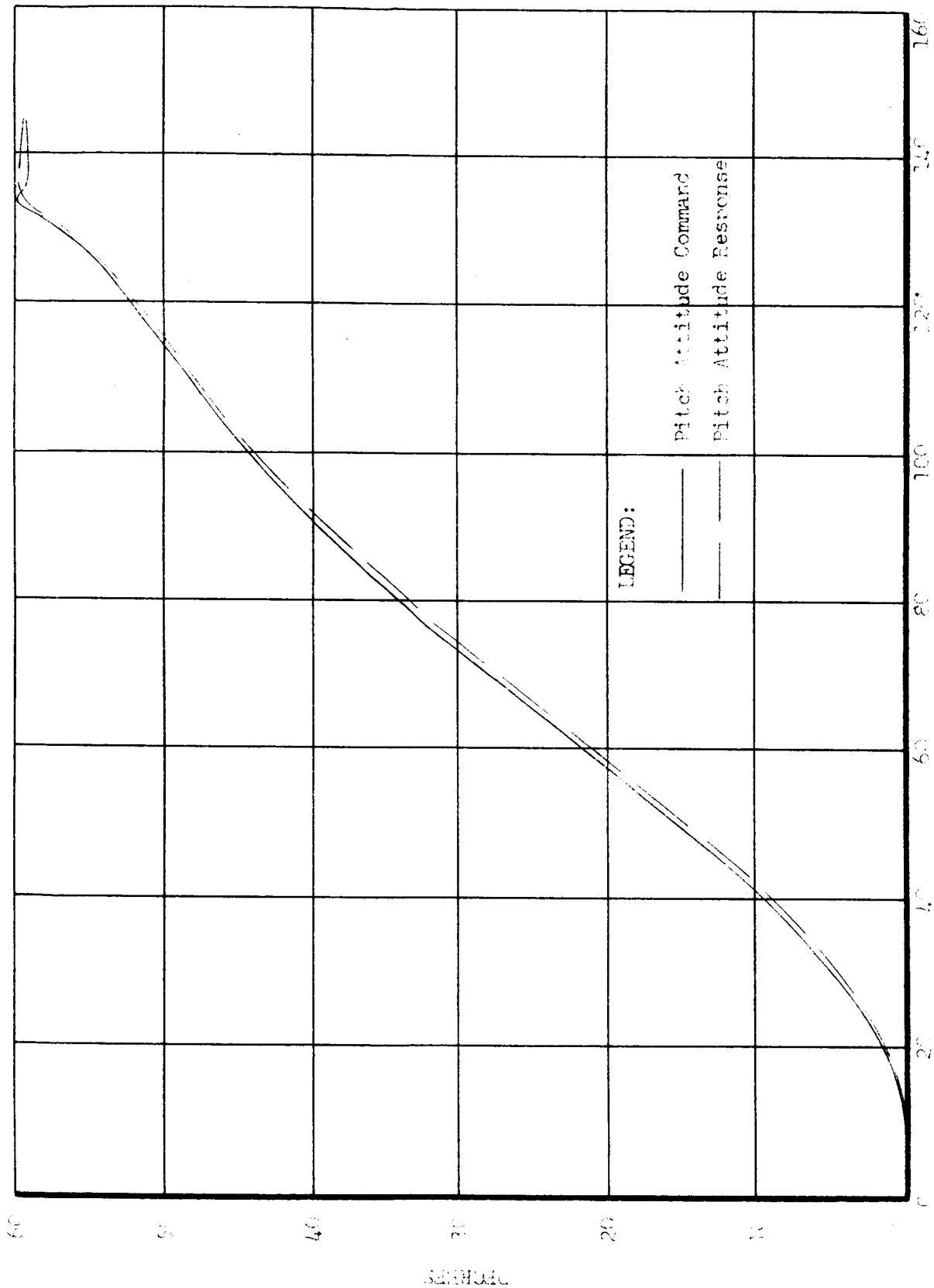
FIGURE 27

SA-204/LM-1 NOMINAL FLIGHT DYNAMIC PRESSURE AND TRIM

PITCH ANGLE OF ATTACK

FLIGHT TIME ~ SEC

SPACE DIVISION CHRYSLER CORPORATION
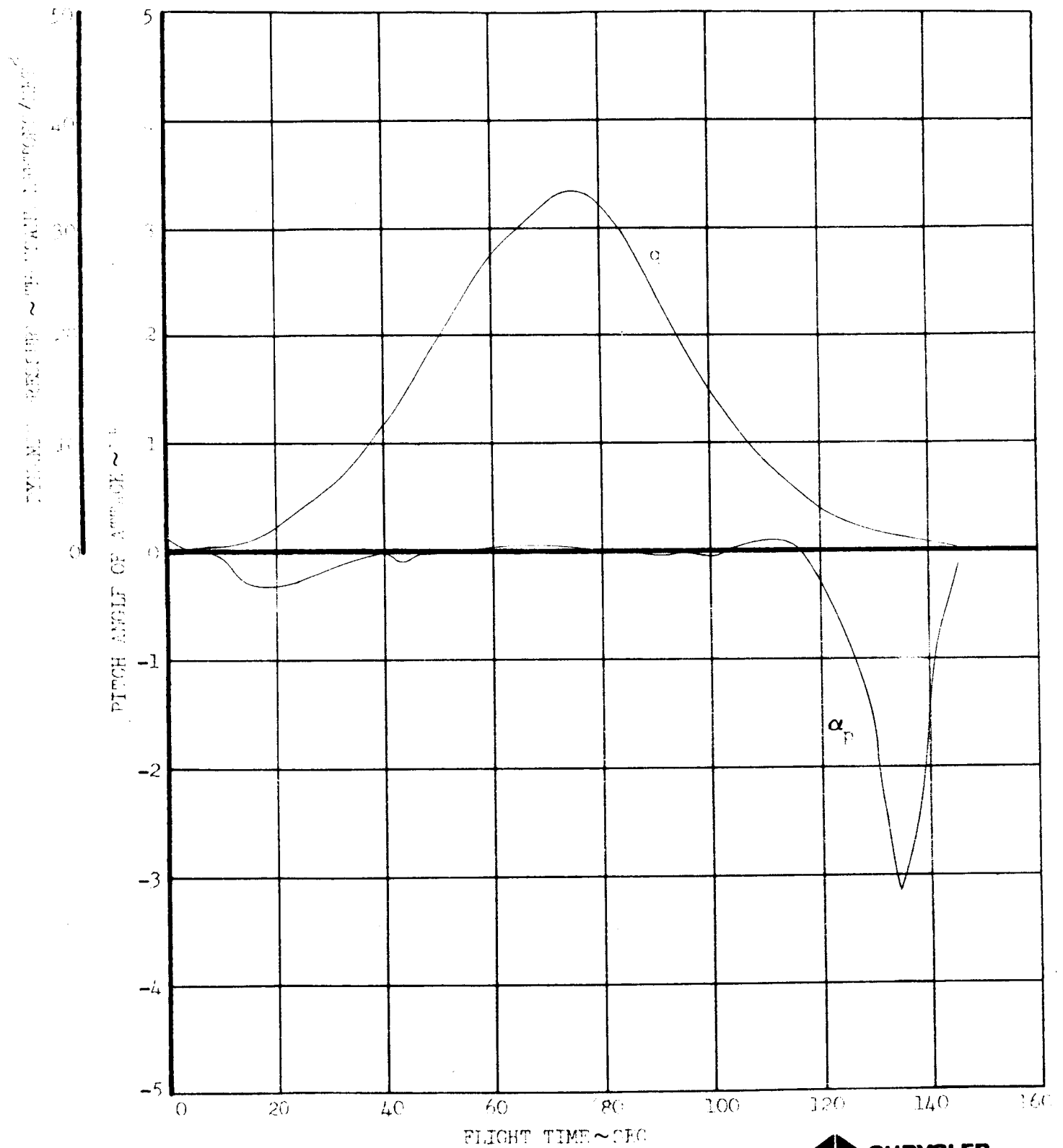
FIGURE 28

SA-204/LM-1 TOTAL VEHICLE PITCH MOMENT OF INERTIA

FLIGHT TIME ~ SEC

I_{p} PITCH MOMENT OF INERTIA ~ MILLION KGM-M^2
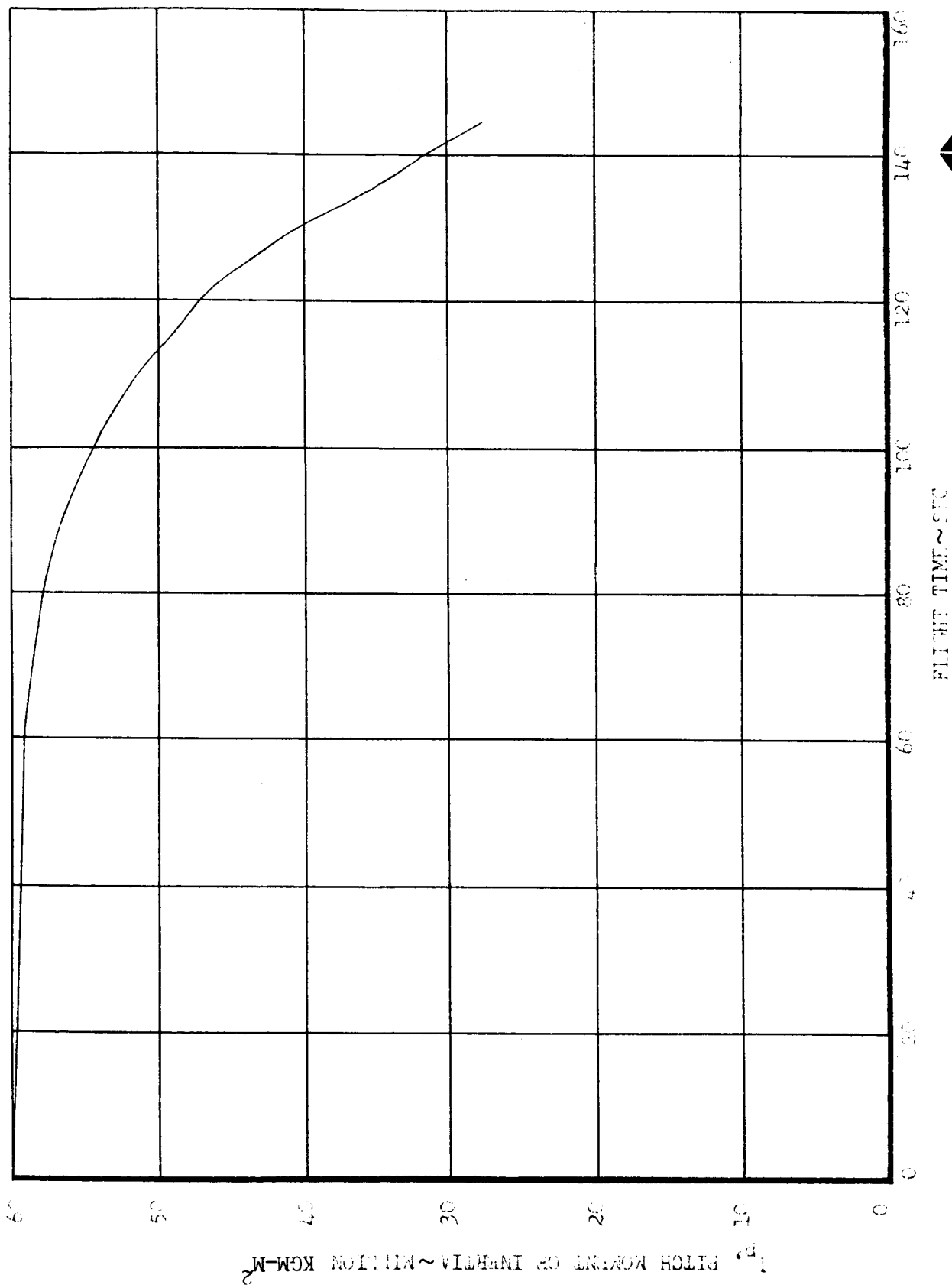
FIGURE 29

SA-204/IM-1 TOTAL VEHICLE AERODYNAMIC CHARACTERISTIC
C_{Z_α}, NORMAL FORCE COEFFICIENT GRADIENT

84431 62618C
JAN 66
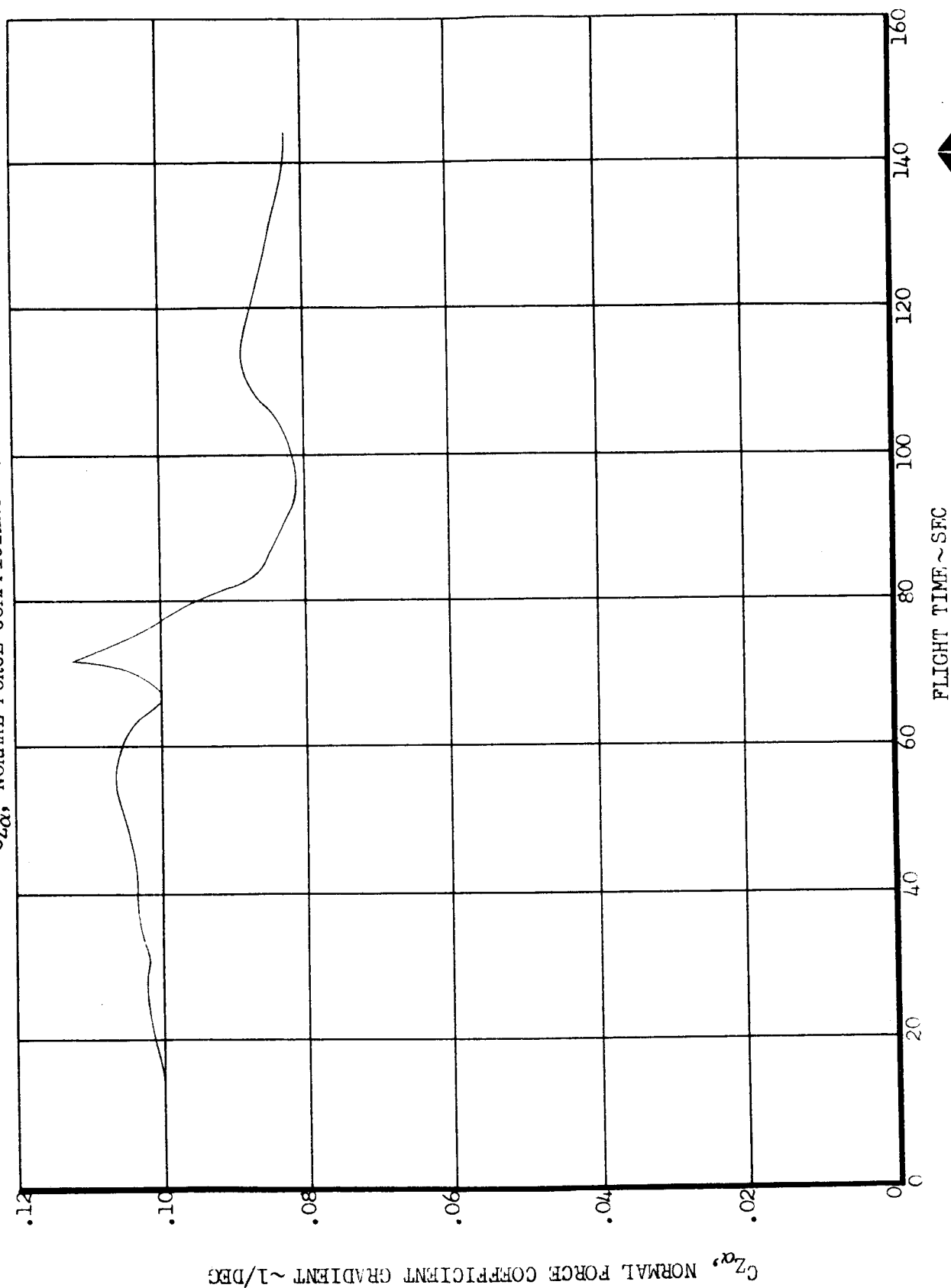
FIGURE 30

SA-204/LM-1 PITCH-ROLL CONTROL CHANNELS
S-IB STAGE

-55-
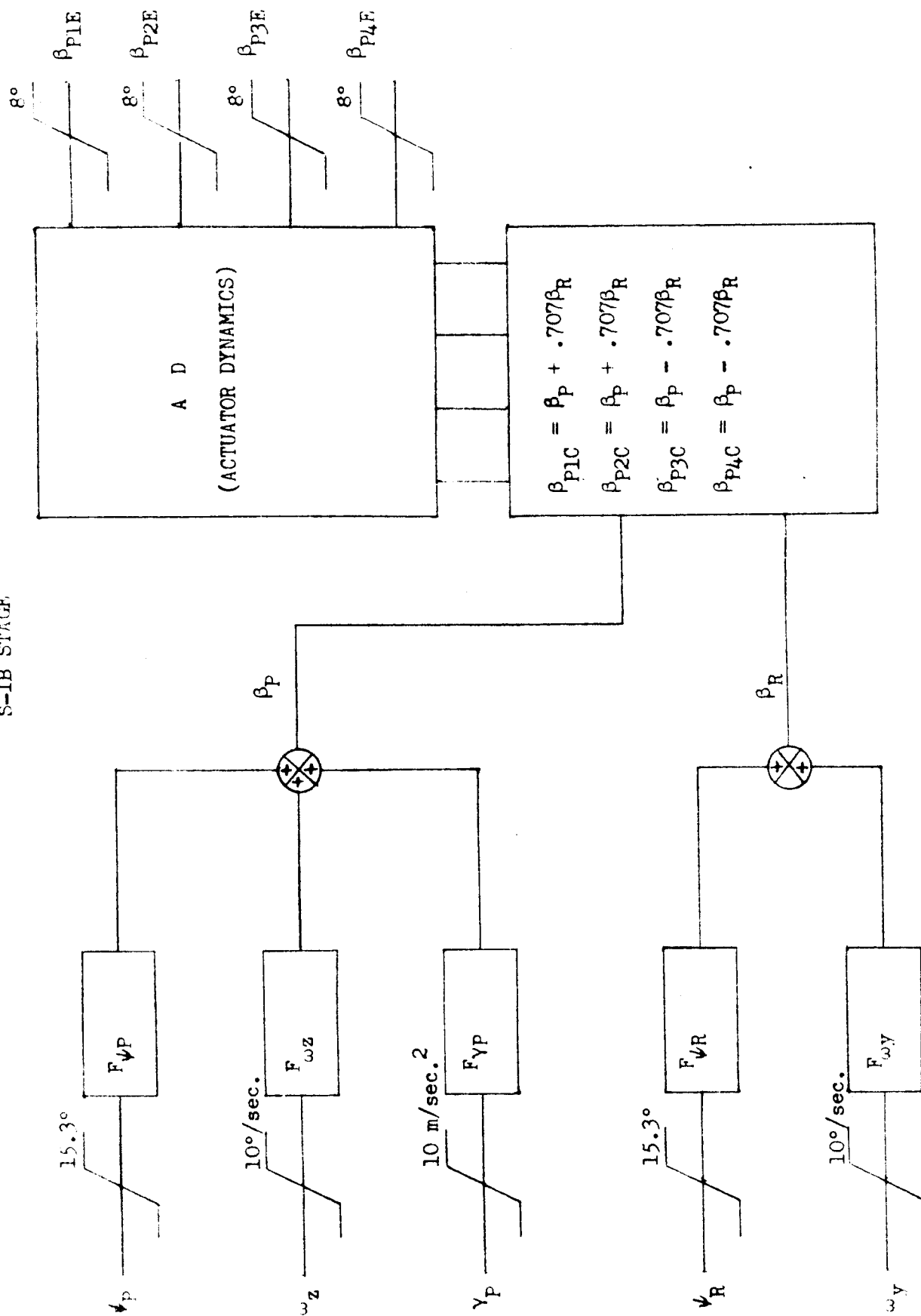
FIGURE 31

SA-204/IM-1 YAW-ROLL CONTROL CHANNELS
S-IB STAGE

$$\beta_{Y1C} = \beta_Y - .707\,\beta_R$$

$$\beta_{Y2C} = \beta_Y + .707\,\beta_R$$

$$\beta_{Y3C} = \beta_Y + .707\,\beta_R$$

$$\beta_{Y4C} = \beta_Y - .707\,\beta_R$$

-56-
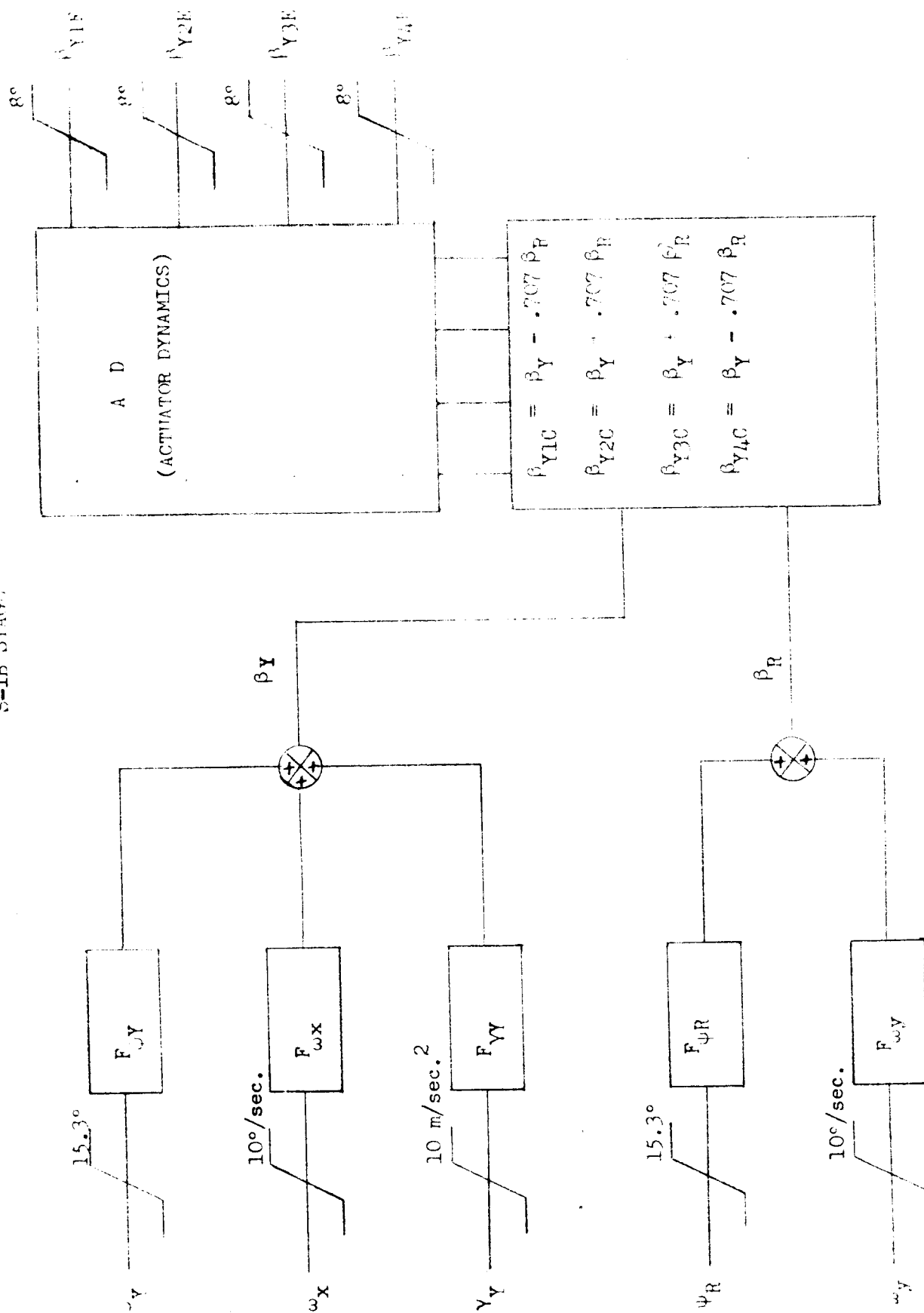
FIGURE 32

SA-204/LM-1 CONTROL SYSTEM GAINS

S-IB STAGE

SPACE DIVISION CHRYSLER CORPORATION
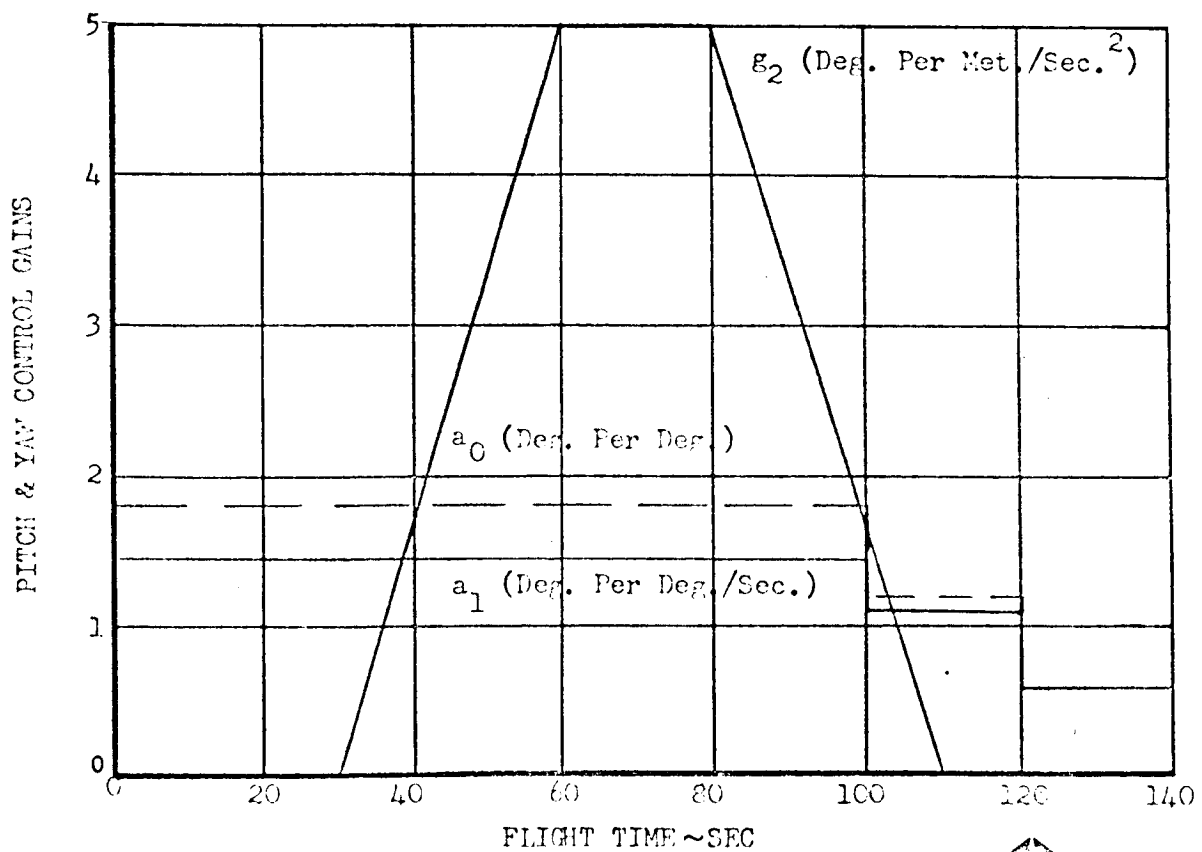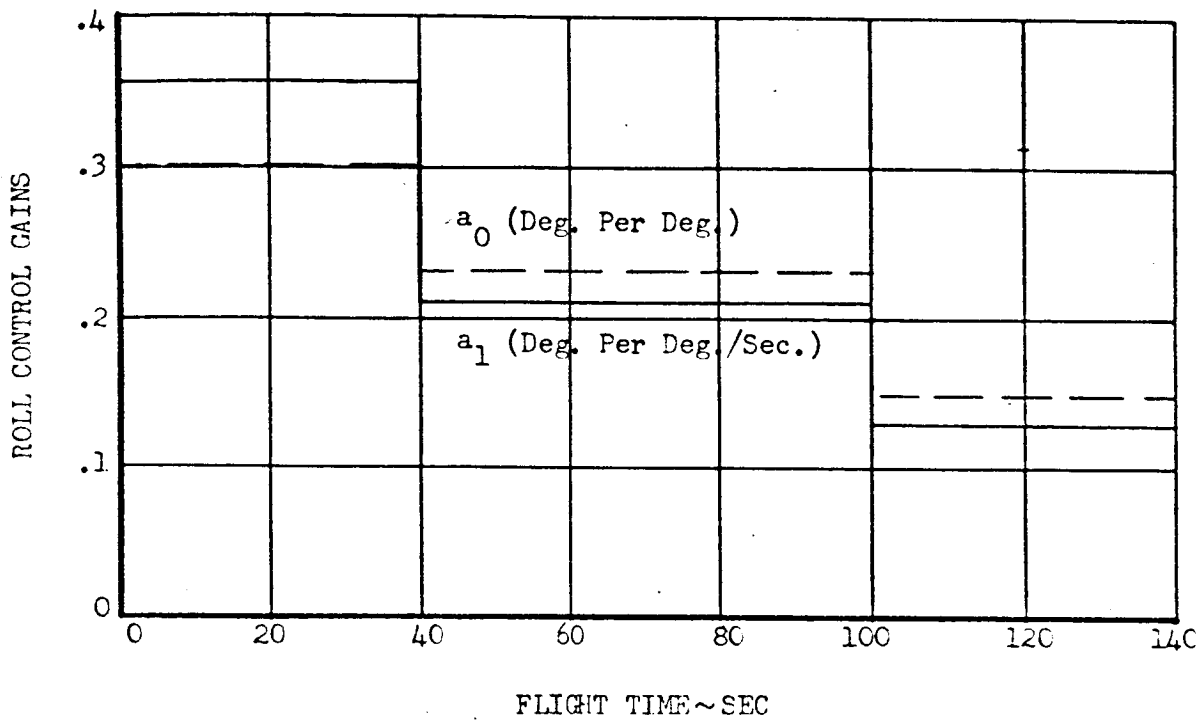
FIGURE 33

SA-204/LM-1 STRUCTURAL LIMITS FOR A 1.25 SAFETY FACTOR

H4-431-026184
JAN 66

ALTITUDE ~ KM

WIND SPEED ~ M/SEC
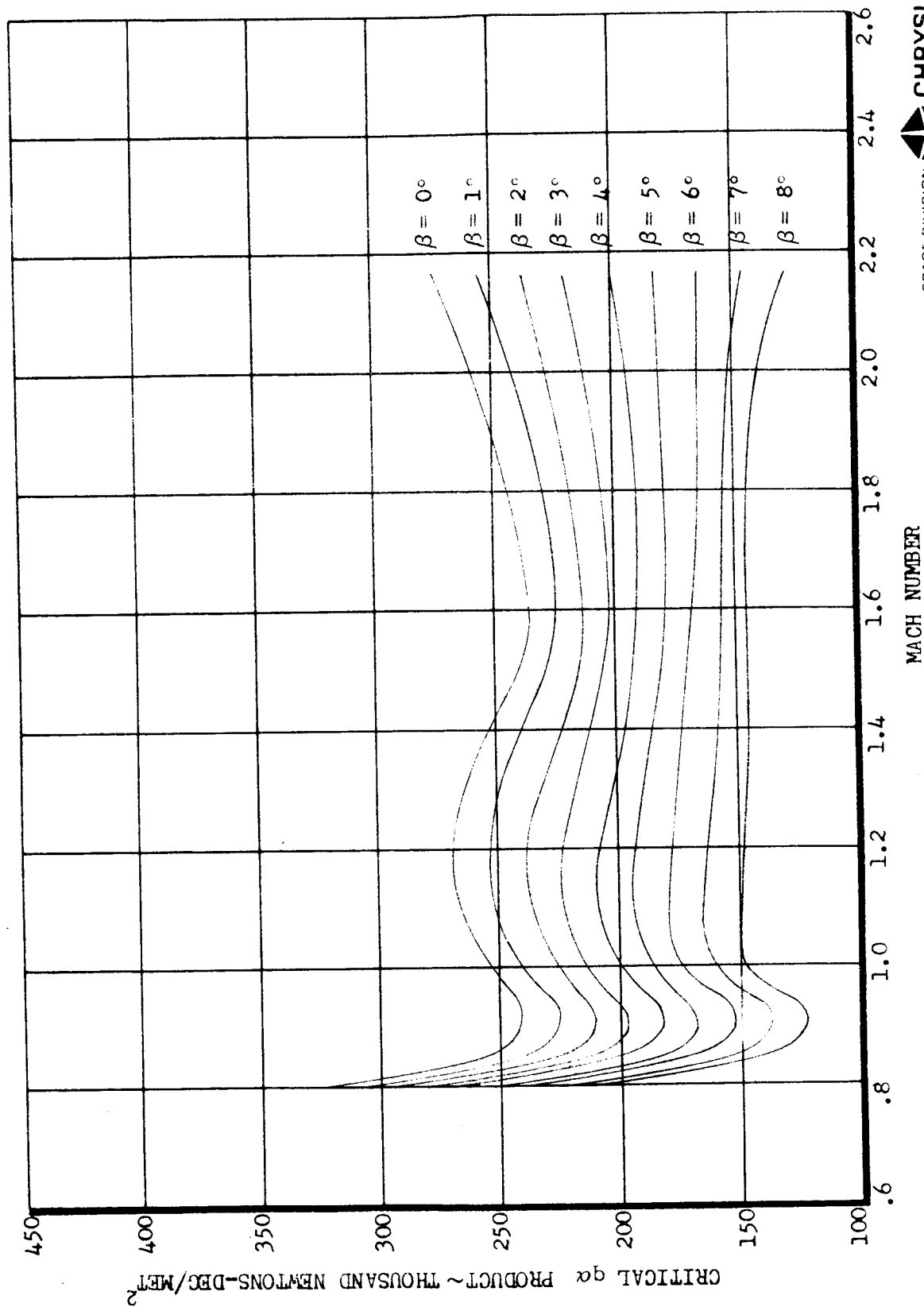
FIGURE 35

MSFC SCALAR DESIGN WINDS

95% QSS ENVELOPE

99% SHEARS AND GUSTS
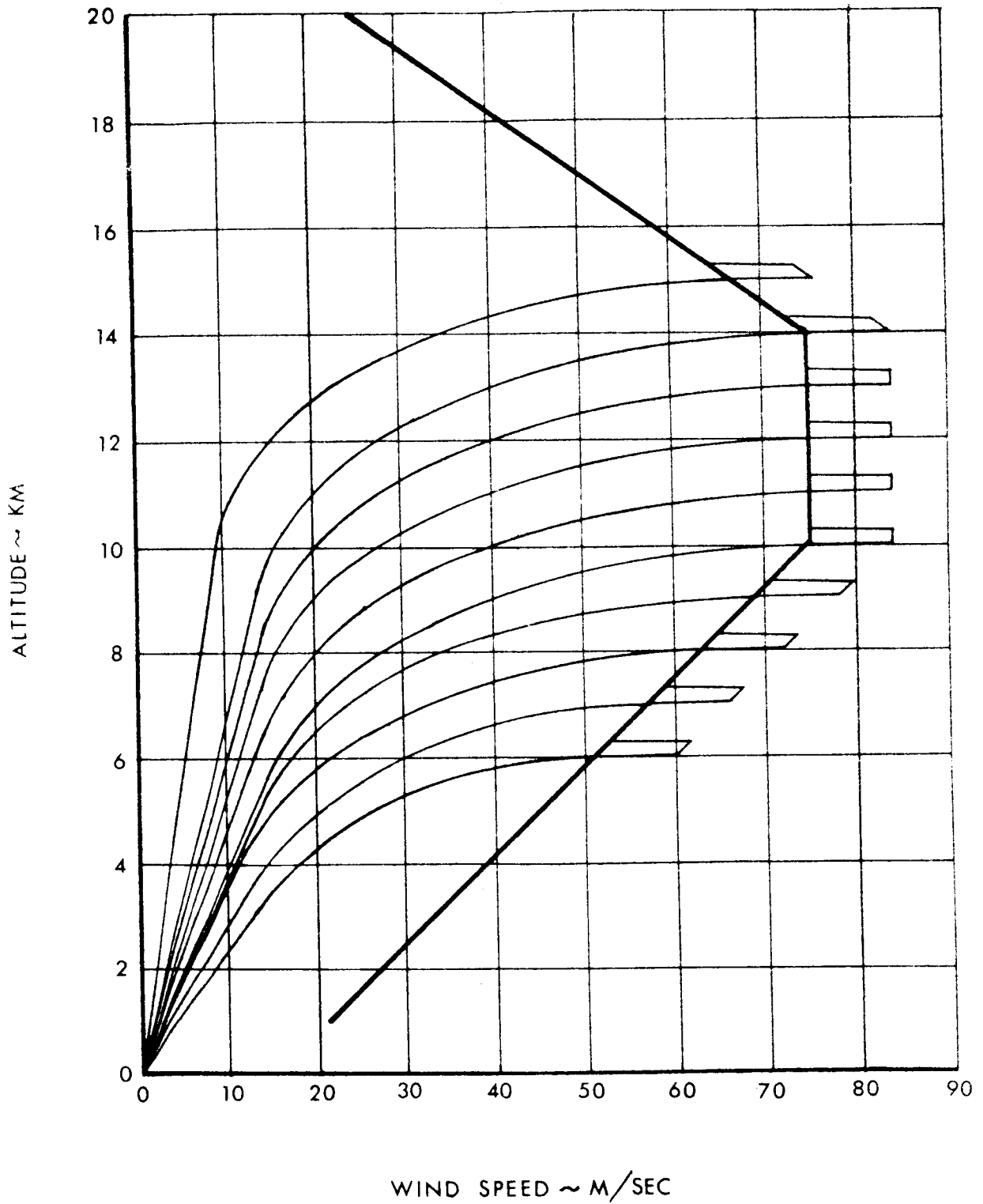
WIND SPEED ~ M/SEC

FIGURE 36

SA-204/LM-1 CRITICAL αq RATIO RESPONSE TO

THE MOST RESTRICTIVE 95% QSS TAILWIND
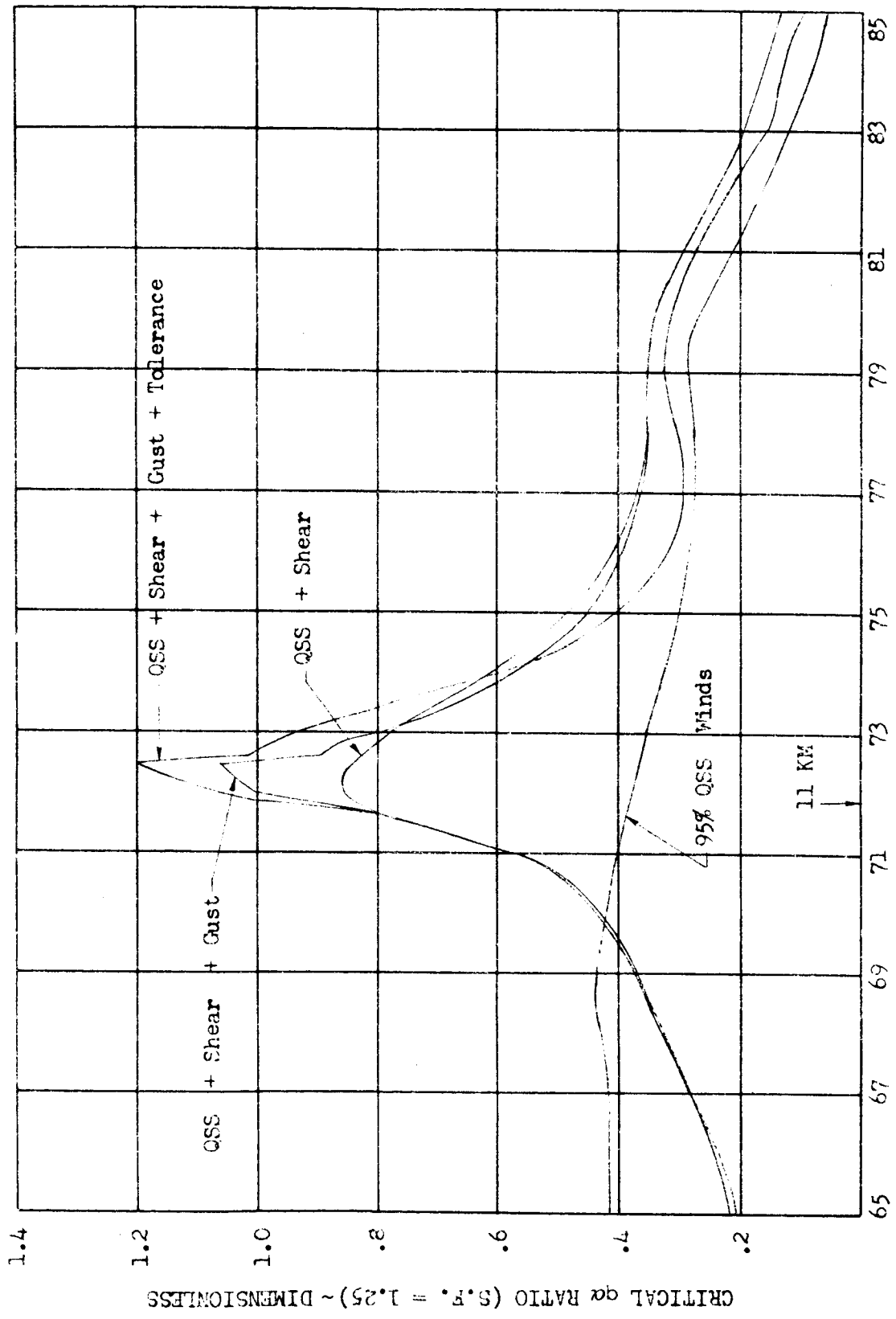
FIGURE 32

SA-204/LM-1 CRITICAL qα RATIO (S.F. = 1.25) VS SEC WIND SPEED

FOR EACH WIND DIRECTION AT THE WORST GUST ALTITUDE (11 KM.)

CHRYSLER
CORPORATION

SPACE DIVISION

-62-
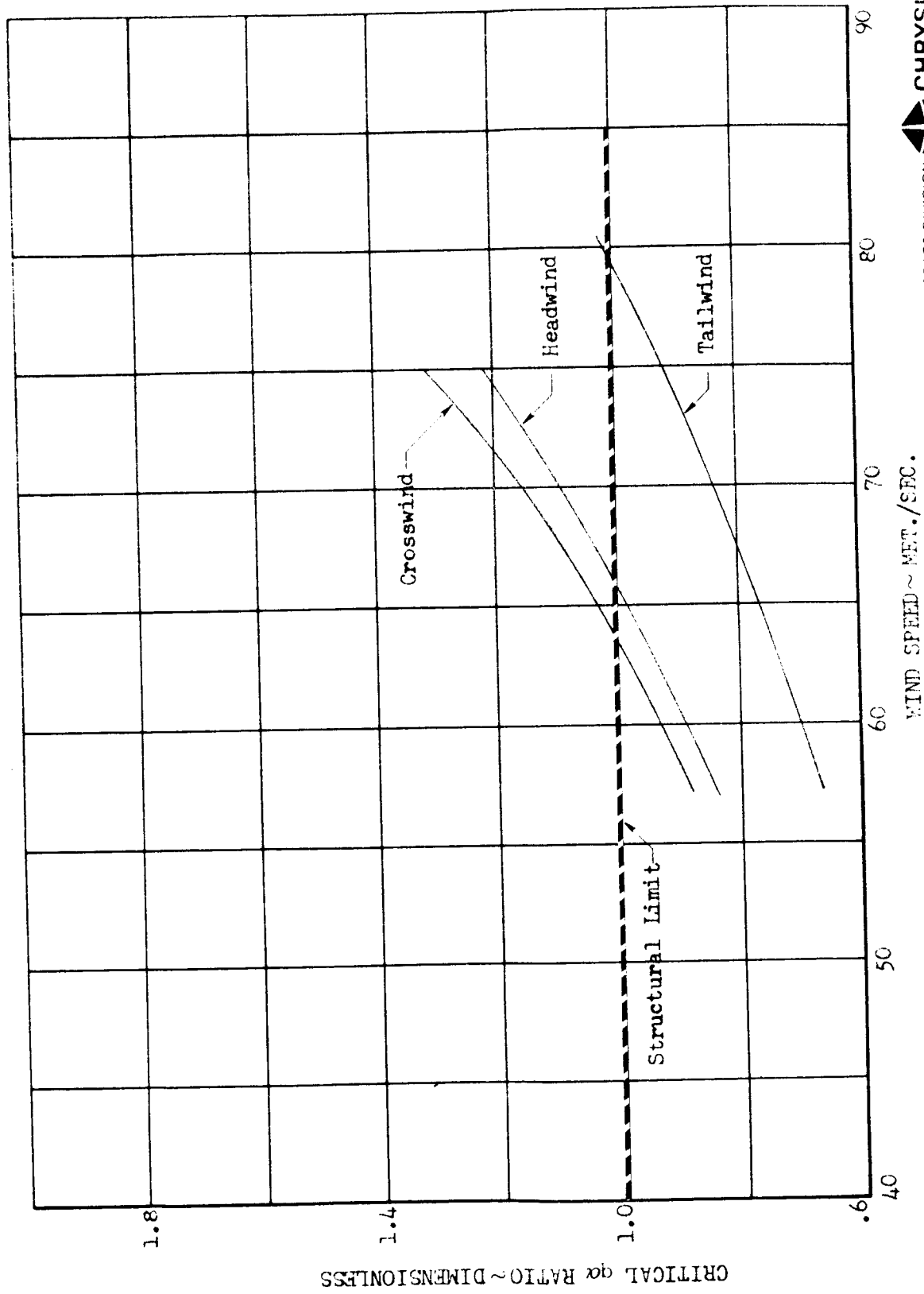
FIGURE 38

SA-204/LM-1 BOOST FLIGHT WIND SPEED LIMITS I

TAILWIND

HEADWIND

Jan.
Feb.
Mar.

Envelope of 95
Percentile Winds

Wind Speed Limit Based
Upon Structural Integrity

WIND SPEED ~ M/SEC

ALTITUDE ~ KILOMETERS

16   14   12   10   8   6   4

100   80   60   40   20   0   20   40   60   80   100
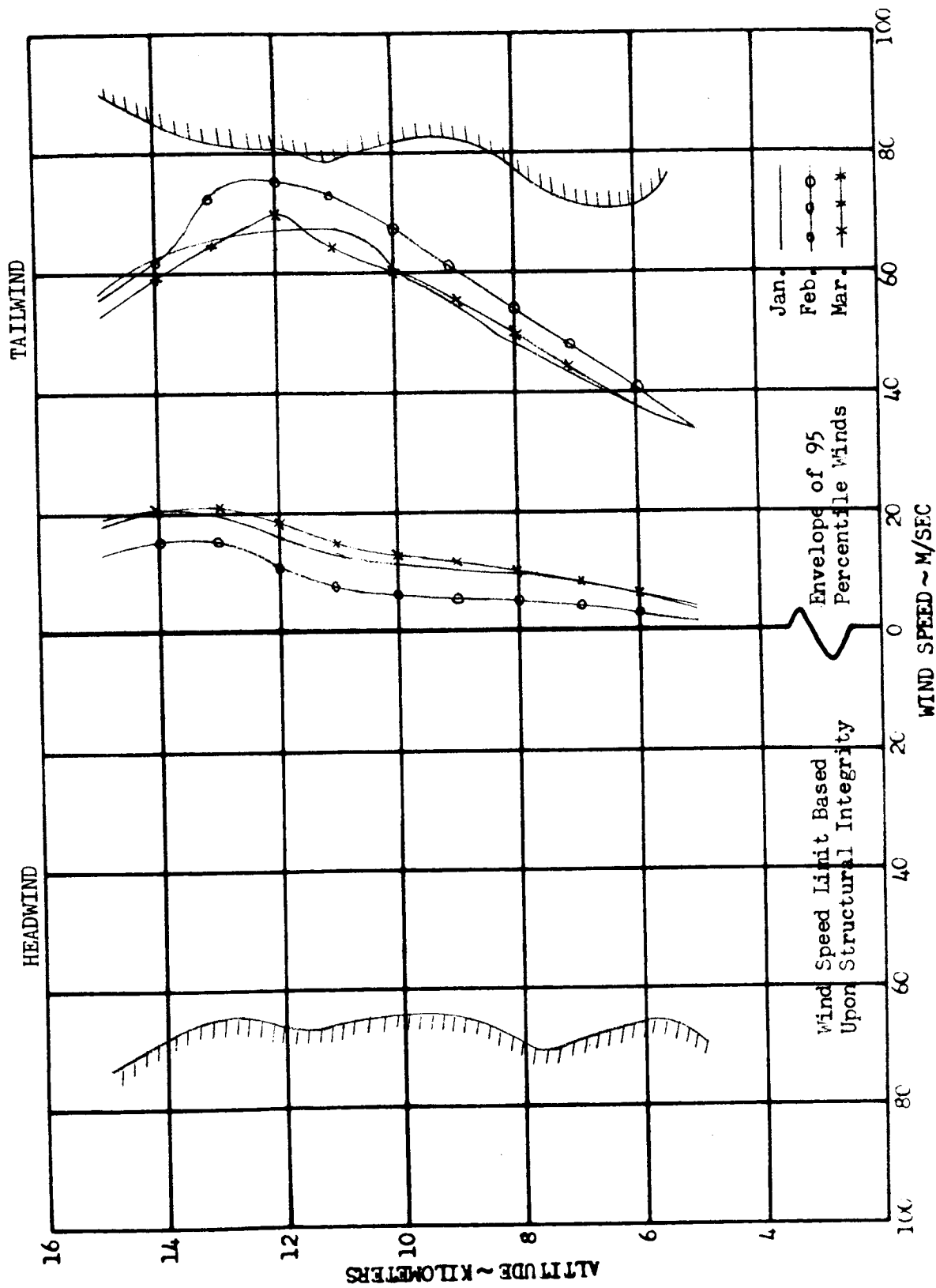
FIGURE 39

SA-204/LM-1 BOOST FLIGHT WIND SPEED LIMITS II

-64-
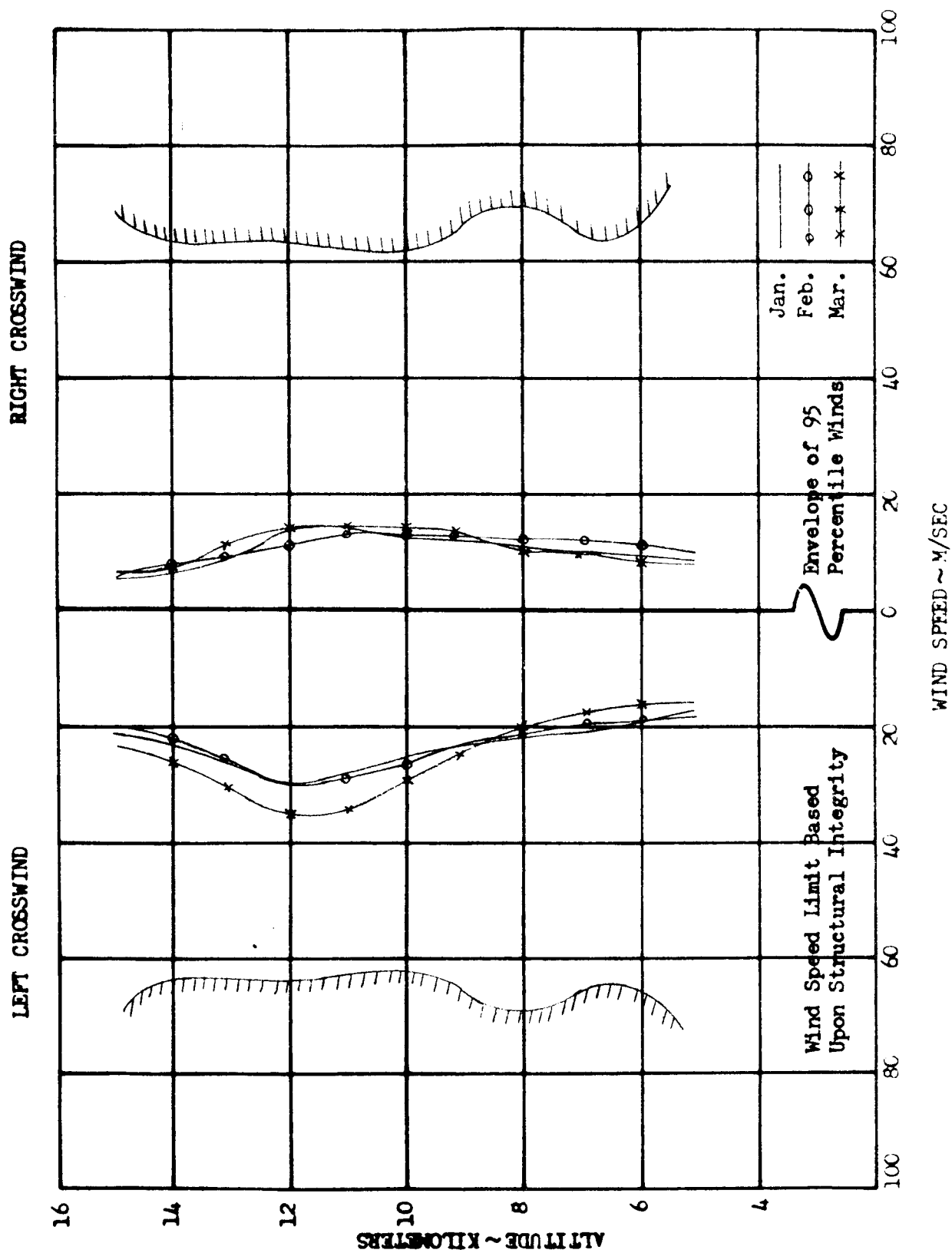
FIGURE 40

SA-204/LM-1 BOOST FLIGHT WIND SPEED LIMIT AT MOST

RESTRICTIVE ALTITUDE (11 KM.)
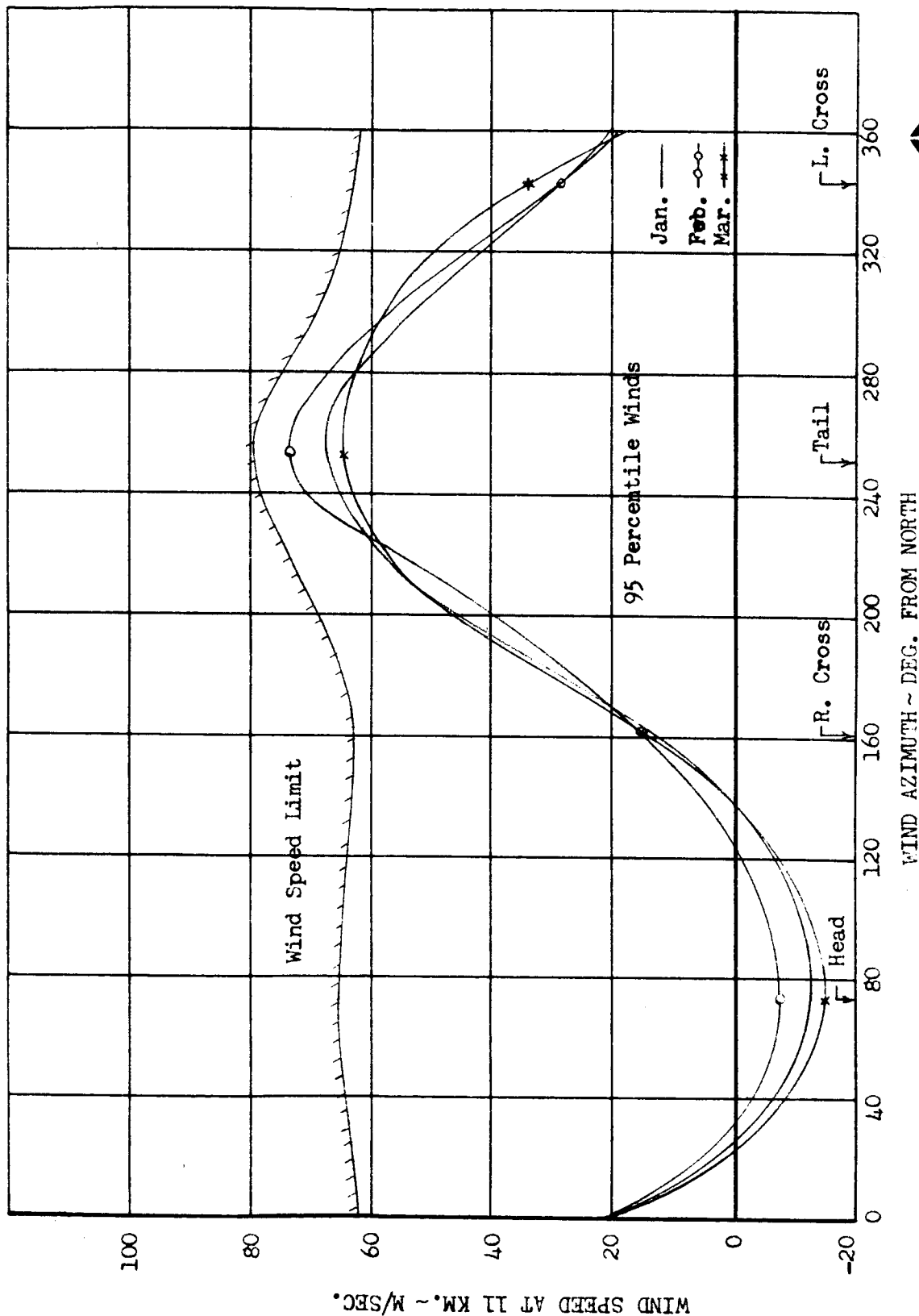
FIGURE 41

SA-204/LM-1 PITCH ATTITUDE COMMAND TIME HISTORIES FOR A
SPECTRUM OF ENGINE FAILURE TIMES AND THE AS-204 ENGINE
OUT STEERING COMPENSATION

Nominal

Engine Failure at   0 Sec
                    45 Sec
                    55 Sec

PITCH ATTITUDE COMMAND ~ DEG

FLIGHT TIME ~ SEC

CHRYSLER
CORPORATION

SPACE DIVISION
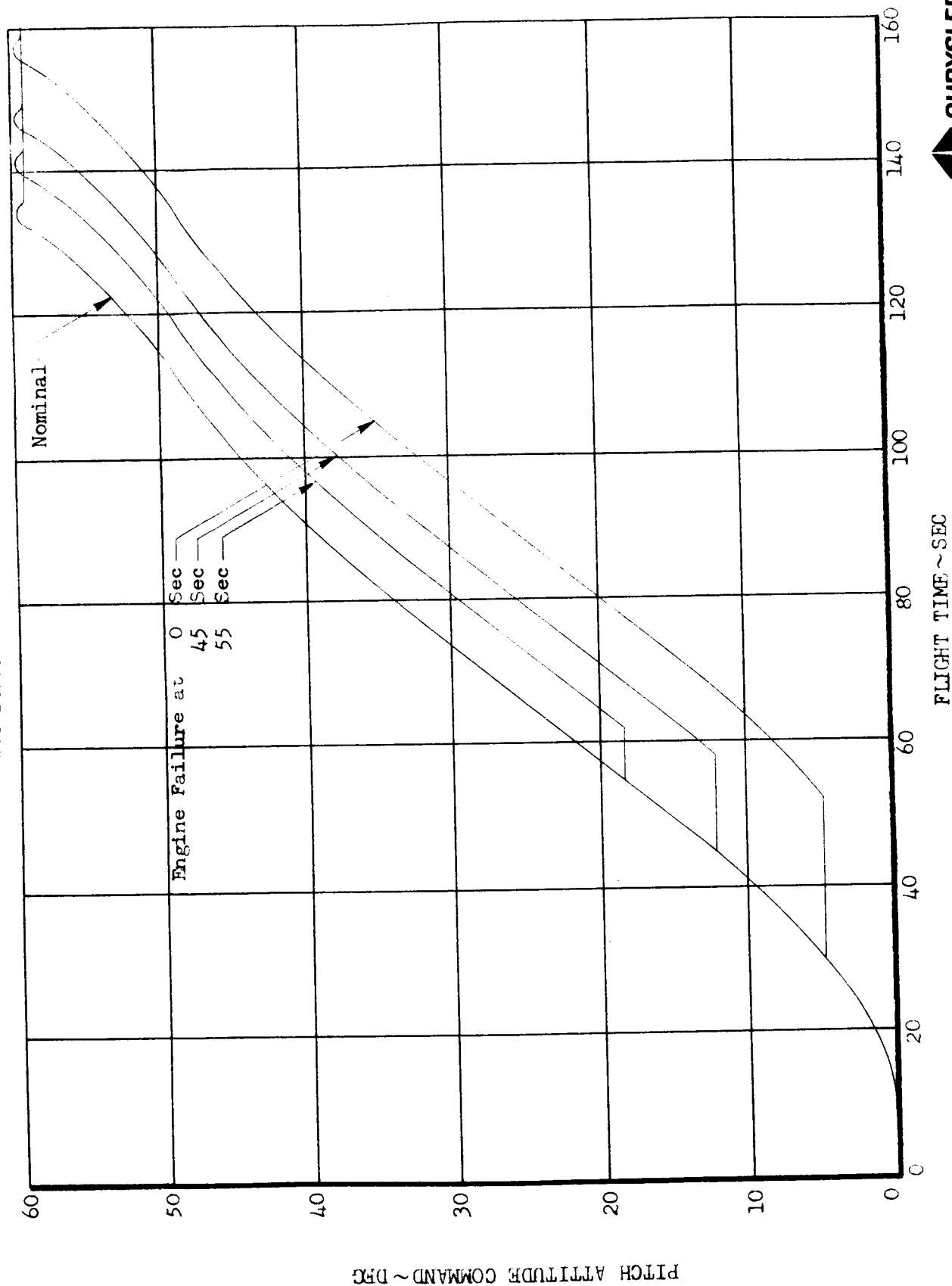
FIGURE 42

AS-204 ENGINE OUT STEERING COMPENSATION

CHI FREEZE INHIBIT INTERVAL

FLIGHT TIME OF ENGINE FAILURE ~ SEC

CHI FREEZE TIME INTERVAL ~ SECONDS

CHRYSLER
CORPORATION
SPACE DIVISION
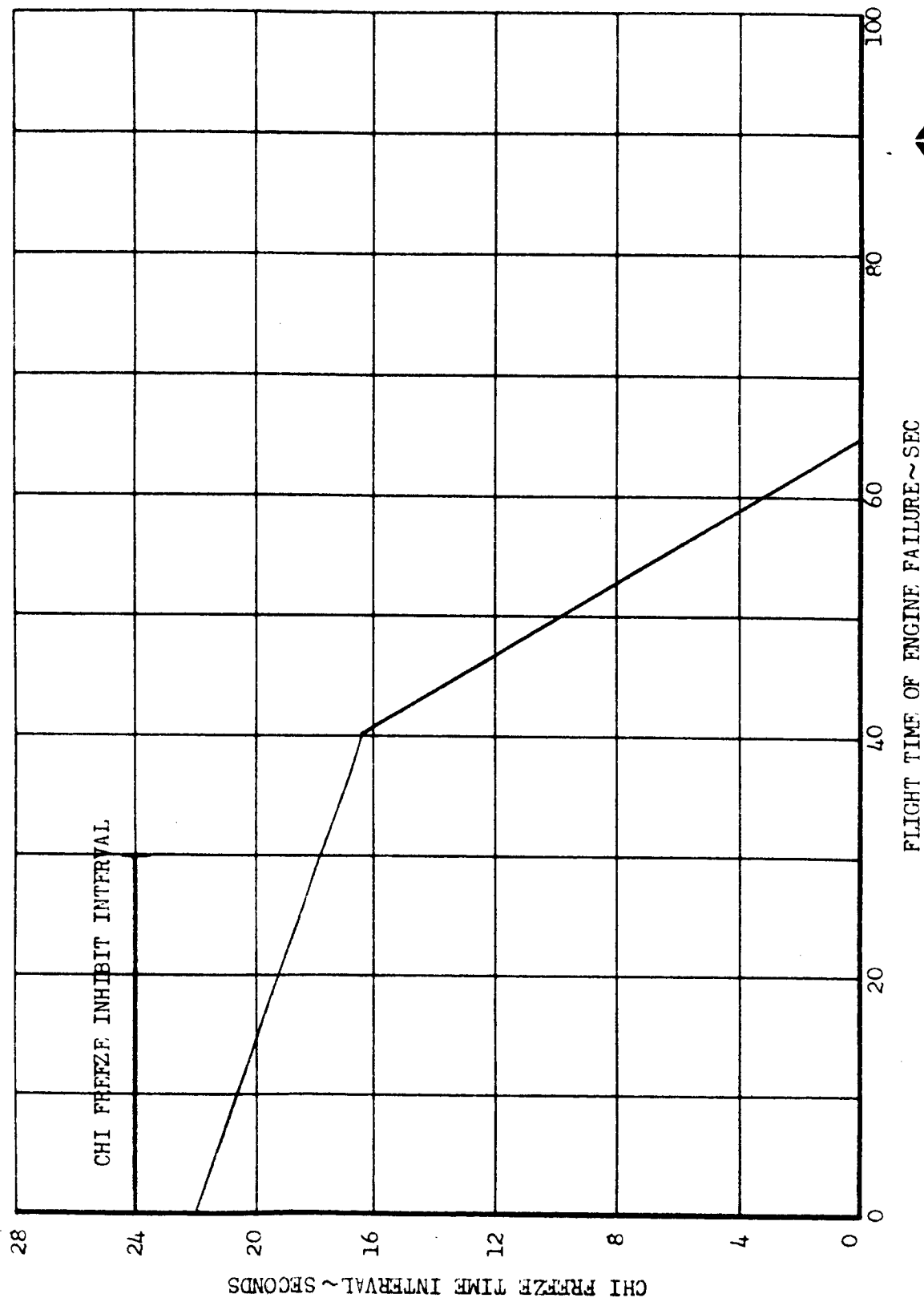
FIGURE 43

SA-204/IM-1 TYPICAL THRUST TIME HISTORIES

FOR A SPECTRUM OF OUTBOARD ENGINE FAILURES

Nominal

Outboard Engine Failure
at

0 Seconds ———
75 Seconds ———
Nominal ———

THRUST ~ THOUSAND NEWTONS

FLIGHT TIME ~ SEC

CHRYSLER
CORPORATION

SPACE DIVISION

84-431-62618A
JAN 66

-68-
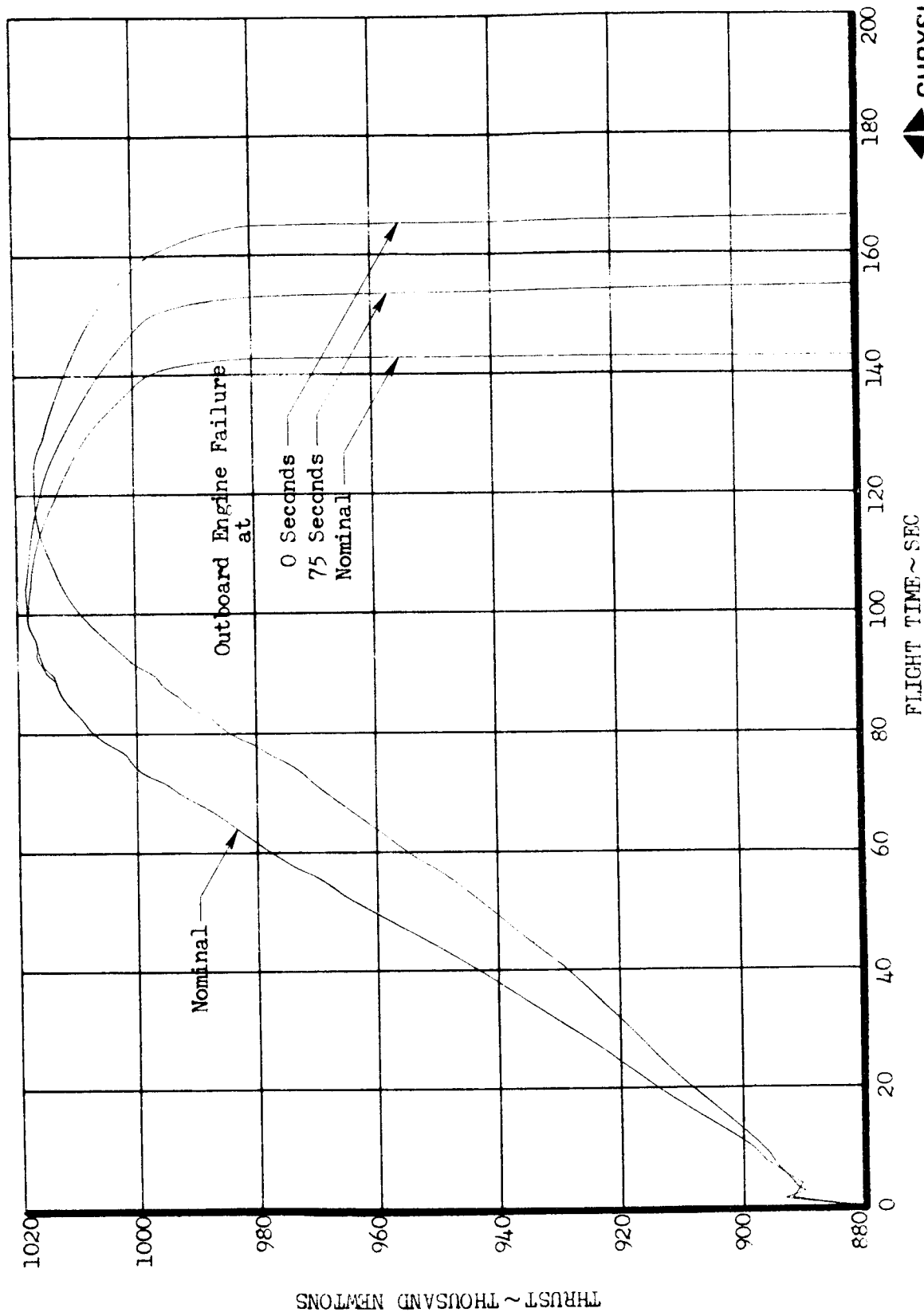
FIGURE 44

SA-204/LM-1 MASS LOSS TIME HISTORIES FOR A SPECTRUM OF

OUTBOARD ENGINE FAILURE TIMES
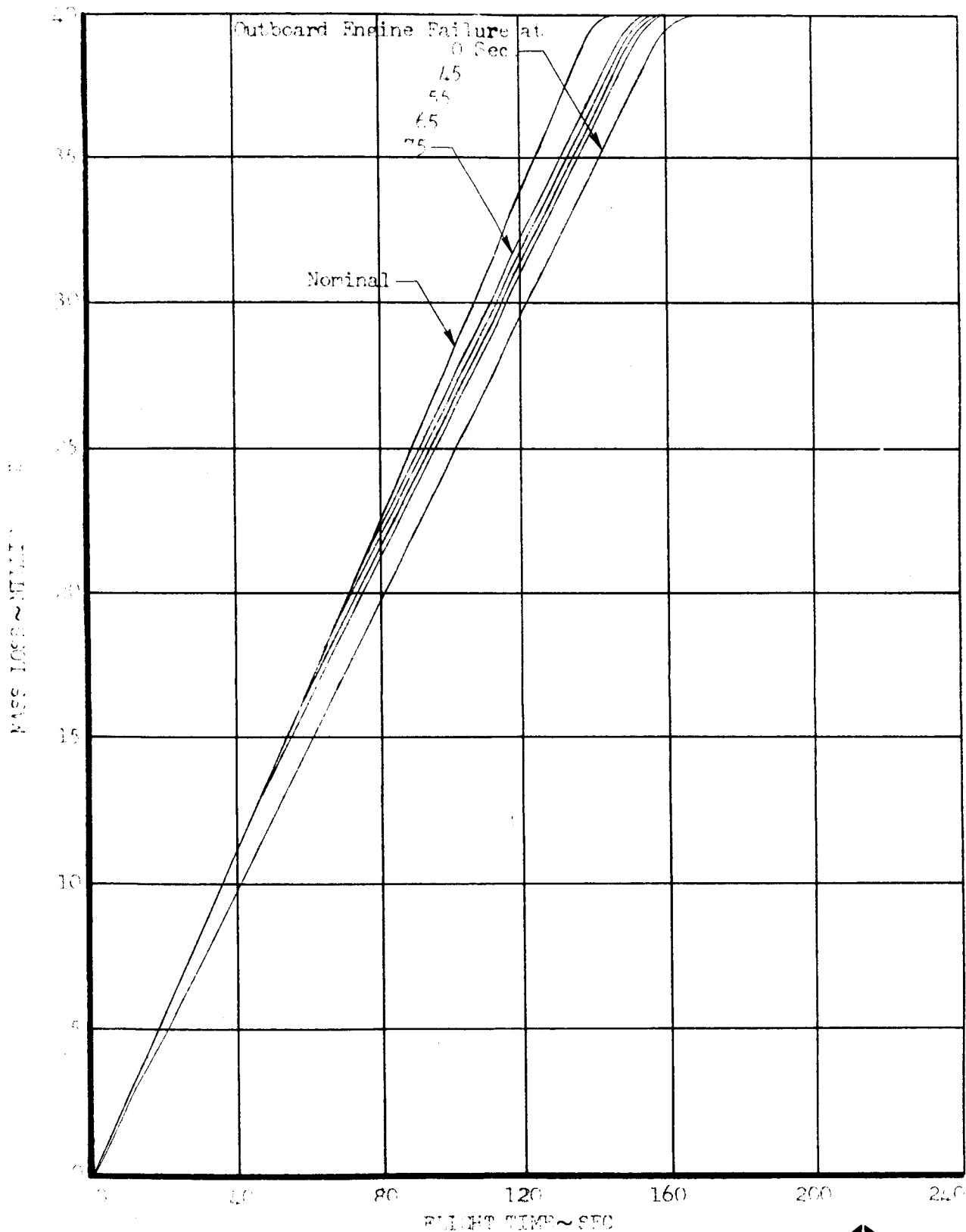
SPACE DIVISION CHRYSLER CORPORATION

FIGURE 45

SA-204/LM-1 PITCH AND YAW CHANNELS

S-IVB STAGE
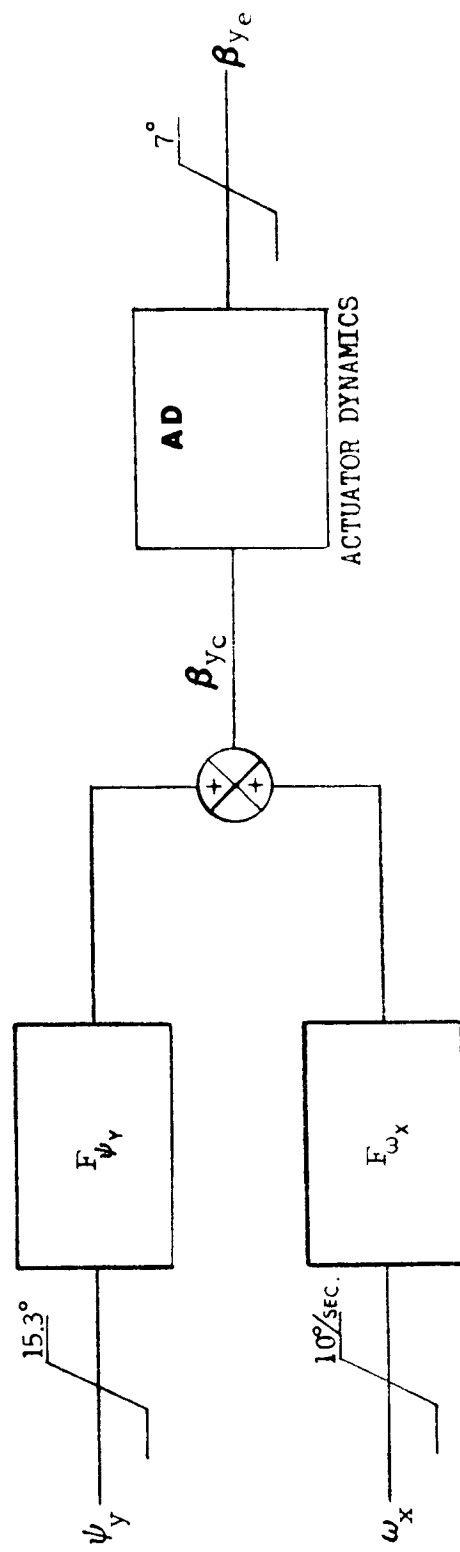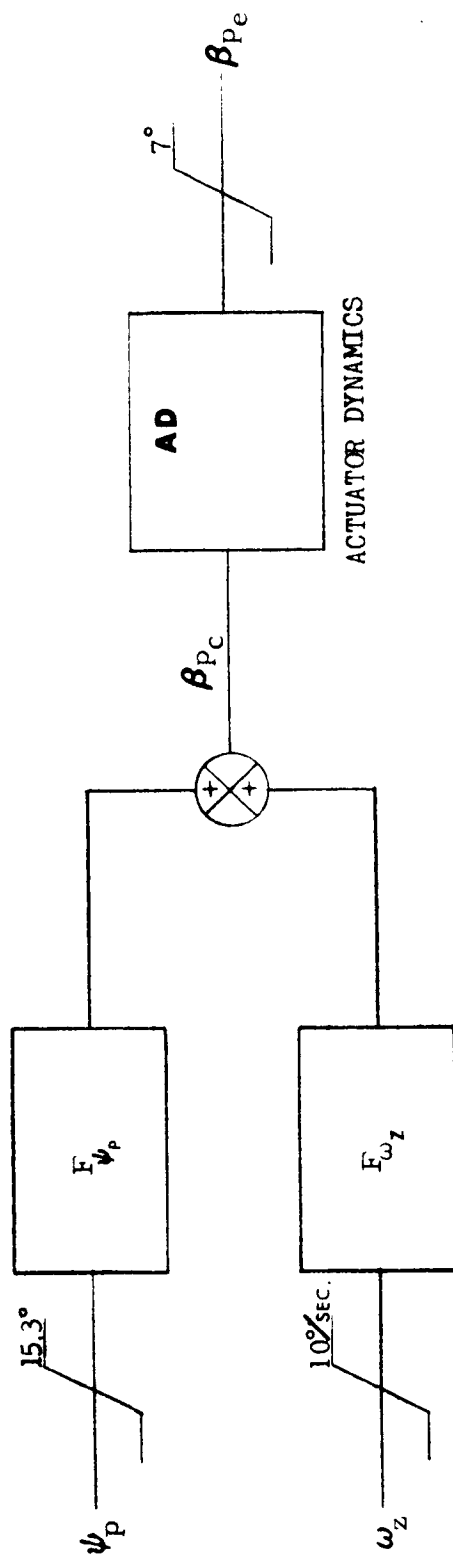
FIGURE 46

SA-204/LM-1 PITCH AND YAW CONTROL SYSTEM GAINS

S-IVB STAGE
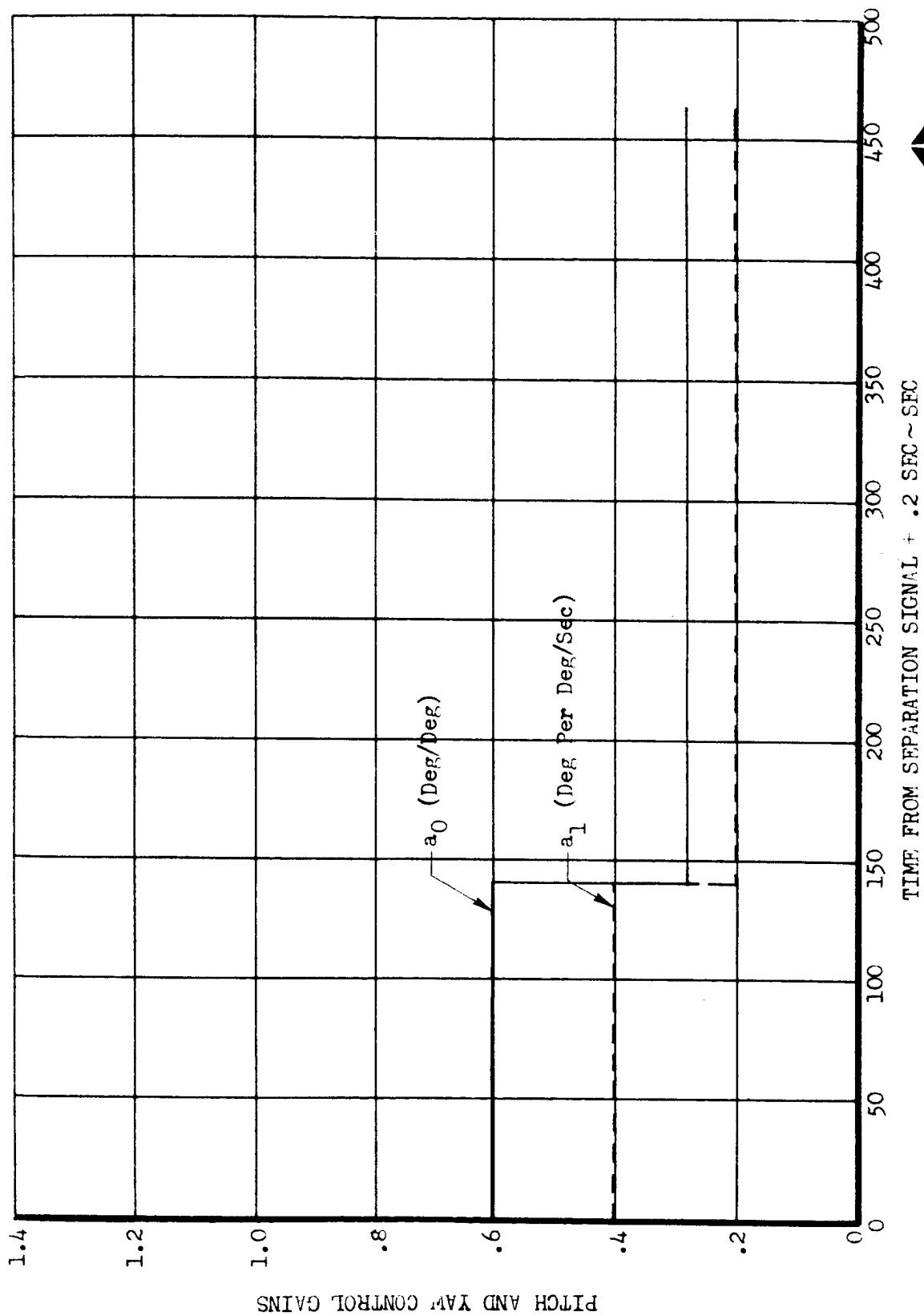
FIGURE 47

EXTREME VALUES OF MONTHLY 95 PERCENTILE WIND ENVELOPES

75° FLIGHT AZIMUTH
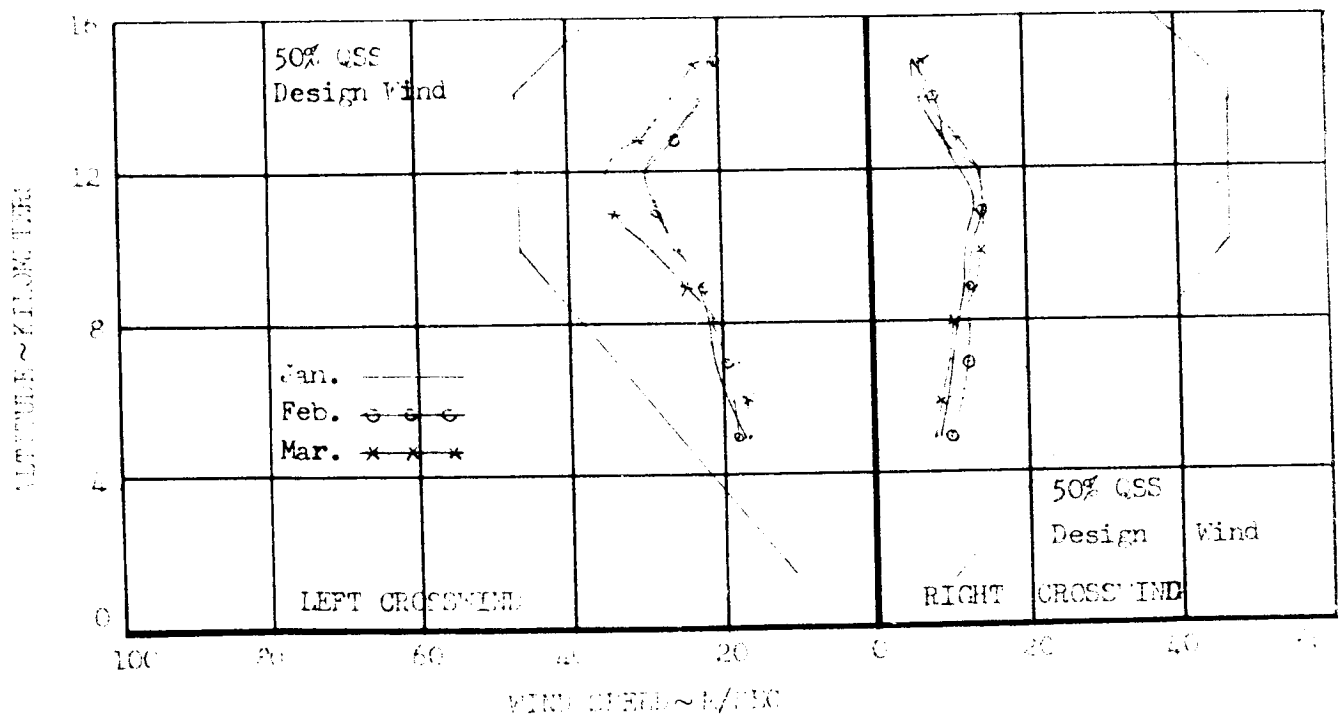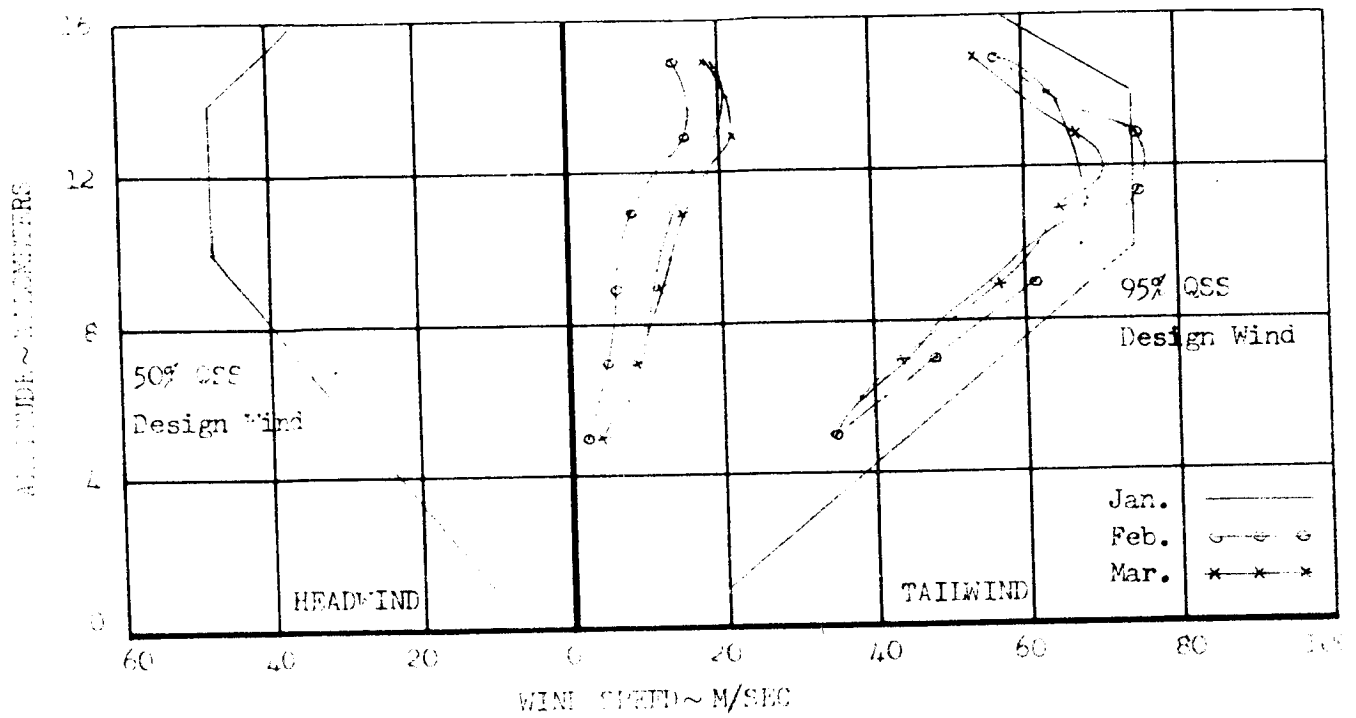
FIGURE 48

SA-204/LM-1 ENVELOPES OF PEAK CONTROL GIMBAL DEFLECTION

NO ENGINE FAILURE

FLIGHT TIME OF PEAK RESPONSE TO GUST ~ SEC

MAXIMUM CONTROL GIMBAL DEFLECTION ~ DEG.

Left Crosswind (50% QSS)

Right Crosswind (50% QSS)

SPACE DIVISION CHRYSLER CORPORATION
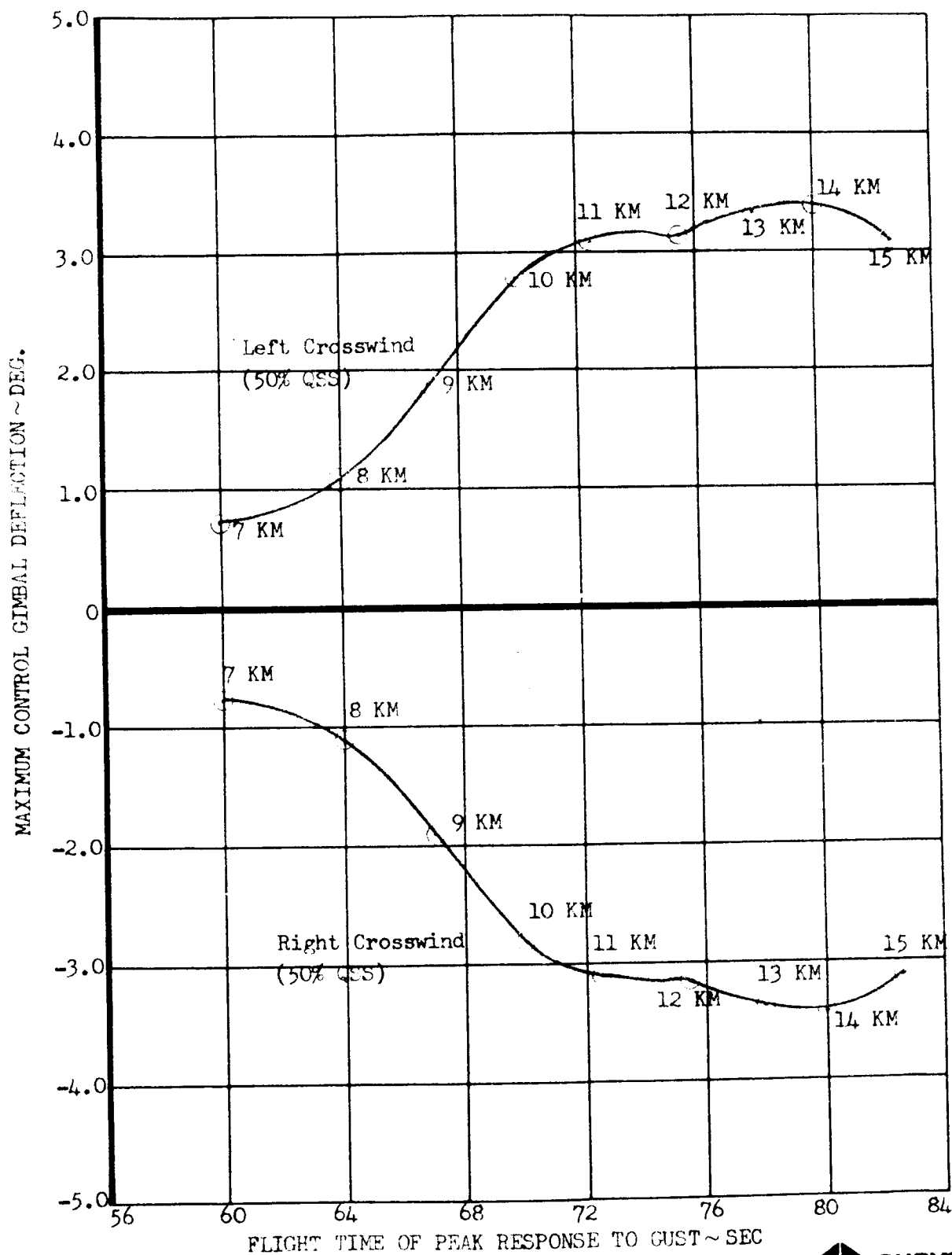
FIGURE 50

SA-204/LM-1 ENVELOPES OF PEAK BENDING MOMENT
CRITICAL RATIOS (S.F. = 1.25)
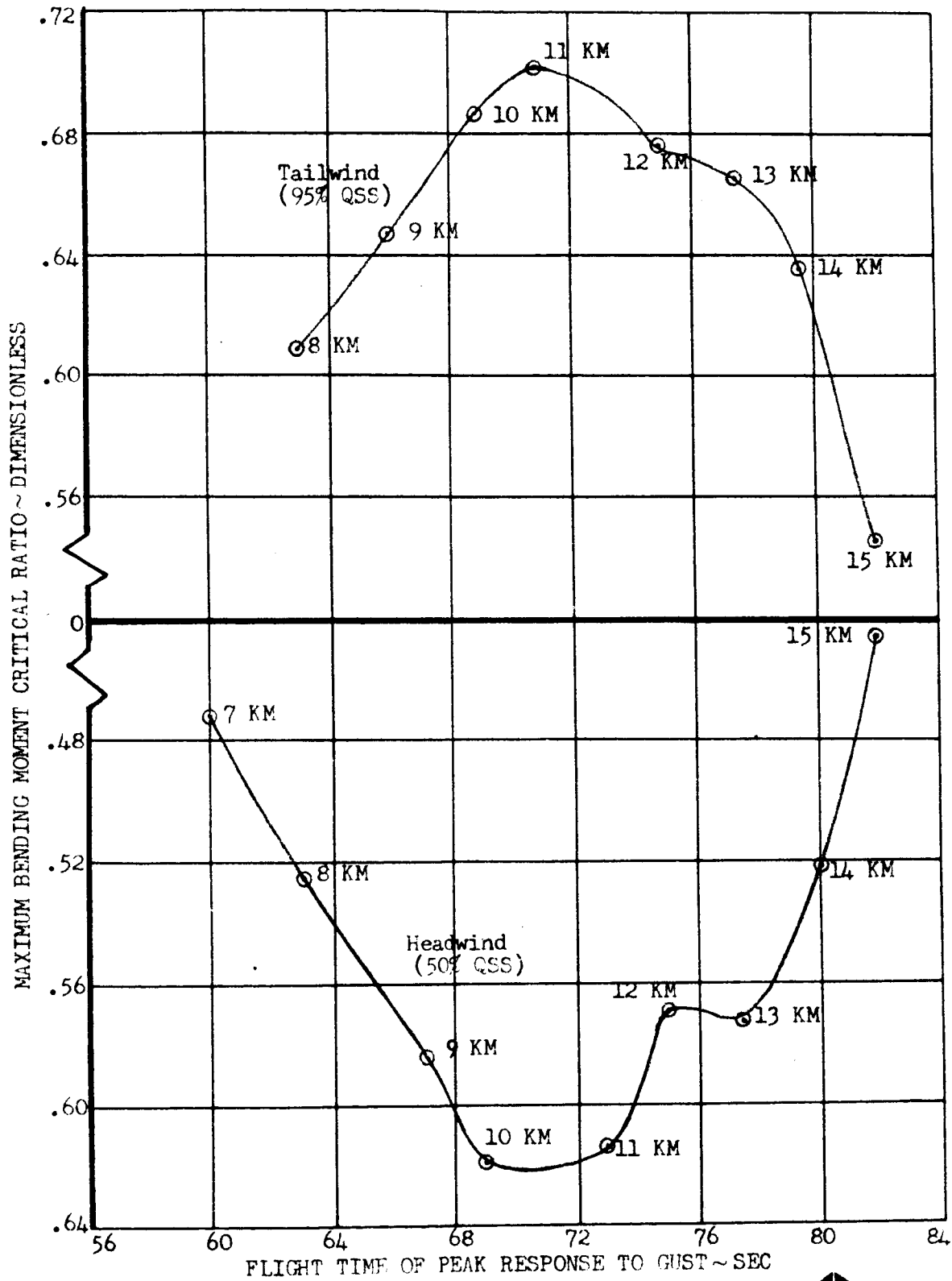
NO ENGINE FAILURE

FIGURE 51

SA-204/LM-1 ENVELOPES OF PEAK BENDING MOMENT CRITICAL RATIOS
(S.F. = 1.25)
NO ENGINE FAILURE

FLIGHT TIME OF PEAK RESPONSE TO GUST ~ SEC.

SPACE DIVISION CHRYSLER CORPORATION
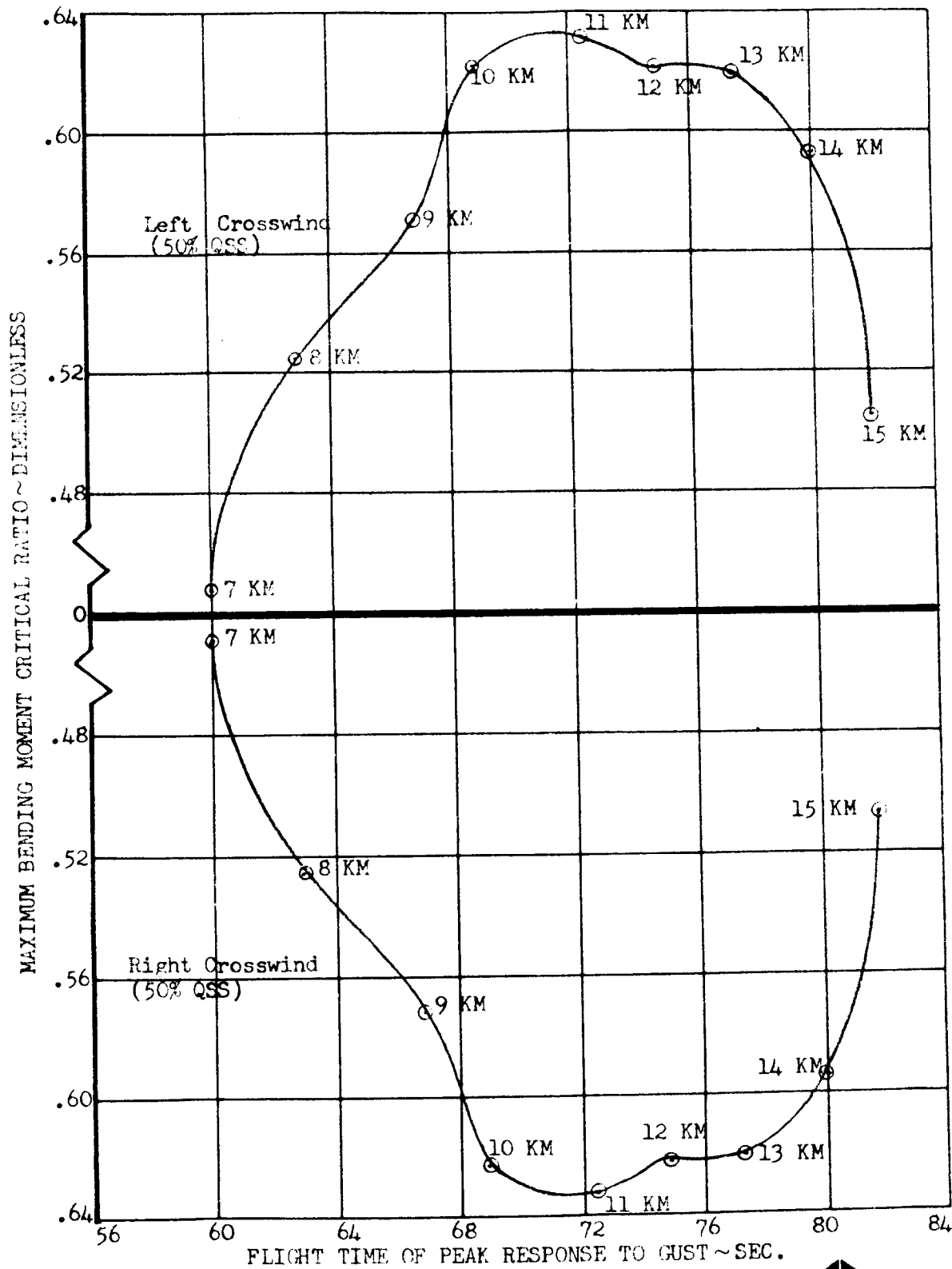
FIGURE 52

SA-204/LM-1 ENVELOPES OF MAXIMUM CONTROL GIMBAL DEFLECTIONS

FOR ENGINE NO. 3 FAILURES DURING BOOST WITH NO WINDS

-77-
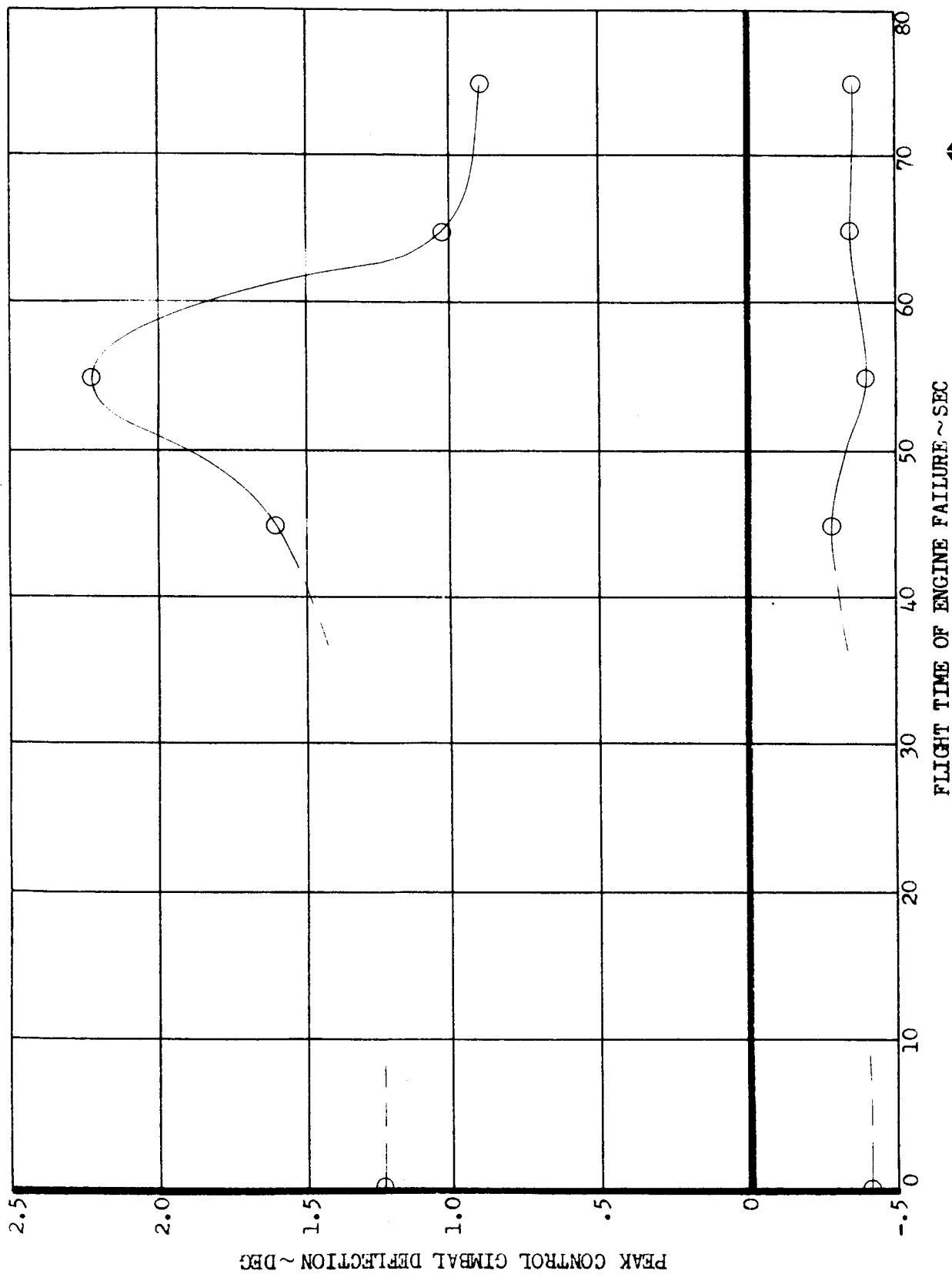
FIGURE 53

SA-204/LM-1 ENVELOPES OF MAXIMUM CONTROL GIMBAL DEFLECTIONS
FOR ENGINE NO. 4 FAILURES DURING BOOST WITH NO WINDS

84 431 62618C
JAN 66

-78-
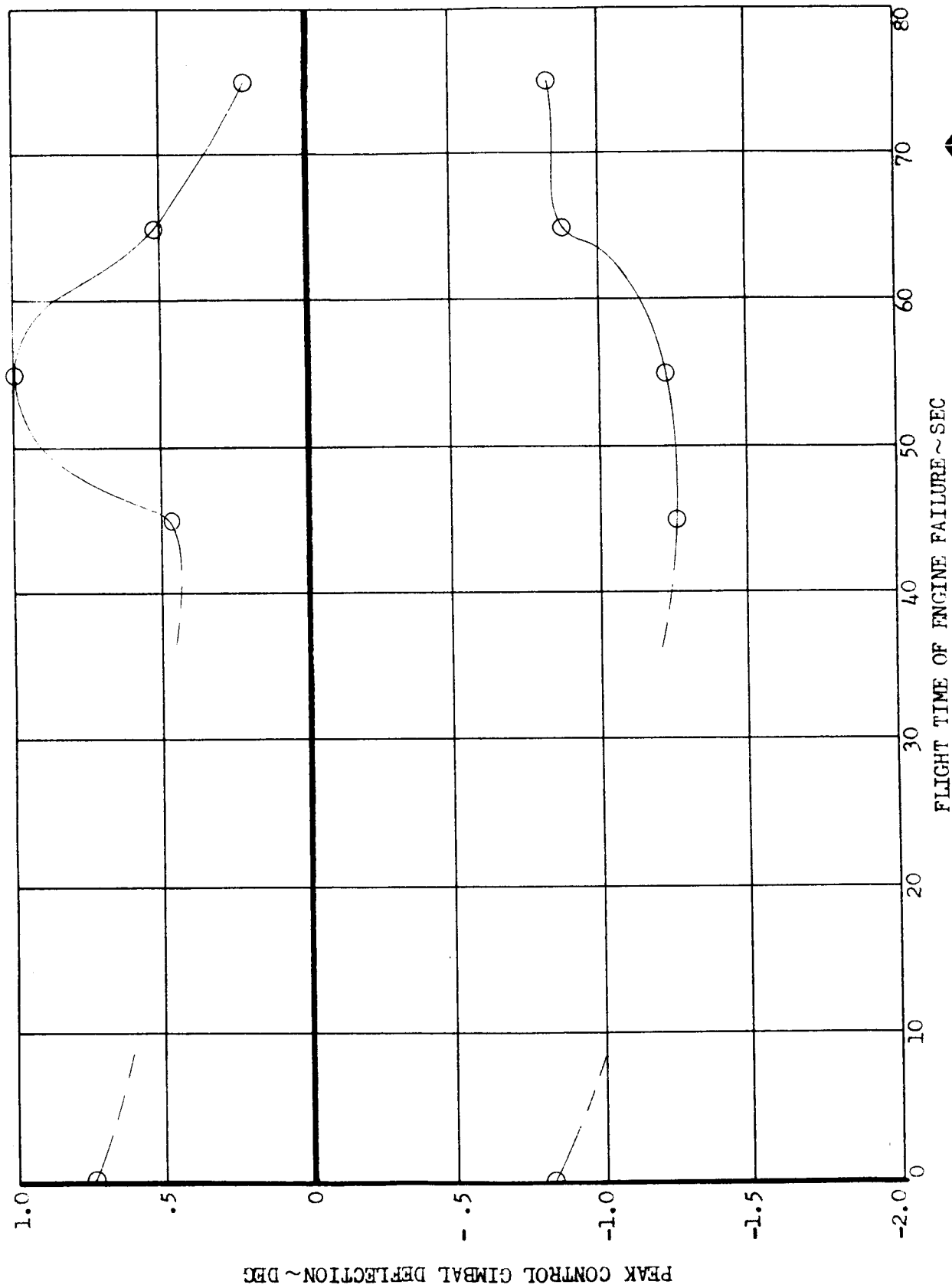
FIGURE 54

SA-204/LM-1 ENVELOPES OF MAXIMUM BENDING MOMENT CRITICAL RATIOS (S.F. = 1.25)

FOR ENGINE NO. 3 FAILURES AND ENGINE NO. 4 FAILURES DURING BOOST WITH NO WINDS

84 431 6 2618C
JAN 66
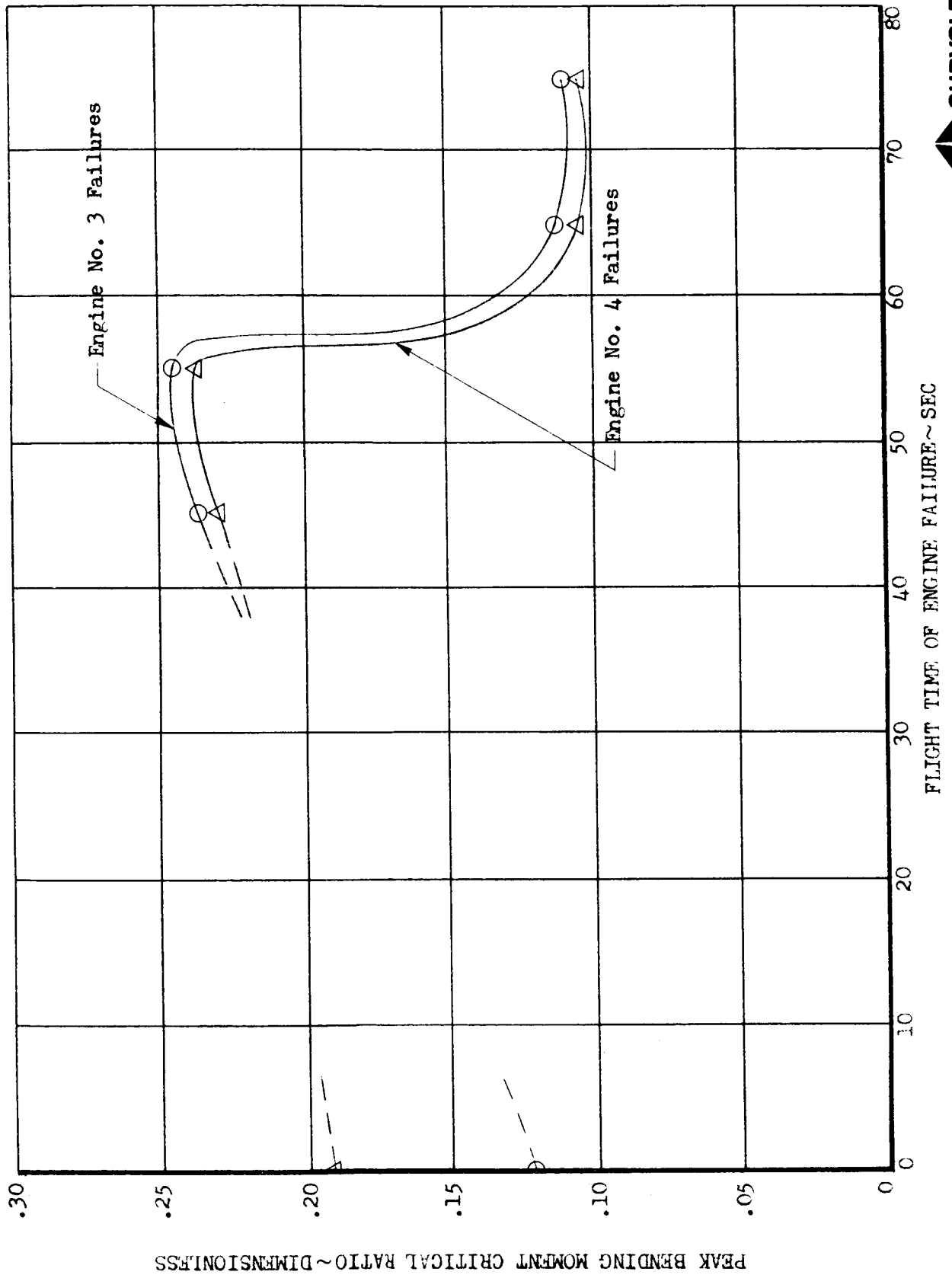
FIGURE 55

SA-204/LM-1 STAGING AERODYNAMIC MOMENT ON S-IVB STAGE
FOR ENGINE NO. 3 FAILURES AND ENGINE NO. 4 FAILURES DURING BOOST WITH NO WINDS

Engine No. 4 Failures

Engine No. 3 Failures

Nominal

FLIGHT TIME OF ENGINE FAILURE ~ SEC

SEPARATION TOTAL S-IVB AERODYNAMIC MOMENT
~ THOUSAND NEWTON-MET

CHRYSLER CORPORATION

SPACE DIVISION

84 431 62618C
JAN 66
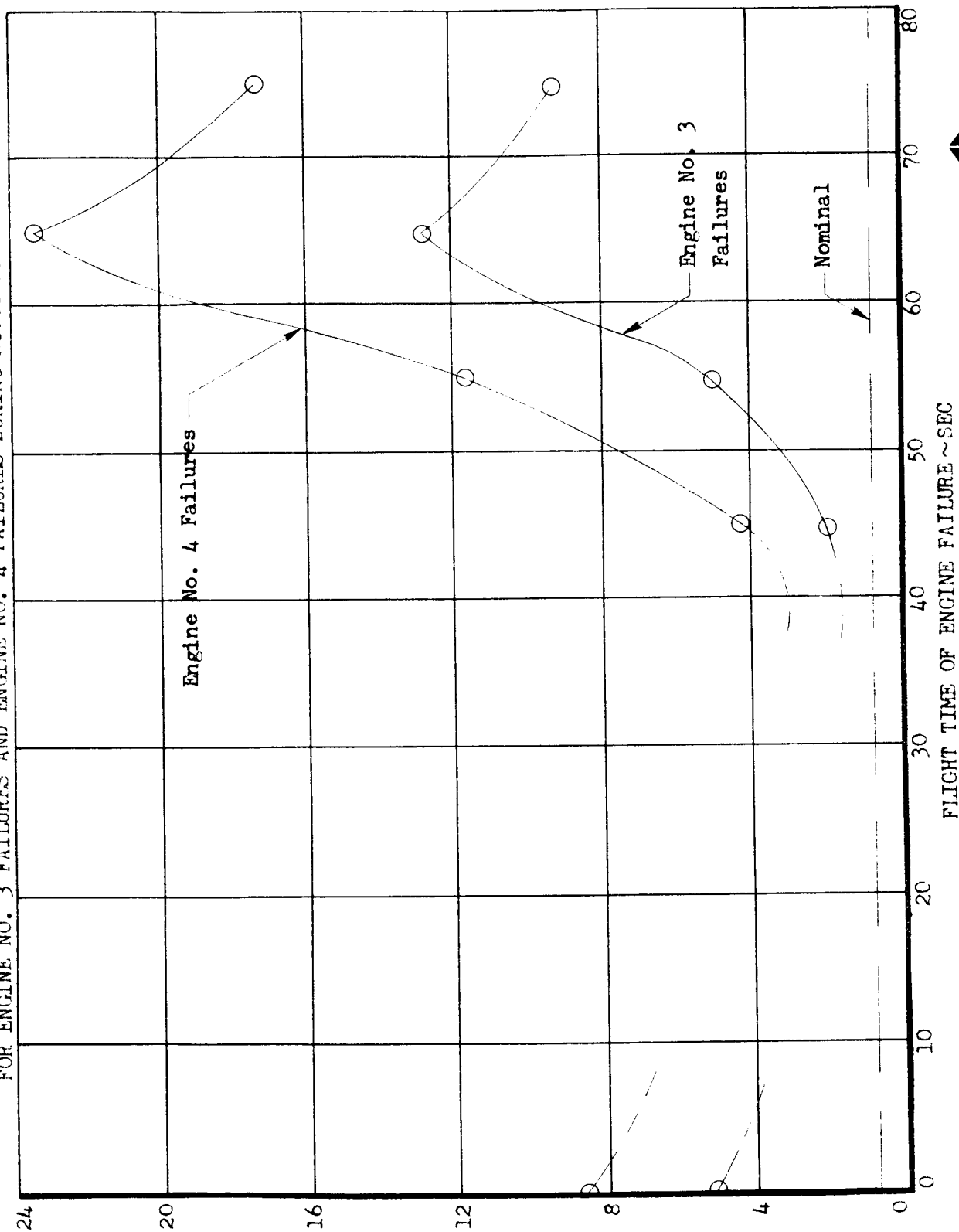
FIGURE 56

SA-204/LM-1 STAGING DYNAMIC PRESSURE TIMES TOTAL ANGLE OF ATTACK
FOR ENGINE NO. 3 FAILURES AND ENGINE NO. 4 FAILURES DURING BOOST WITH NO WINDS

SEPARATION DYNAMIC PRESSURE TIMES TOTAL ANGLE OF ATTACK
~DEG-NEWTONS/MET^2

FLIGHT TIME OF ENGINE FAILURE ~ SEC
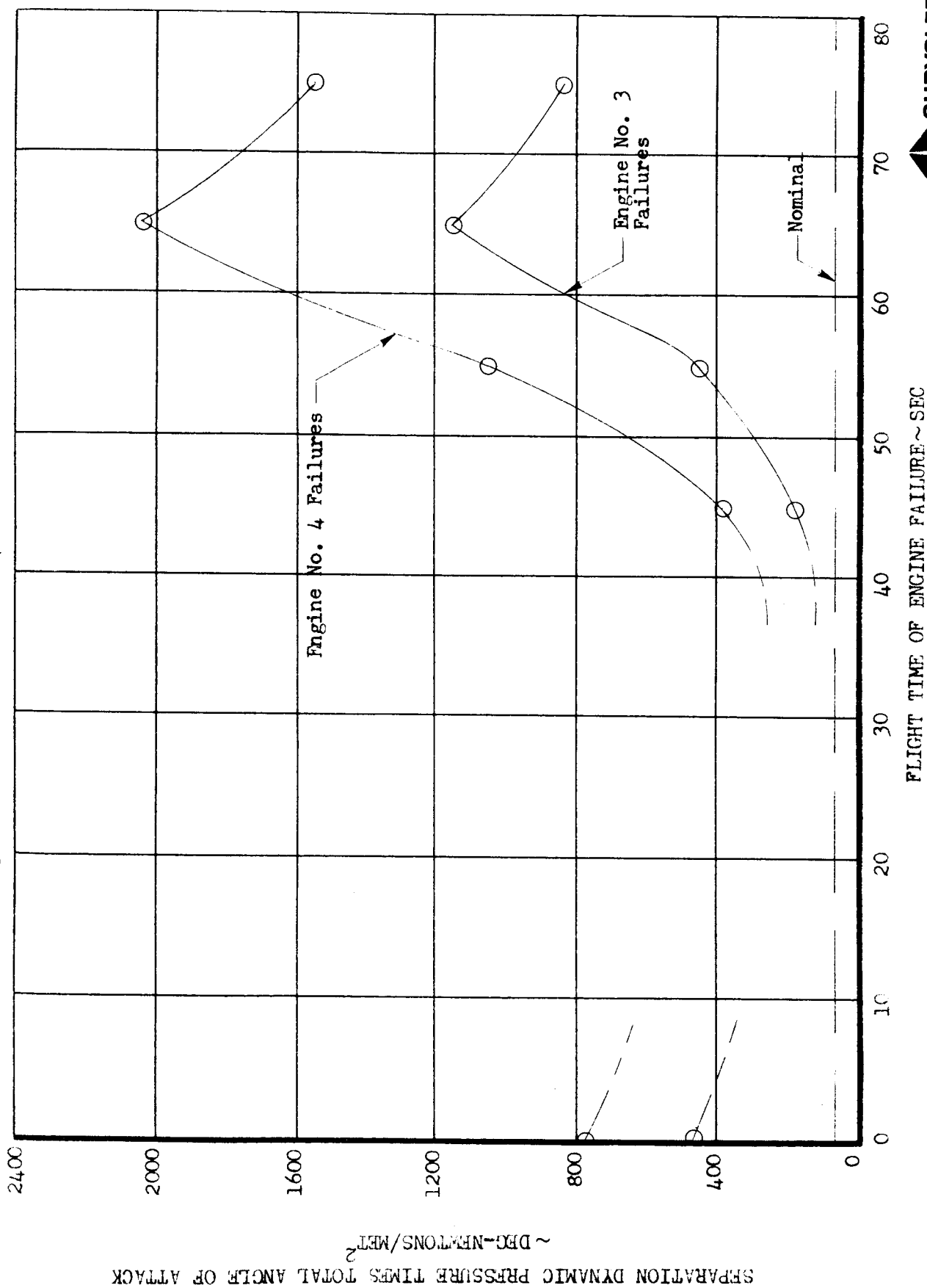
FIGURE 17

SA-204/LM-1 ENVELOPES OF POST SEPARATION S-IVB MAXIMUM MAGNITUDE OF ATTITUDE ERROR

FOR WORST CASE ENGINE FAILURES DURING BOOST WITH NO WINDS

FIGURE 33

SA-204/LM-1 ENVELOPES OF POST SEPARATION S-IVB MAXIMUM MAGNITUDE OF ATTITUDE RATE

FOR WORST CASE ENGINE FAILURES DURING BOOST WITH NO WINDS
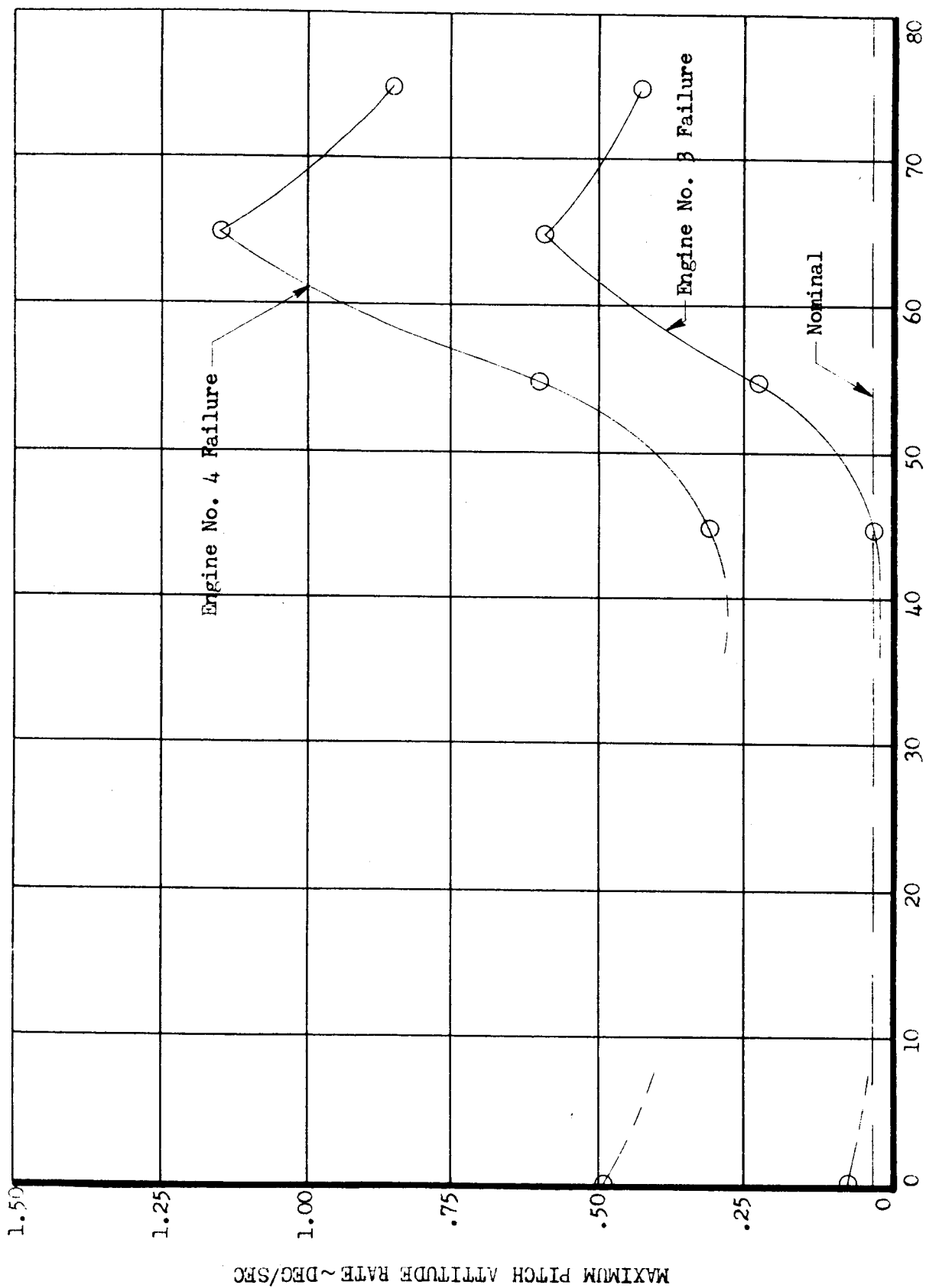
Engine No. 4 Failure

Engine No. 3 Failure

Nominal

FLIGHT TIME OF ENGINE FAILURE ~ SEC

MAXIMUM PITCH ATTITUDE RATE ~ DEG/SEC

S-IVB POST SEPARATION

1.50   1.25   1.00   .75   .50   .25   0

0   10   20   30   40   50   60   70   80

SA-204/LM-1 ENVELOPES OF POST SEPARATION S-IVB MAXIMUM MAGNITUDE OF CONTROL GIMBAL DEFLECTION

FOR WORST CASE ENGINE FAILURES DURING BOOST WITH NO AGING

Engine No. 4 Failure

Engine No. 3 Failure

Nominal

FLIGHT TIME OF ENGINE FAILURE ~ SEC

MAXIMUM PITCH CONTROL GIMBAL DEFLECTION ~ DEG

S-IVB POST SEPARATION

2.4 2.0 1.6 1.2 .8 .4 0

0 10 20 30 40 50 60 70 80

-84-

84 431 62618C
JAN 66
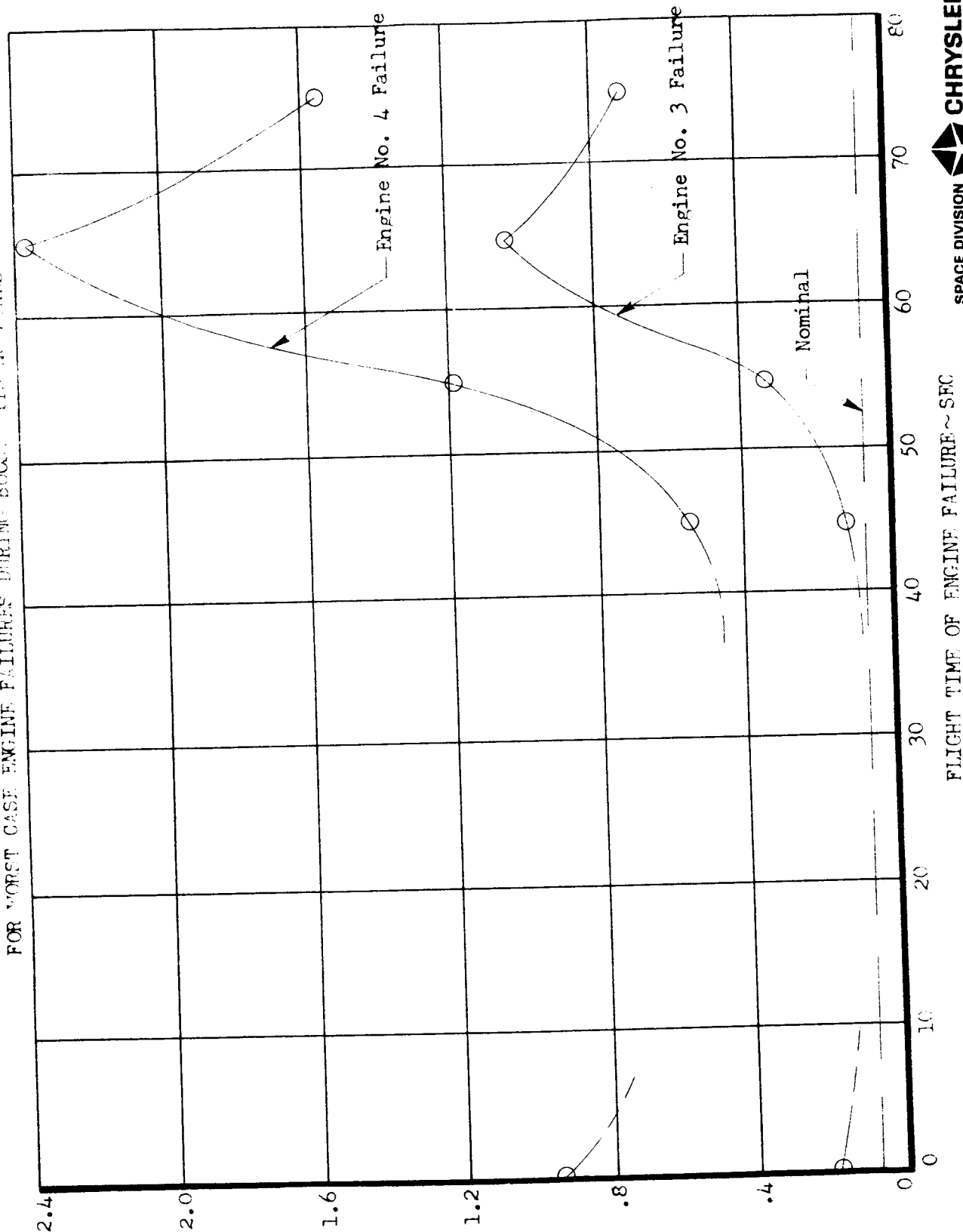
FIGURE 60

SA-204/LM-1 ENVELOPES OF PEAK CONTROL GIMBAL DEFLECTION RESPONSES

TO A SPECTRUM OF 50% QSS HEADWINDS AND

CROSSWINDS FOR ENGINE NO. 3 FAILURES

SPACE DIVISION CHRYSLER CORPORATION

-85-
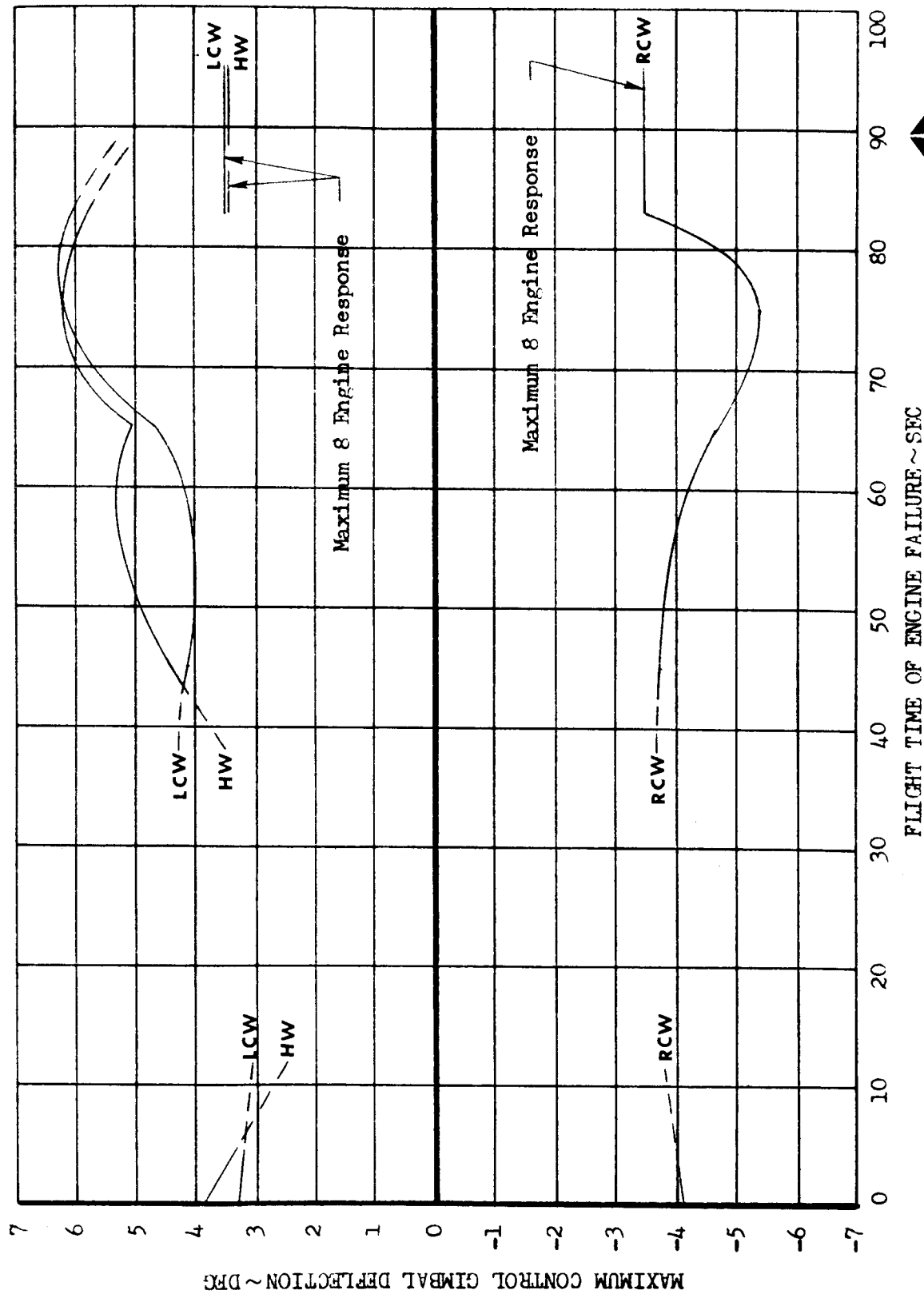
FIGURE 61

SA-204/LM-1 ENVELOPES OF PEAK CONTROL GIMBAL DEFLECTION RESPONSES
TO A SPECTRUM OF 50% QSS HEADWINDS AND
CROSSWINDS FOR ENGINE NO. 4 FAILURES

-86-
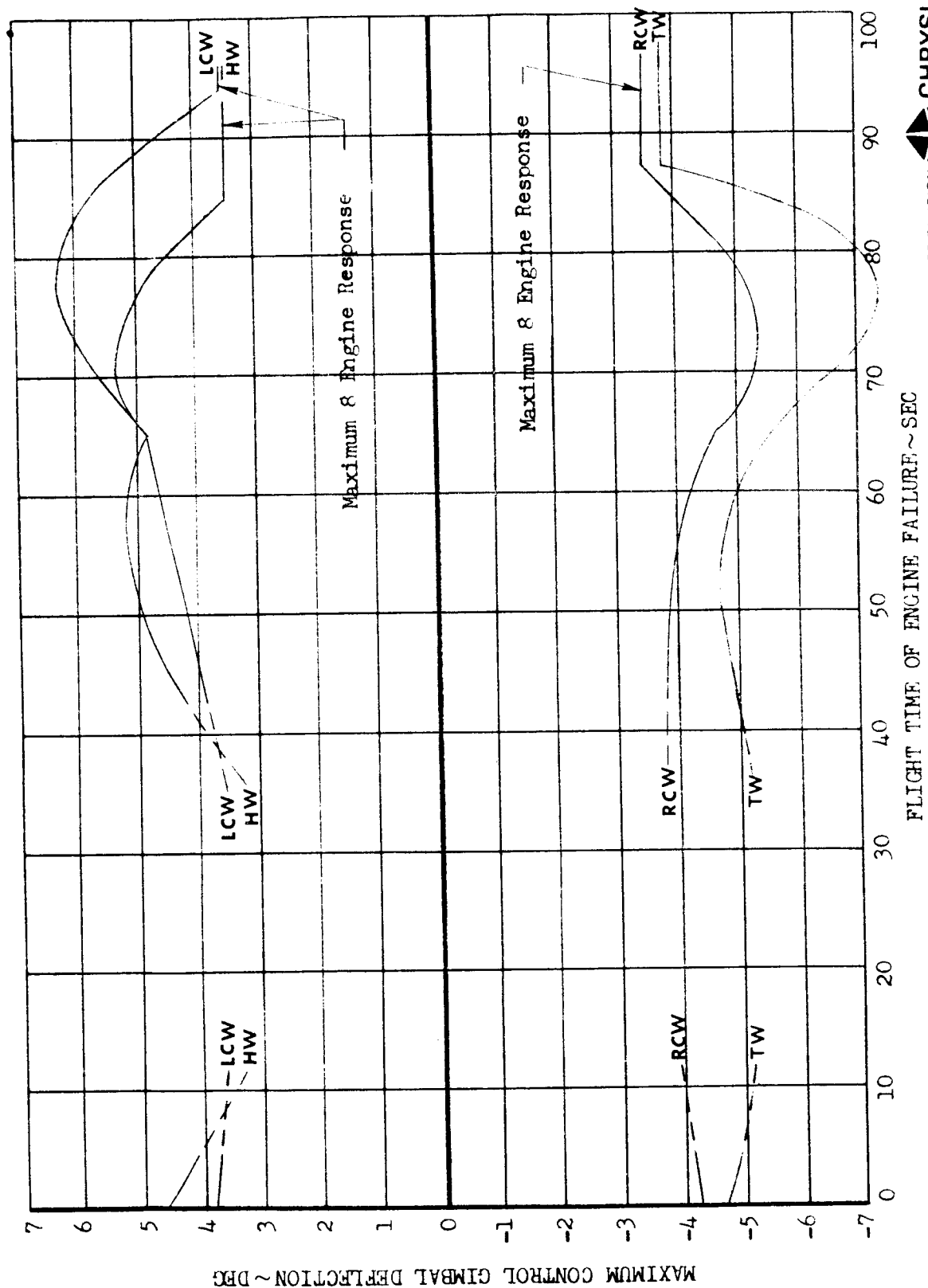
FIGURE 62

SA-204/LM-1 ENVELOPES OF PEAK BENDING MOMENT CRITICAL RATIO
RESPONSES (S.F. = 1.25) TO A SPECTRUM OF 50% QSS
HEADWINDS AND CROSSWINDS FOR ENGINE NO. 3 FAILURES
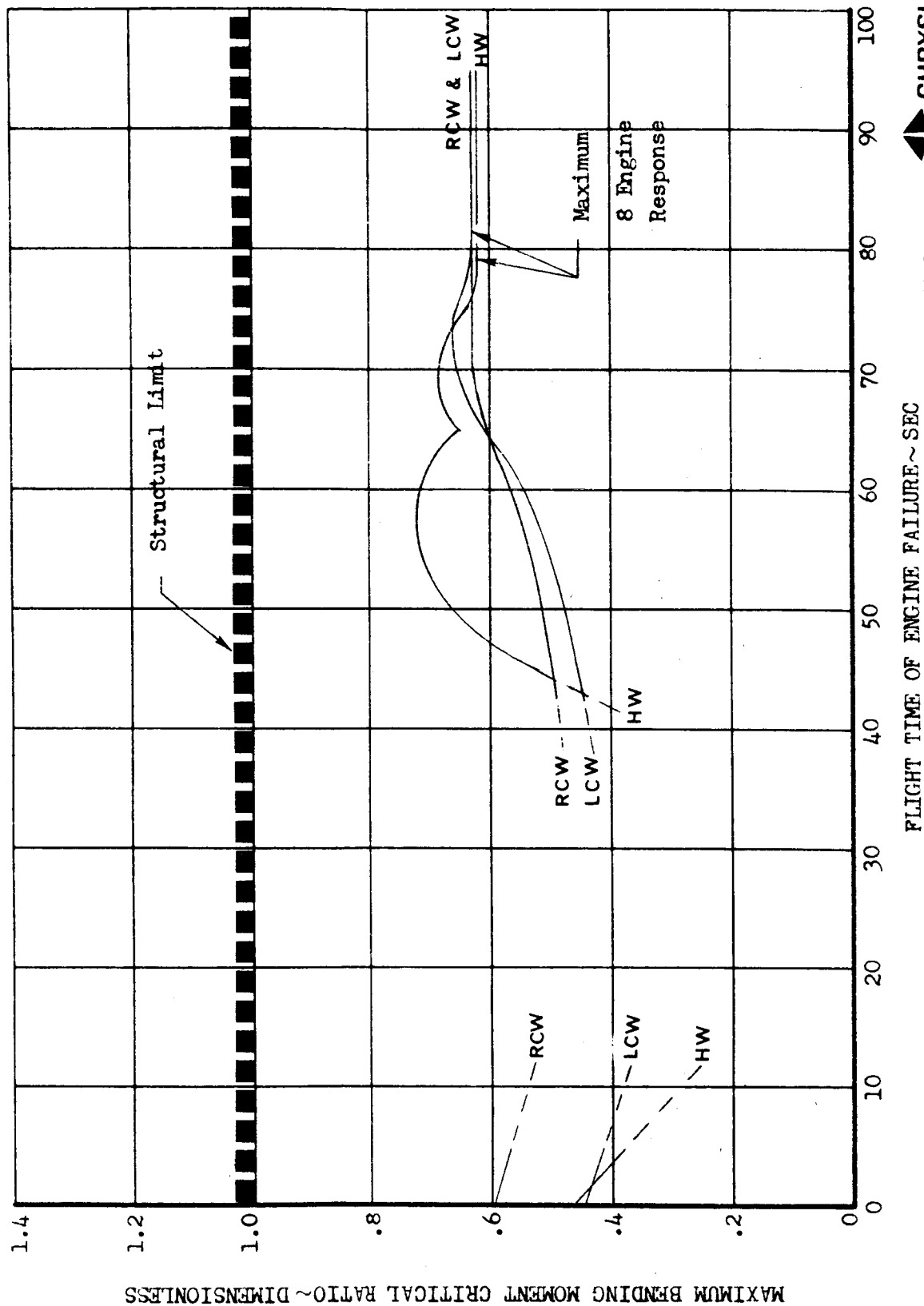
FIGURE 63

SA-204/IM-1 ENVELOPES OF PEAK BENDING MOMENT CRITICAL RATIO
RESPONSES (S.F. = 1.25) TO A SPECTRUM OF 50% GSS
HEADWINDS AND CROSSWINDS FOR ENGINE NO. 4 FAILURES
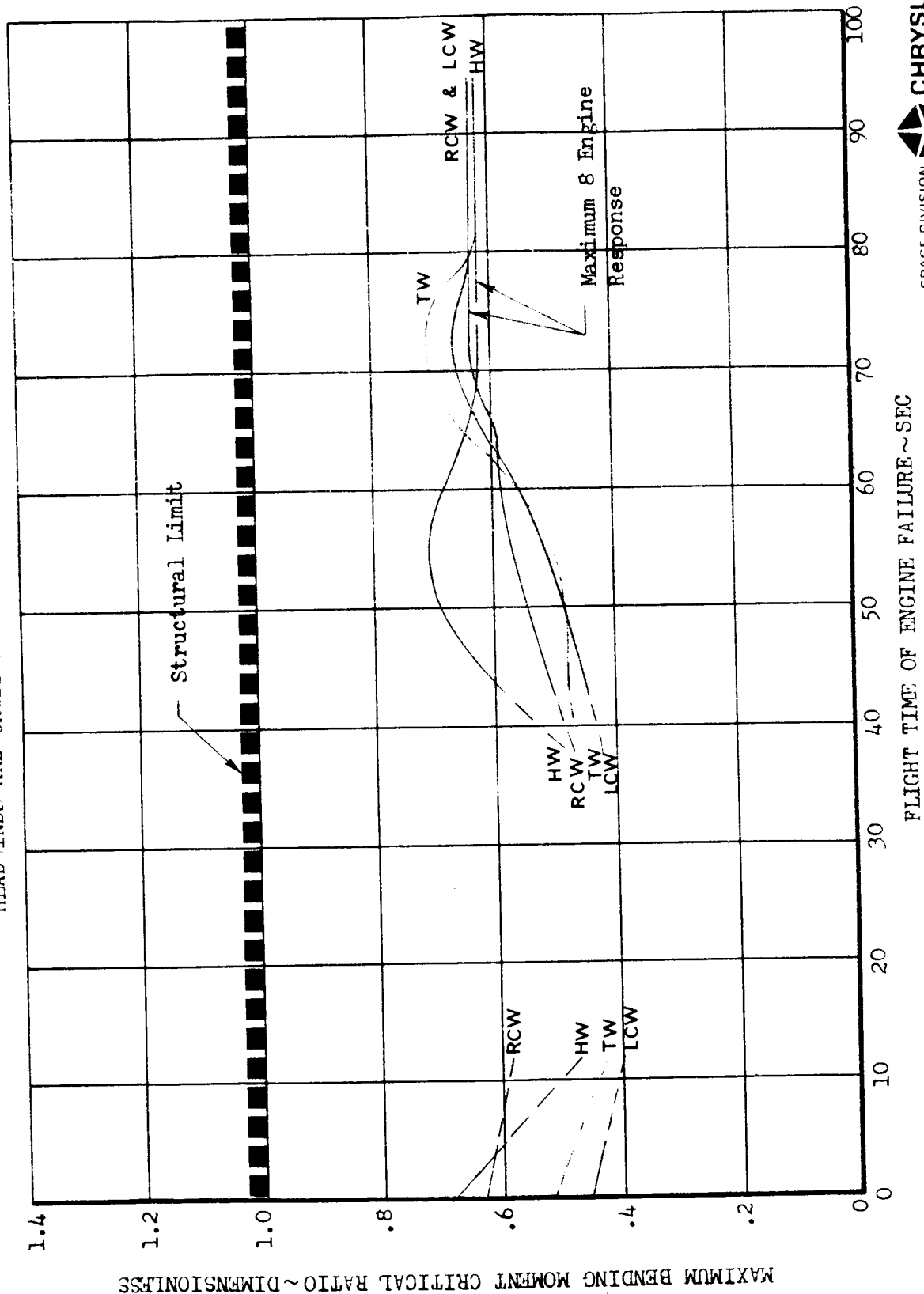
FIGURE 64

SA-204/LM-1 ENVELOPES OF PEAK ROLL ATTITUDE ERROR RESPONSES TO
A SPECTRUM OF 50% QSS HEADWINDS AND CROSSWINDS
FOR ENGINE NO. 3 FAILURES

CHRYSLER
CORPORATION

SPACE DIVISION
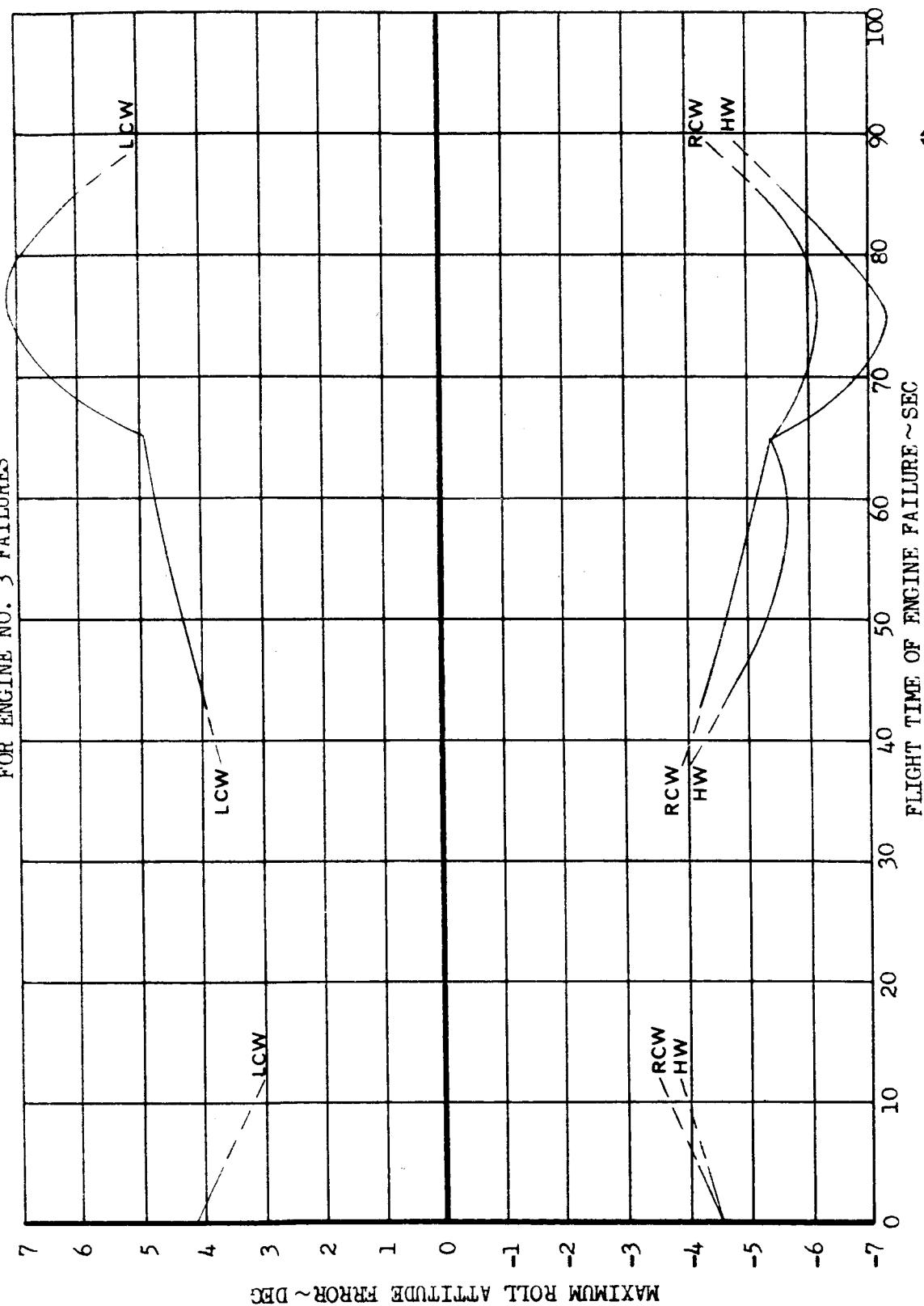
FIGURE 65

SA-204/LM-1 ENVELOPES OF PEAK ROLL ATTITUDE ERROR RESPONSES
TO A SPECTRUM OF 50% QSS HEADWINDS AND
CROSSWINDS FOR ENGINE NO. 4 FAILURES
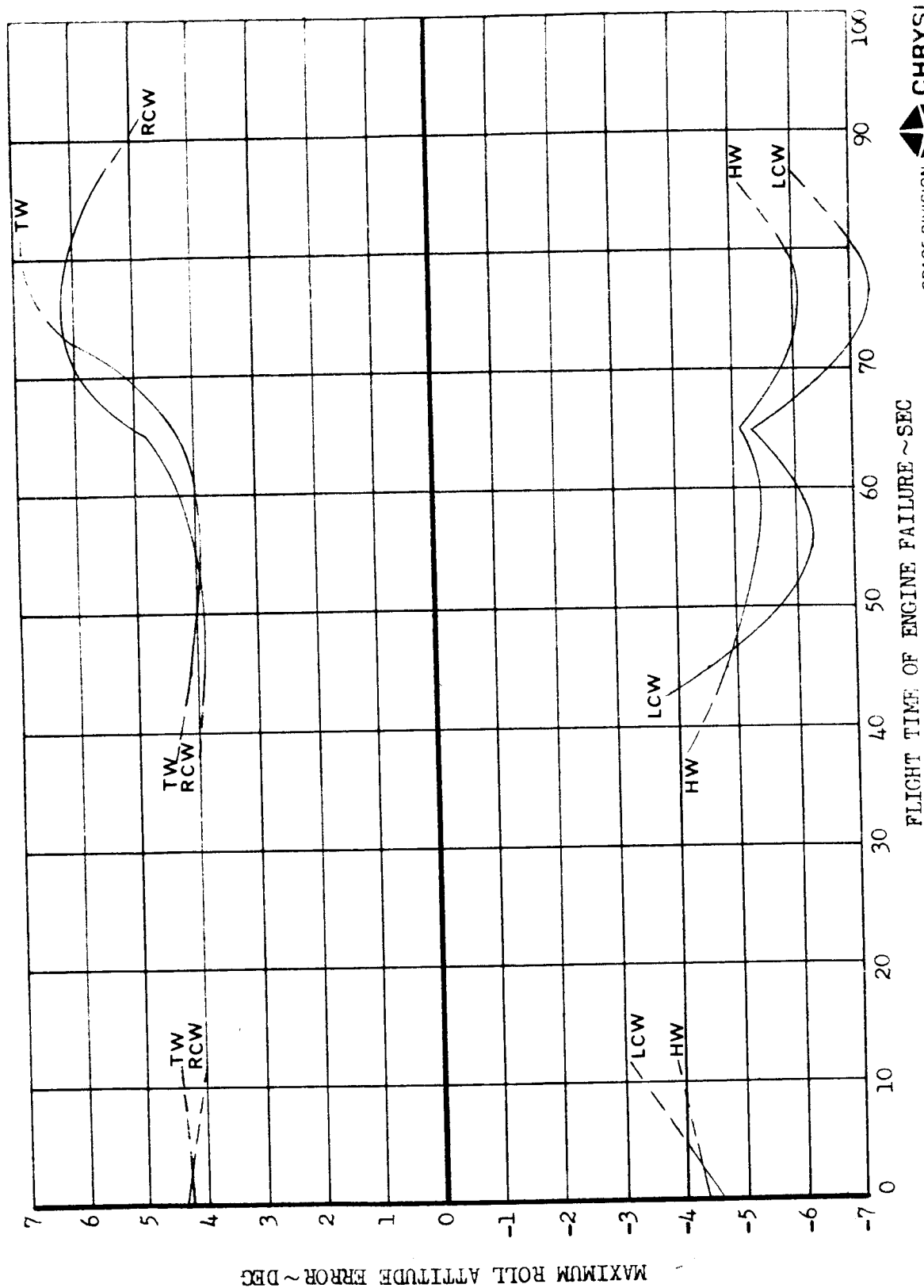
FIGURE 66

SA-204/LM-1 SEPARATION PLANE CLEARANCE SCHEMATIC

Retro-4

Drift When
Retro-2 Out

Outboard Interstage Wall, 3.30 Met.

Ring Frame, 3.133 Met.

X_M

Y_M

Z_M

Ullage-1

Drift When
Retro-1 Out

Retro-3

Ullage-2

Retro-1

Drift When
Retro-3 Out

Drift When
Retro-4 Out

Retro-2

Ullage-3

Radius of J-2 Bell in
Null Position, 1.022 Met.
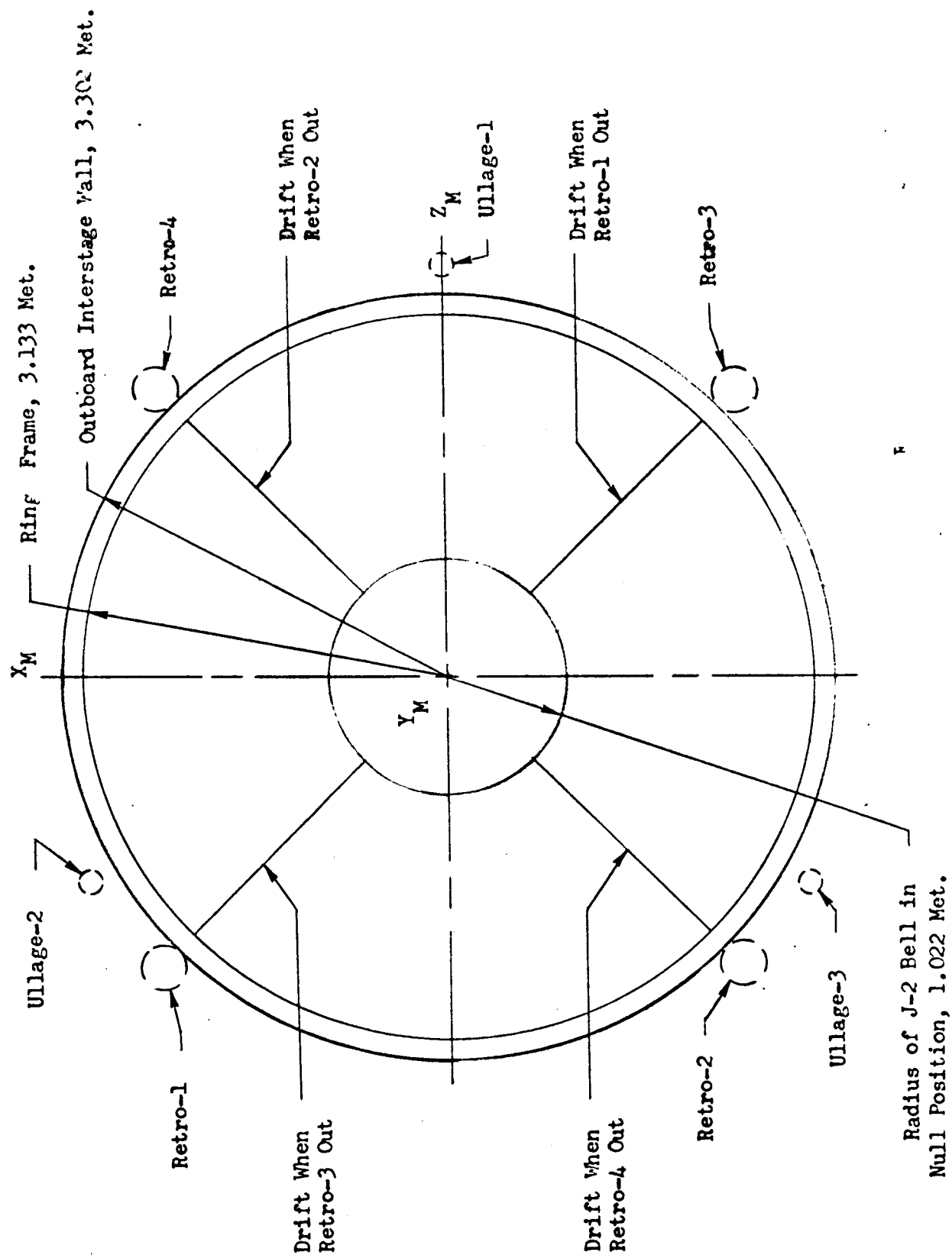
FIGURE 27

SA-204/LM-1 STAGE SEPARATION SINGLE ENGINE THRUST CURVES

TIME FROM SEPARATION STRUCTURE SEVERED ~ SEC

Engines No. 2 and No. 4

Engines No. 1 and No. 3

SPACE DIVISION **CHRYSLER** CORPORATION

FIGURE 68

SA-204/LM-1 STAGE SEPARATION S-IB MOMENT SCHEMATIC

Top of Interstage

←143.28→

STA 1116.844

Point of Thrust Application of 23405 Newtons Normal Force Due To Plume Impingement

₵ of Retro Thrust Canted 9.5°, Engine - 3

₵ of Retro Thrust Canted 9.5°, Engine - 1

H-1 No. 3

H-1 No. 1

Y_M

Retro -3

45°

Retro - 1

STA 469.487

CP

Z_M

X_M

STA 379.488

CG

Plan View Looking Aft

STA 100.000

Gimbal Station Plane

₵ of H-1 Thrust Canted 6°, Engine - 3

₵ of H-1 Thrust Canted 6°, Engine - 1
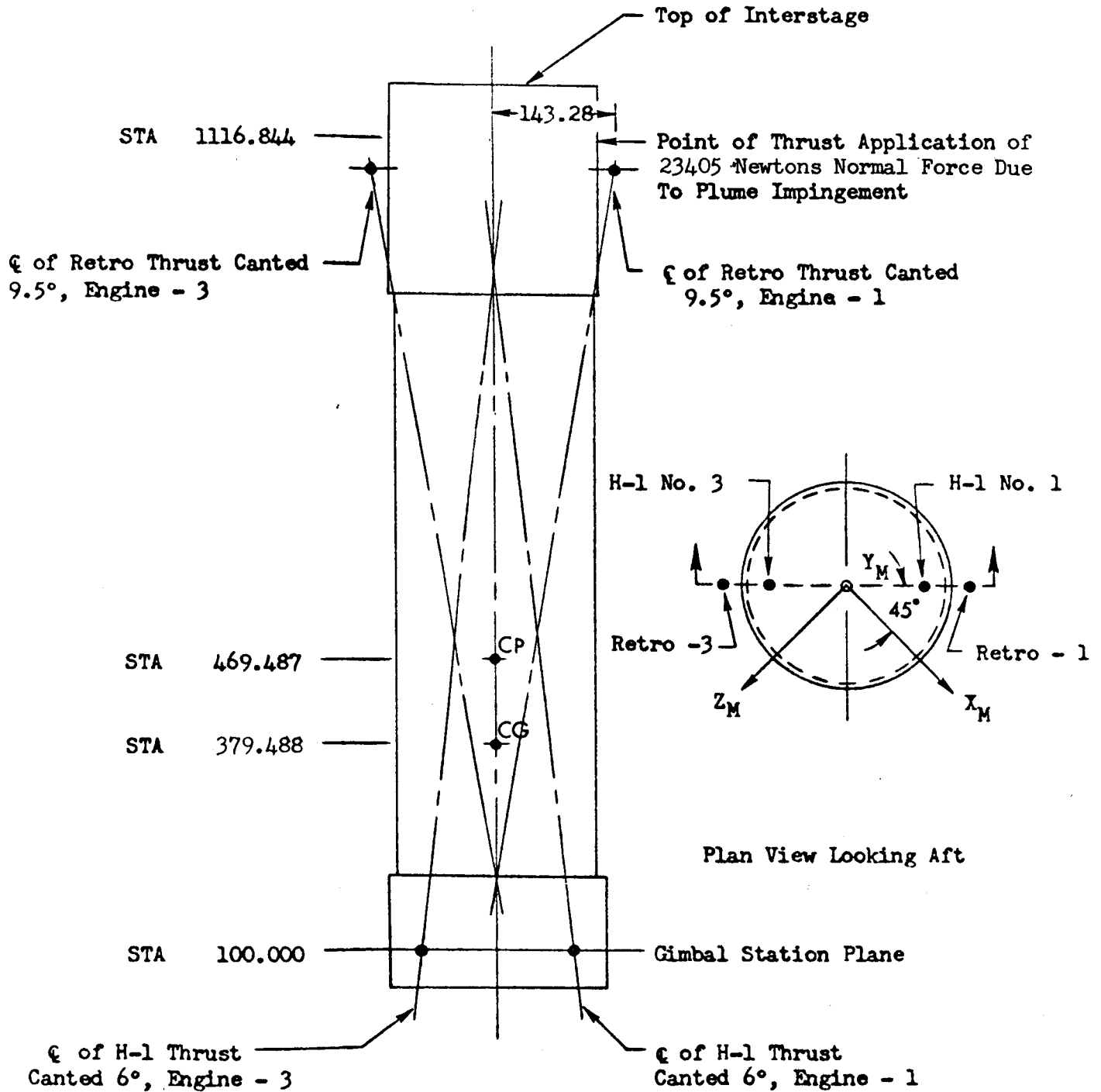
FIGURE 69

SA-204/LM-1 STAGE SEPARATION S-IVB MOMENT SCHEMATIC

Plan View Looking Aft

STA   1772.337

STA   1336.432

ULLAGE No. 2

9 in.

STA   1163.800

Point of Thrust Application
Due to Plume Impingment

Max Normal Force = 890 Newtons
Max Axial Force = 32928 Newtons

STA   1086.157 ——————— Gimbal Station Plane
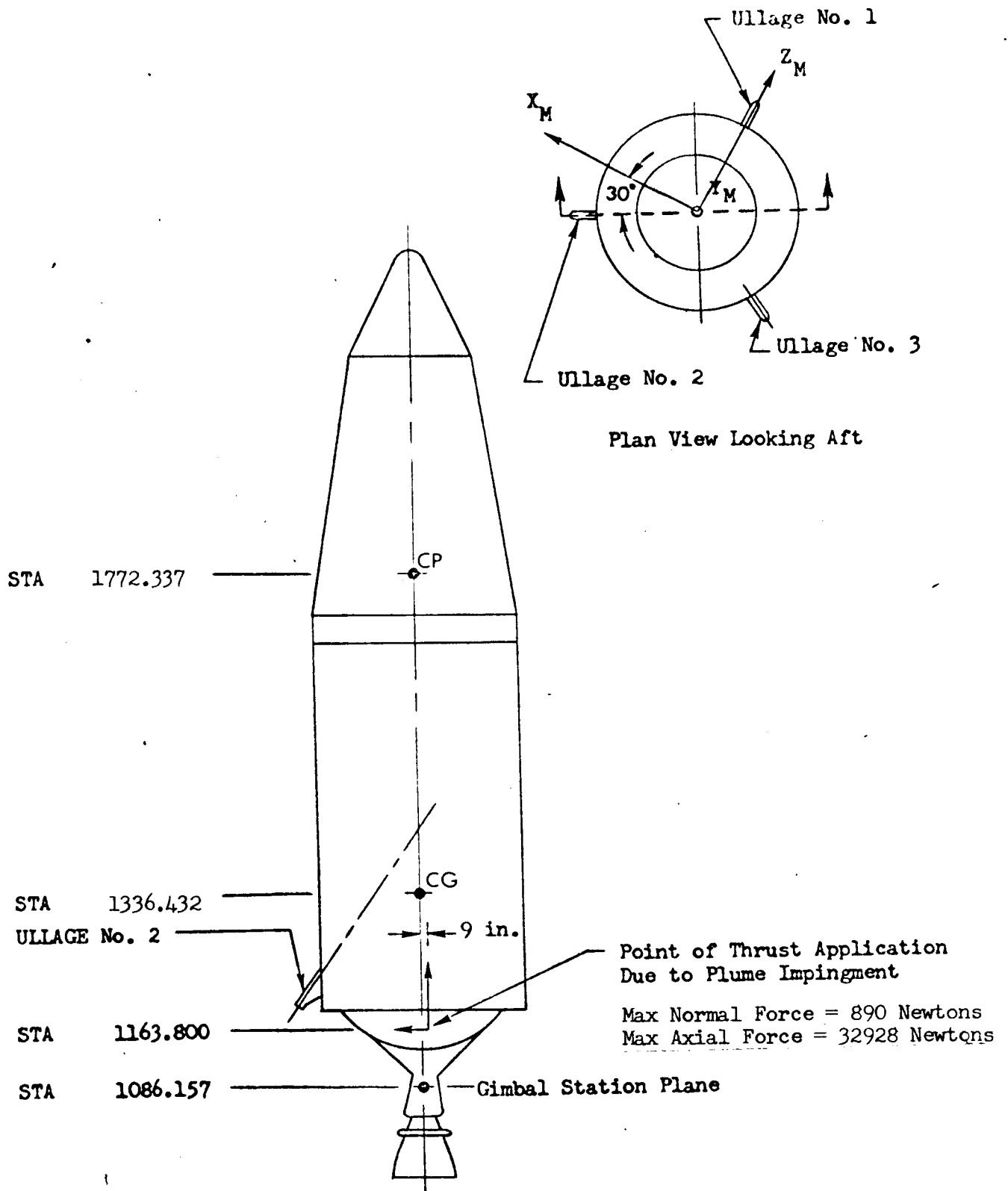
FIGURE 70

SA-204/LM-1 PEAK DYNAMIC RESPONSES DURING POST SEPARATION S-IVB MOTION

S-IVB ATTITUDE ERRORS

-95-
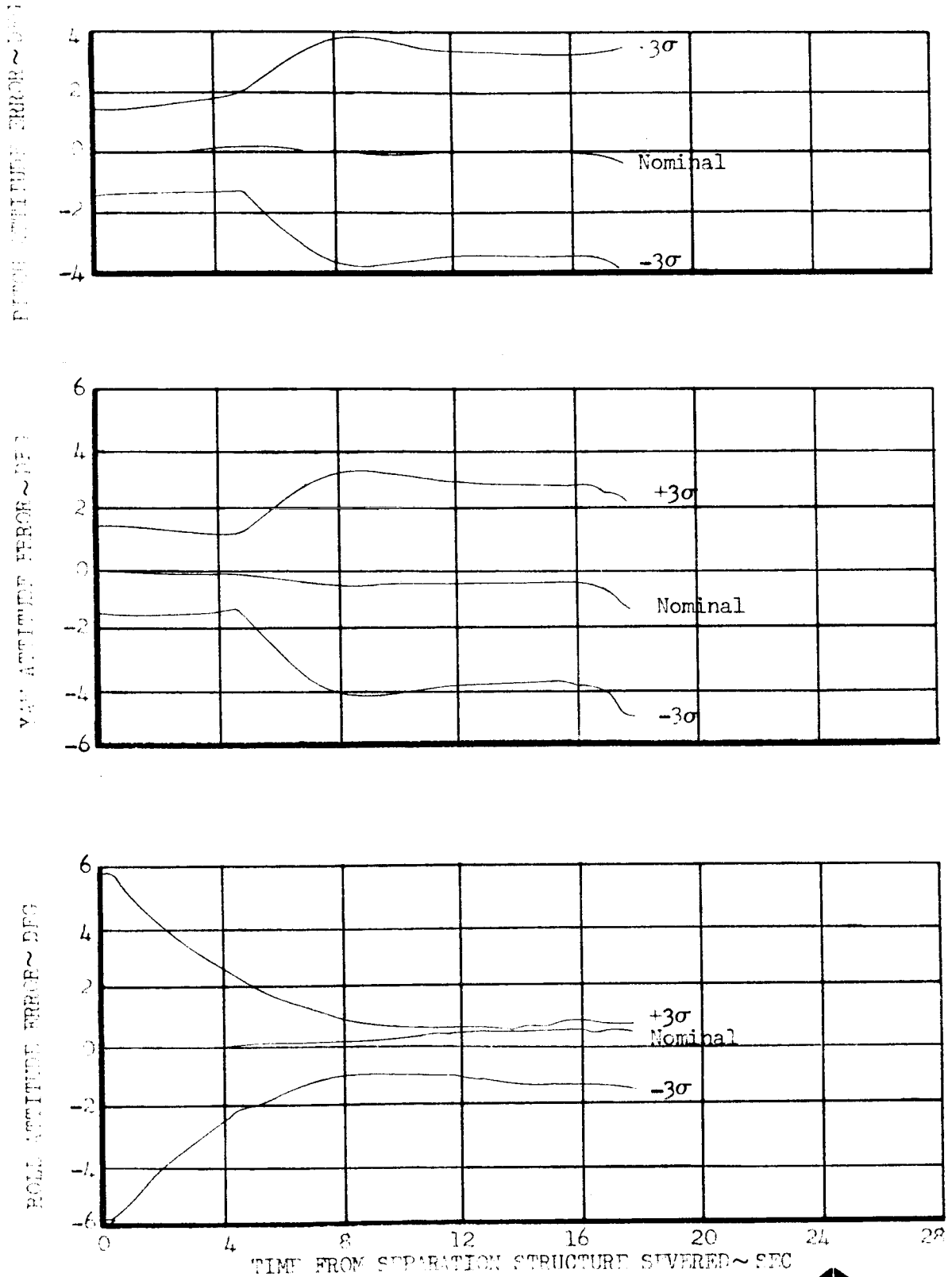
FIGURE 71

SA-204/LM-1 PEAK DYNAMIC RESPONSES DURING POST SEPARATION S-IVB MOTION

S-IVB BODY ATTITUDE RATES

TIME FROM SEPARATION STRUCTURE SEVERED ~ SEC

SPACE DIVISION CHRYSLER CORPORATION
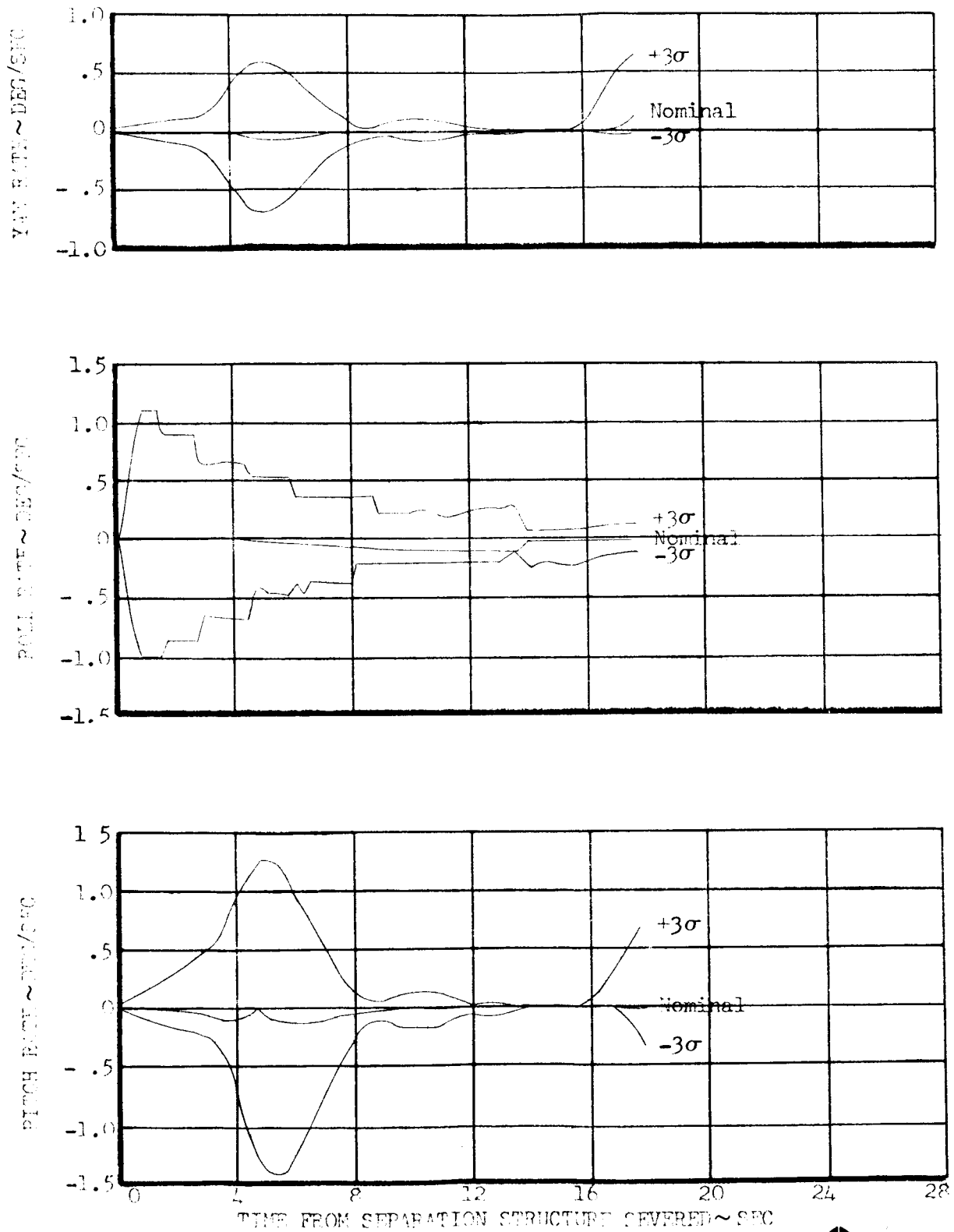
FIGURE 72

SA-204/LM-1 PEAK DYNAMIC RESPONSES DURING POST SEPARATION S-IVB MOTION

J-2 GIMBAL DEFLECTION

TIME FROM SEPARATION STRUCTURE SEVERED ~ SEC

FIGURE 73
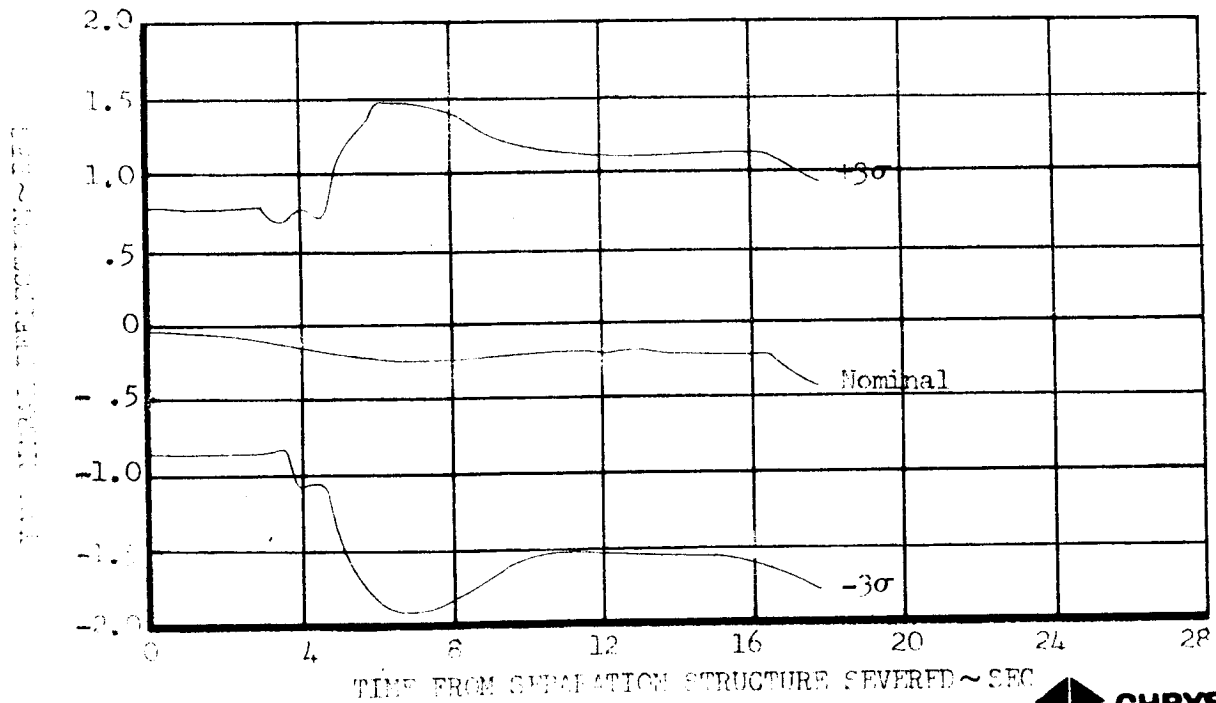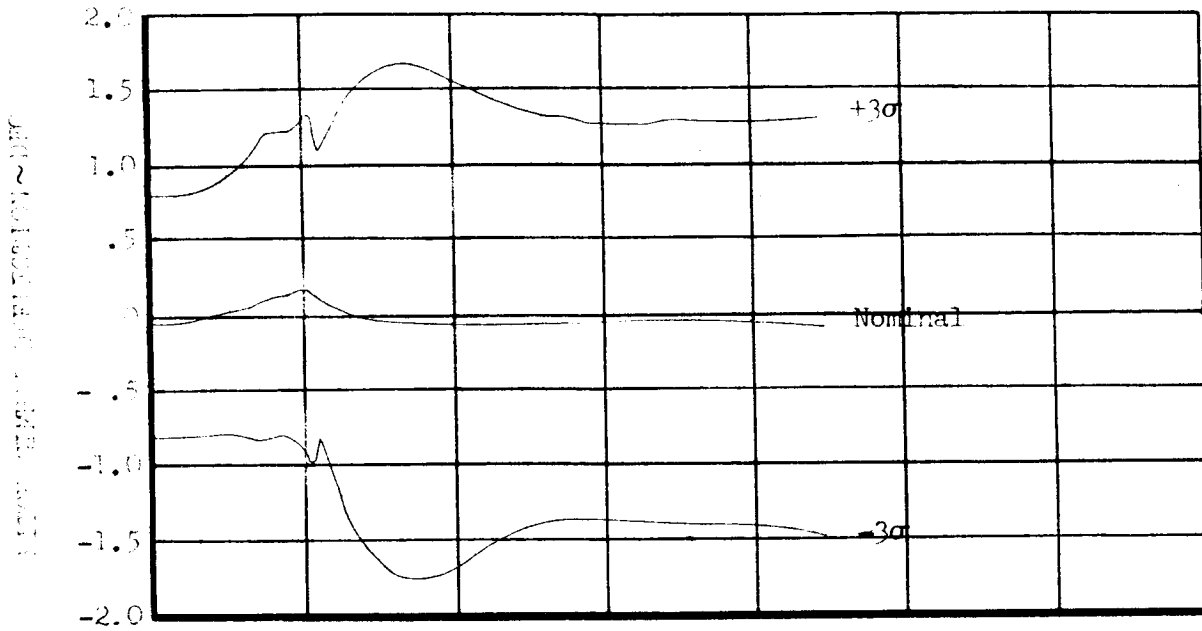
SA-204/LM-1 SEPARATION RELATIVE MOTION FOR SINGLE RETRO FAILURE
PROFILE VIEW

Separation Plane

Nulled J-2 Drift,
Retro 3 Out

Nulled J-2 Drift,
Retro 1 Out

Canted J-2 Drift,
Retro 1 Out

Canted J-2
Drift, Retro
3 Out

4°

5.4°

S-IB/S-IVB
Interstage
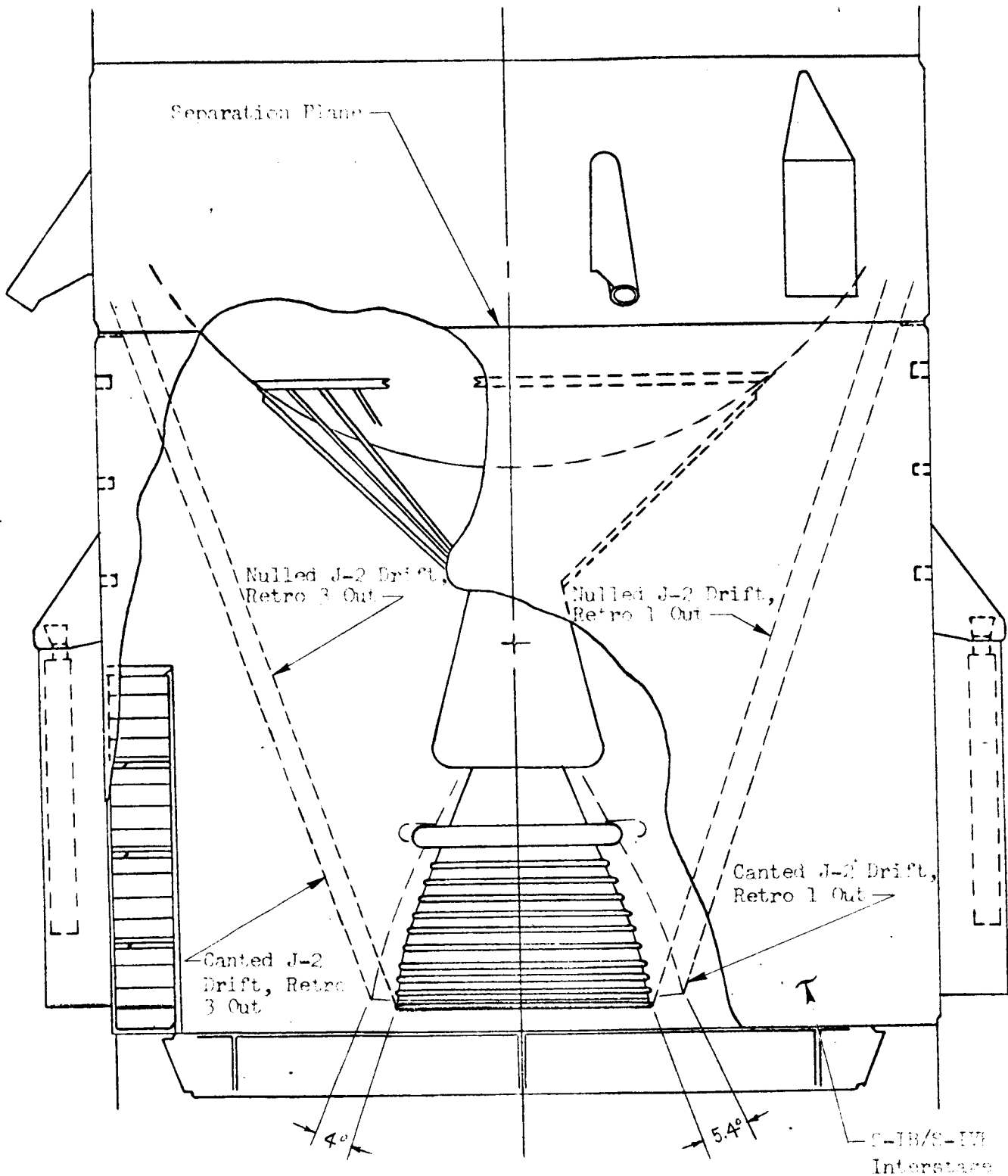
Results Shown Here Assume 732 Km. of the Residual S-IB Stage Pro-
pellants Become Unseated During Retro Action

TABLE 1

SA-204/LM-1 LIFTOFF SUMMARY

OBSTRUCTION	TIME REQUIRED TO CLEAR OBSTRUCTION (SEC)	DRIFT PER UNIT CG OFFSET (MET/MET)	DRIFT PER UNIT COMPOSITE THRUST MISALIGNMENT (MET/DEG)	DRIFT PER UNIT COMPOSITE CONTROL DEFLECTION ERROR (MET/DEG)
Swing Arm #4 Platform Top	6.55	29.66	3.71	1.86
Tower Top	7.50	40.35	5.27	2.63
Lightning Mast Top	8.20	49.21	6.56	3.28

OBSTRUCTION	INITIAL AVAILABLE CLEARANCE (MET)	FINAL AVAILABLE CLEARANCE 95%QSS(MET) DESIGN WINDS	3σ JAN. WINDS	MINIMUM % OF INITIAL CLEARANCE 95%QSS DESIGN WINDS	3σ JAN. WINDS
Swing Arm #4 Platform Top	5.42	2.28	.98	42.1	18.1
Tower Top	7.40	3.25	1.58	43.9	21.4
Lightning Mast Top	11.44	6.30	3.75	55.1	32.8

TABLE 2

H-1 ENGINE THRUST MISALIGNMENT CONTRIBUTORS

CONTRIBUTOR		$\Delta\beta$(Deg.)	
		CONTROL	FIXED
Electrical Nulls			
1. P & Y	.1°	.180	——
2. Rate Gyro P & Y	.125°/s	.180	——
3. Servo Amp	.6 MA	.075	——
4. Servo Valve	.6 MA	.075	——
5. Actuator Pot	178. MV	.069	——
Mechanical Misalignment			
6. Pad to First Ref. Plane P & Y	6 '	.180	——
7. S-IB S-IVB P & Y	6 '	.180	——
8. S-IVB IU P & Y	6 '	.180	——
9. IU Platform P & Y	15 '	.450	——
Undetectable Bias			
9. Unsymetrical Engine Thrust	30 '	.636	.636
10. Engine to S-IB Ref. Plane	30 '	.639	.639
11. Actuator Tie Points	21 '	.445	——

TABLE 3

SA-204/LM-1 LAUNCH VEHICLE OPERATIONAL FLIGHT TRAJECTORY
FLIGHT SEQUENCE OF EVENTS

NOMINAL FLIGHT TIME (HR:MIN:SEC)	TIME (SEC)	PROGRAM TIME (SEC)	EVENT
- 0:0:05.0	- 5.00	----	Guidance Reference Release (GRR).
- 0:0:03.1	- 3.10	----	Initiate S-IB Mainstage Ignition Sequence.
0:0:00.0	0.00	----	First Motion.
0:0:00.2	0.20	$(0.0)_1$	Lift-off Signal. Initiate Time Base 1.
0:0:10.2	10.20	$(10.0)_1$	Initiate Pitch and Roll Maneuvers.
0:0:40.2	40.20	$(40.0)_1$	Control Gain Switch Point.
0:1:15.0	75.00	----	Maximum Dynamic Pressure.
0:1:40.2	100.20	$(100.0)_1$	Control Gain Switch Point.
0:2:00.2	120.20	$(120.0)_1$	Control Gain Switch Point.
0:2:13.2	133.20	$(133.)_1$	Tilt Arrest.
0:2:14.3	134.29	$(134.1)_1$	Enable S-IB Propellant Level Sensors.
0:2:17.8	137.79	$(0.0)_2$	Level Sensor Activation; Initiate Time Base 2.
0:2:20.9	140.89	$(3.1)_2$	Inboard Engine Cutoff (IECO).
0:2:23.9	143.89	$(0.0)_3$	Outboard Engine Cutoff (OECO); Initiate Time Base 3.
0:2:25.2	145.19	$(1.3)_3$	Separation Signal.
0:2:25.3	145.27	$(1.4)_3$	S-IB/S-IVB Physical Separation; Control Gain Switch Point.
0:2:26.6	146.59	$(2.7)_3$	J-2 Engine Start Command.
0:2:28.9	148.94	----	Ullage Burn Out.
0:2:29.9	149.89	----	90% J-2 Thrust Level.
0:2:32.6	152.59	$(8.7)_3$	Command PU System Activation.
0:2:37.2	157.19	$(13.3)_3$	Jettison Ullage Rocket Motors.
0:2:40.9	160.89	$(17.0)_3$	Command Active Guidance Initiation.
0:4:47.6	287.59	$(143.7)_3$	Control Gain Switch Point.
0:7:57.3	477.25	----	EMR Shift Sensed by IGM.
0:9:52.3	592.26	----	Guidance Cutoff Signal (GCS).

TABLE 3 (continued)

SA-204/LM-1 LAUNCH VEHICLE OPERATIONAL FLIGHT TRAJECTORY
FLIGHT SEQUENCE OF EVENTS

NOMINAL FLIGHT TIME (HR:MIN:SEC)	TIME (SEC)	PROGRAM TIME (SEC)	EVENT
0:9:52.5	592.46	$(0.0)_4$	Initiate Time Base 4. (Reflects an approximate 0.2 second systems delay).
0:10:02.3	602.26	---	Orbital Insertion.
0:10:37.3	637.46	$(45.)_4$	Nose Cone Jettisoned.
0:53:55.	3235.	---	LM Separation.
4:30:00.	16200.	---	Loss of S-IVB/IU Attitude Control.

TABLE 4

SA-204/LM-1 LAUNCH VEHICLE MASS BREAKDOWN
(KILOGRAMS)

Spacecraft*	16,485	
Instrument Unit	2,087	
S-IVB Stage Dry	10,611	
S-IVB Residuals	1,090	
Useable Reserve Propellant (Includes FPR)	1,393	
Injection Mass		31,666
J-2 Thrust Decay Propellant and LOX Venting	111	
S-IVB Cutoff Mass		31,777
S-IVB Propellant Consumed	102,026	
S-IVB APS Propellant Consumed	2	
Ullage Cases	98	
S-IVB "90% Thrust" Mass		133,903
S-IVB GH2 Start Tank	2	
S-IVB Buildup Propellant Consumed	199	
Ullage Propellant Consumed	83	
S-IVB Detonation Package	2	
S-IVB Stage Mass at Separation		134,189
S-IVB Aft Frame Hardware	14	
S-IB/S-IVB Interstage	2,970	
S-IB Dry Mass	38,699	
S-IB Residuals and Reserves	4,760	
S-IVB Frost Consumed	45	
S-IB Frost Consumed	454	
S-IB Seal Purge Consumed	3	
S-IB Fuel Additive Consumed	12	
S-IB Gearbox Lubricant Consumed	328	
Inboard Engine Thrust Decay Prpt Consumed	971	
Outboard Engine Thrust Decay Prpt Consumed		
To Separation	893	
S-IB Mainstage Propellant Consumed	400,270	
Vehicle Liftoff Mass		583,608

*SLA	1,792
Lunar Module	14,209
Nose Cone	484
	16,485

TABLE 5

SA-204/LM-1 CONTROL SYSTEM COMPONENT
TRANSFER FUNCTIONS
S-IB STAGE

Pitch and Yaw Attitude Error $(\psi_{p,y})$

$$F_{\psi_{p,y}} = \frac{A_{op,y}}{0.1320S + 1.0} \qquad\qquad (0 \leq T < 100)$$

$$F_{\psi_{p,y}} = \frac{A_{op,y}}{0.1380S + 1.0} \qquad\qquad (100 \leq T < 120)$$

$$F_{\psi_{p,y}} = \frac{A_{op,y}}{0.1440S + 1.0} \qquad\qquad (120 \leq T \leq OECO)$$

Roll Attitude Error (ψ_r)

$$F_{\psi_r} = \frac{A_{or}}{0.1584S + 1.0} \qquad\qquad (0 \leq T < 40)$$

$$F_{\psi_r} = \frac{A_{or}}{0.1634S + 1.0} \qquad\qquad (40 \leq T < 100)$$

$$F_{\psi_r} = \frac{A_{or}}{0.1692S + 1.0} \qquad\qquad (100 \leq T \leq OECO)$$

Pitch and Yaw Attitude Rate $(\omega_{z,x})$

$$F_{\omega_{z,x}} = \frac{A_{1p,y}(0.0003640S^2 + 0.0010405 + 1.0)}{0.0000668S^3 + 0.01650S^2 + 0.1560S + 1.0}$$

Roll Attitude Rate (ω_y)

$$F_{\omega_y} = \frac{A_{1r}(0.0021S^2 + 0.012S + 1.0)}{0.0006193S^3 + 0.01358S^2 + 0.1597S + 1.0}$$

Pitch and Yaw Accelerometer $(\gamma_{p,y})$

$$F_{\gamma_{p,y}} = \frac{G2}{0.5S^2 + 5.1S + 1.0}$$

Actuator Dynamics

$$AD = \frac{1.0}{0.00001942S^3 + 0.0007963S^2 + 0.05576S + 1.0}$$

TABLE 6

CONTROL DATA FOR VARIOUS WIND MAGNITUDES AND DIRECTIONS

57 m/sec Headwind

ALTITUDE (Km)	TIME (Sec)	α_{ss} (Deg)	ΔSHEAR (Deg)	ΔGUSTS (Deg)	$\Delta C1,C2$ (Deg)
10	69.0	2.40	2.30	1.02	0
11	71.7	1.72	2.65	0.94	0
12	75.0	1.51	2.45	0.97	0.1
13	77.5	1.64	2.43	0.92	0.12

ALTITUDE (Km)	TIME (Sec)	β_{ss} (Deg)	ΔSHEAR (Deg)	ΔGUSTS (Deg)	$\Delta C1,C2$ (Deg)
10	69.8	1.32	1.95	1.01	1.53
11	72.5	0.56	2.77	1.07	1.43
12	75.2	0.61	2.71	1.12	1.72
13	77.7	1.04	2.86	1.09	1.31

75 m/sec Headwind

ALTITUDE (Km)	TIME (Sec)	α_{ss} (Deg)	ΔSHEAR (Deg)	ΔGUSTS (Deg)	$\Delta C1,C2$ (Deg)
10	69.0	3.06	3.04	1.03	0
11	71.7	2.16	3.55	0.88	.08
12	75.0	1.95	3.37	0.86	.22
13	77.5	2.12	3.25	0.86	.21

ALTITUDE (Km)	TIME (Sec)	β_{ss} (Deg)	ΔSHEAR (Deg)	ΔGUSTS (Deg)	$\Delta C1,C2$ (Deg)
10	69.8	1.79	2.80	1.20	2.11
11	72.5	0.62	4.08	1.15	1.98
12	75.2	0.93	4.00	1.22	1.85
13	77.7	1.46	4.09	1.15	1.90

TABLE 6 (Continued)

CONTROL DATA FOR VARIOUS WIND MAGNITUDES AND DIRECTIONS

57 m/sec Crosswind

ALTITUDE (Km)	TIME (Sec)	α_{ss} (Deg)	ΔSHEAR (Deg)	ΔGUSTS (Deg)	ΔC1,C2 (Deg)
10	69.0	2.95	2.50	1.27	0
11	71.7	2.27	2.96	1.19	0
12	75.0	1.83	3.13	1.16	0
13	77.5	1.93	2.90	1.14	0.12

ALTITUDE (Km)	TIME (Sec)	β_{ss} (Deg)	ΔSHEAR (Deg)	ΔGUSTS (Deg)	ΔC1,C2 (Deg)
10	69.8	1.64	1.62	1.16	1.66
11	72.5	1.06	2.40	0.91	1.54
12	75.2	0.51	3.10	0.99	1.50
13	77.7	1.03	2.88	1.03	1.41

75 m/sec Crosswind

ALTITUDE (Km)	TIME (Sec)	α_{ss} (Deg)	ΔSHEAR (Deg)	ΔGUSTS (Deg)	ΔC1,C2 (Deg)
10	69.0	3.90	3.35	1.35	0
11	71.8	3.05	3.90	1.20	0
12	74.5	2.45	4.15	1.10	.05
13	77.0	2.43	4.12	0.95	.15

ALTITUDE (Km)	TIME (Sec)	β_{ss} (Deg)	ΔSHEAR (Deg)	ΔGUSTS (Deg)	ΔC1,C2 (Deg)
10	69.8	2.08	2.72	1.15	2.20
11	72.5	1.58	3.08	1.17	2.07
12	75.2	0.80	4.05	1.00	1.95
13	77.7	1.45	3.80	1.10	1.85

TABLE 6 (Continued)

CONTROL DATA FOR VARIOUS WIND MAGNITUDES AND DIRECTIONS

57 m/sec Tailwind

ALTITUDE (Km)	TIME (Sec)	α_{ss} (Deg)	ΔSHEAR (Deg)	ΔGUSTS (Deg)	$\Delta C1, C2$ (Deg)
10	69.0	2.86	2.31	1.24	0
11	71.8	2.19	2.68	1.18	0
12	75.0	1.78	2.79	1.09	0
13	77.5	1.58	2.69	1.05	0

ALTITUDE (Km)	TIME (Sec)	β_{ss} (Deg)	ΔSHEAR (Deg)	ΔGUSTS (Deg)	$\Delta C1, C2$ (Deg)
10	69.8	1.40	0.63	0.56	1.38
11	72.5	1.05	1.56	0.78	1.23
12	75.2	0.60	2.12	0.62	1.16
13	77.8	0.57	2.21	0.70	1.07

75 m/sec Tailwind

ALTITUDE (Km)	TIME (Sec)	α_{ss} (Deg)	ΔSHEAR (Deg)	ΔGUSTS (Deg)	$\Delta C1, C2$ (Deg)
10	69.0	3.80	3.10	1.32	0
11	71.8	3.08	3.49	1.23	0
12	74.5	2.50	3.69	1.13	0
13	77.0	2.10	3.77	1.09	0

ALTITUDE (Km)	TIME (Sec)	β_{ss} (Deg)	ΔSHEAR (Deg)	ΔGUSTS (Deg)	$\Delta C1, C2$ (Deg)
10	69.8	1.54	1.09	0.46	1.82
11	72.5	1.51	2.08	0.73	1.63
12	75.2	0.98	2.42	0.72	1.49
13	77.8	0.62	3.01	0.62	1.39

TABLE 7

SA-204/LM-1 PREDICTED ENGINE SHUTDOWN TIMES

FOR A SPECTRUM OF EARLY ENGINE FAILURE TIMES

INBOARD ENGINE FAILURE TIME (SEC)	PREDICTED PROPELLANT SENSOR LEVEL UNCOVER TIME (SEC)	PREDICTED INBOARD ENGINE CUTOFF TIME (SEC)	PREDICTED OUTBOARD ENGINE CUTOFF TIME (SEC)	PREDICTED SEPARATION STRUCTURE SEVERED TIME (SEC)
0	157.476	160.576	164.351	165.730
45	151.050	154.151	157.925	159.304
55	149.619	152.719	156.493	157.872
65	148.191	151.292	155.066	156.445
75	146.762	149.863	153.637	155.016
80	146.048	149.148	152.923	154.302

OUTBOARD ENGINE FAILURE TIME (SEC)	PREDICTED PROPELLANT SENSOR LEVEL UNCOVER TIME (SEC)	PREDICTED INBOARD ENGINE CUTOFF TIME (SEC)	PREDICTED OUTBOARD ENGINE CUTOFF TIME (SEC)	PREDICTED SEPARATION STRUCTURE SEVERED TIME (SEC)
0	157.476	160.576	165.609	166.988
45	151.050	154.151	159.183	160.562
55	149.619	152.719	157.751	159.130
65	148.191	151.292	156.324	157.703
75	146.762	149.863	154.895	156.274
80	146.048	149.148	154.181	155.560
Nominal	137.792	140.892	143.892	145.271

TABLE 8

SA-204/LM-1 CONTROL SYSTEM

COMPONENT TRANSFER FUNCTIONS

S-IVB STAGE

Pitch and Yaw Attitude Error ($\psi_{p,y}$)

$$F\psi_{p,y} = \frac{a_{o_{p,y}}}{0.1545S + 1.0}$$

OECO + 1.5 sec to OECO + 141.5 sec

$$F\psi_{p,y} = \frac{a_{o_{p,y}}}{0.1556S + 1.0}$$

OECO + 141.5 sec to S-IVB Burnout

Pitch and Yaw Attitude Rate ($\omega_{z,x}$)

$$F\omega_{z,x} = \frac{a_{1_{p,y}} (0.14 \times 10^{-3} s^2 + 0.4 \times 10^{-3} s + 1.0)}{0.7225 \times 10^{-4} s^3 + 0.3759 \times 10^{-2} s^2 + 0.7917 \times 10^{-1} s + 1.0}$$

OECO + 1.5 sec to OECO + 141.5 sec

$$F\omega_{z,x} = \frac{a_{1_{p,y}} (0.14 \times 10^{-3} s^2 + 0.4 \times 10^{-3} s + 1.0)}{0.7462 \times 10^{-4} s^3 + 0.3842 \times 10^{-2} s^2 + 0.7974 \times 10^{-1} s + 1.0}$$

OECO + 141.5 sec to S-IVB Burnout

Actuator Dynamics

$$AD = \frac{1.0}{0.34542 \times 10^{-4} s^3 + 0.16582 \times 10^{-2} s^2 + 0.62686 \times 10^{-1} s + 1.0}$$

TABLE 9

MONTHLY 95 PERCENTILE HEADWIND ENVELOPE

COMPARISON WITH QSS DESIGN WIND ENVELOPES

FOR 75° FLIGHT AZIMUTH

	5KM	6KM	7KM	8KM	9KM	10KM	11KM	12KM	13KM	14KM	15KM
*JANUARY	+ 4.3	+ 6.9	+ 8.7	+ 9.9	+10.5	+11.5	+12.9	+15.9	+19.6	+20.5	+19.2
FEBRUARY	+ 1.7	+ 3.0	+ 4.3	+ 5.3	+ 5.5	+ 6.2	+ 7.7	+11.2	+15.4	+15.5	+13.3
MARCH	+ 3.6	+ 6.3	+ 8.1	+ 9.6	+11.6	+13.2	+14.6	+18.8	+21.2	+20.7	+18.2
APRIL	- 5.1	- 5.1	- 4.1	- 2.3	- 1.5	- 1.7	- 1.0	- 1.1	+ 2.0	+ 3.6	+ 4.0
MAY	- 6.1	- 5.9	- 5.5	- 6.6	- 6.6	- 7.5	- 7.3	- 7.3	- 5.8	- 3.3	- 4.1
JUNE	- 4.6	- 4.9	- 5.9	- 6.6	- 8.0	- 9.7	-10.6	-12.5	-12.8	-12.6	-12.8
JULY	- 5.9	- 6.5	- 7.7	- 8.4	-11.0	-12.9	-15.3	-18.4	-19.3	-17.1	-15.0
AUGUST	- 6.2	- 6.8	- 7.6	- 8.7	-10.3	-12.4	-13.7	-16.9	-17.0	-16.4	-13.0
SEPTEMBER	- 7.4	- 7.8	- 7.4	- 7.7	- 8.5	-10.0	-12.1	-13.1	-14.2	-14.0	-12.1
OCTOBER	- 4.0	- 3.5	- 2.9	- 2.3	- 2.2	- 2.1	- 3.2	- 2.3	- 2.6	- 2.9	- 2.1
NOVEMBER	- 4.7	- 3.7	- 2.5	- 1.8	- 2.0	- 2.3	- 2.0	- 0.5	- 0.1	+ 1.0	+ 1.0
DECEMBER	- 0.6	+ 0.4	+ 2.3	+ 2.7	+ 2.9	+ 4.3	+ 5.6	+ 8.1	+11.3	+12.4	+11.5
MAXIMUM	- 7.4	- 7.8	- 7.7	- 8.7	-11.0	-12.9	-15.3	-18.4	-19.3	-17.1	-15.0
ANNUAL	- 4.9	- 4.9	- 5.2	- 5.8	- 6.7	- 8.2	- 9.3	-10.4	-11.5	-10.7	- 9.7
**50% QSS	26.4	30.6	34.7	38.8	42.9	47.0	47.0	47.0	47.0	47.0	41.8
75% QSS	33.1	37.9	42.6	47.4	52.2	57.0	57.0	57.0	57.0	57.0	50.5
90% QSS	40.2	45.8	51.3	56.9	62.4	68.0	68.0	68.0	68.0	68.0	60.3
95% QSS	45.0	51.0	57.0	63.0	69.0	75.0	75.0	75.0	75.0	75.0	66.7
99% QSS	58.4	66.1	73.8	81.5	89.3	97.0	97.0	97.0	97.0	97.0	87.5

*Reference 17   **Reference 6   + Denotes Tailwind
                                              - Denotes Headwind

TABLE 10

MONTHLY 95 PERCENTILE TAILWIND ENVELOPE

COMPARISON WITH QSS DESIGN WIND ENVELOPES

FOR 75° FLIGHT AZIMUTH

	5KM	6KM	7KM	8KM	9KM	10KM	11KM	12KM	13KM	14KM	15KM
*JANUARY	+33.6	+38.4	+44.1	+48.2	+55.4	+60.8	+68.0	+67.5	+66.1	+63.7	+56.3
FEBRUARY	+34.1	+41.0	+48.0	+54.7	+61.2	+67.4	+73.4	+76.1	+74.8	+62.8	+56.3
MARCH	+34.3	+37.9	+43.8	+50.2	+56.7	+61.6	+64.7	+70.5	+66.2	+59.6	+53.6
APRIL	+28.0	+33.0	+36.8	+42.8	+48.5	+55.0	+58.5	+60.5	+61.8	+57.6	+47.4
MAY	+17.6	+19.8	+22.8	+24.5	+27.5	+34.0	+37.8	+43.5	+45.7	+42.0	+33.3
JUNE	+10.2	+11.4	+12.6	+14.1	+16.0	+18.8	+22.0	+26.5	+26.8	+22.0	+16.0
JULY	+ 7.4	+ 7.3	+ 7.0	+ 8.4	+ 9.8	+ 9.9	+12.3	+13.0	+12.3	+ 8.4	+ 4.1
AUGUST	+ 9.0	+ 8.2	+ 8.3	+ 8.7	+ 8.6	+ 9.5	+11.4	+13.2	+12.6	+10.2	+ 7.0
SEPTEMBER	+ 9.7	+10.3	+11.2	+14.1	+16.0	+18.0	+19.8	+21.5	+21.7	+19.5	+14.5
OCTOBER	+16.7	+20.7	+25.2	+29.1	+33.0	+36.8	+40.4	+42.0	+41.0	+37.8	+30.1
NOVEMBER	+25.0	+28.6	+34.2	+39.2	+43.0	+50.0	+54.0	+51.0	+50.3	+45.0	+37.6
DECEMBER	+30.7	+34.2	+40.2	+44.7	+51.8	+57.0	+60.7	+63.6	+62.0	+58.5	+51.7
MAXIMUM	+34.3	+41.0	+48.0	+54.7	+61.2	+67.4	+73.4	+76.1	+74.8	+63.7	+56.3
ANNUAL	+27.6	+32.0	+36.9	+42.0	+47.2	+52.8	+57.2	+59.4	+58.3	+54.1	+46.3
**50% QSS	26.4	30.6	34.7	38.8	42.9	47.0	47.0	47.0	47.0	47.0	41.8
75% QSS	33.1	37.9	42.6	47.4	52.2	57.0	57.0	57.0	57.0	57.0	50.5
90% QSS	40.2	45.8	51.3	56.9	62.4	68.0	68.0	68.0	68.0	68.0	60.3
95% QSS	45.0	51.0	57.0	63.0	69.0	75.0	75.0	75.0	75.0	75.0	66.7
99% QSS	58.4	66.1	73.8	81.5	89.3	97.0	97.0	97.0	97.0	97.0	87.5

* Reference 17   **Reference 6   + Denotes Tailwind
                                               - Denotes Headwind

TABLE 11

MONTHLY 95 PERCENTILE LEFT CROSSWIND ENVELOPE

COMPARISON WITH QSS DESIGN WIND ENVELOPES

FOR 75° FLIGHT AZIMUTH

	5KM	6KM	7KM	8KM	9KM	10KM	11KM	12KM	13KM	14KM	15KM
* JANUARY	-17.2	-19.3	-21.3	-21.7	-23.2	-25.5	-28.6	-30.1	-26.7	-23.0	-21.4
FEBRUARY	-18.4	-18.8	-19.8	-21.8	-22.7	-26.3	-28.6	-29.7	-26.3	-22.5	-20.6
MARCH	-16.5	-16.5	-18.2	-20.5	-24.9	-29.3	-34.6	-35.3	-30.5	-26.8	-23.3
APRIL	-16.3	-19.0	-19.8	-21.8	-25.0	-28.5	-33.5	-36.2	-37.7	-32.8	-25.7
MAY	- 9.8	-11.6	-12.7	-14.7	-17.0	-19.1	-22.0	-24.0	-27.0	-24.0	-20.0
JUNE	- 6.6	- 7.5	- 8.2	- 9.5	-12.2	-15.5	-18.6	-23.6	-25.2	-23.3	-19.2
JULY	- 5.3	- 6.2	- 6.6	- 7.2	- 8.0	- 9.3	-10.7	-12.9	-14.8	-14.6	-11.4
AUGUST	- 5.1	- 5.8	- 5.9	- 6.8	- 7.8	-10.2	-11.6	-12.8	-14.6	-14.0	- 9.0
SEPTEMBER	- 5.5	- 6.5	- 7.1	- 8.0	- 9.0	-12.3	-15.1	-18.6	-20.5	-19.4	-14.3
OCTOBER	-10.8	-12.4	-14.1	-16.7	-20.0	-25.0	-29.4	-30.7	-28.7	-25.0	-20.1
NOVEMBER	-13.2	-14.3	-16.6	-19.3	-22.5	-26.7	-31.0	-30.8	-28.8	-23.6	-19.2
DECEMBER	-13.2	-15.6	-16.5	-18.7	-22.4	-24.3	-26.0	-26.7	-25.7	-20.7	-18.8
MAXIMUM	-18.4	-19.3	-21.3	-21.8	-25.0	-28.5	-34.6	-36.2	-37.7	-32.8	-25.7
ANNUAL	-12.4	-13.8	-15.6	-17.5	-19.9	-23.3	-26.4	-28.1	-26.8	-23.4	-19.9
**50% QSS	26.4	30.6	34.7	38.8	42.9	47.0	47.0	47.0	47.0	47.0	41.8
75% QSS	33.1	37.9	42.6	47.4	52.2	57.0	57.0	57.0	57.0	57.0	50.5
90% QSS	40.2	45.8	51.3	56.9	62.4	68.0	68.0	68.0	68.0	68.0	60.3
95% QSS	45.0	51.0	57.0	63.0	69.0	75.0	75.0	75.0	75.0	75.0	66.7
99% QSS	58.4	66.1	73.8	81.5	89.3	97.0	97.0	97.0	97.0	97.0	87.5

*Reference 17   **Reference 6   + Denotes Right Crosswind
                                                - Denotes Left Crosswind

TABLE 12

MONTHLY 95 PERCENTILE RIGHT CROSSWIND ENVELOPE

COMPARISON WITH QSS DESIGN WIND ENVELOPES

FOR 75° FLIGHT AZIMUTH

	5KM	6KM	7KM	8KM	9KM	10KM	11KM	12KM	13KM	14KM	15KM
*JANUARY	+ 8.5	+ 9.8	+10.2	+11.2	+12.0	+12.2	+13.6	+11.2	+ 9.3	+ 6.5	+ 5.5
FEBRUARY	+ 9.8	+11.4	+12.3	+12.2	+12.8	+12.8	+14.4	+14.0	+ 9.2	+ 7.9	+ 5.4
MARCH	+ 8.0	+ 8.4	+10.0	+10.4	+13.6	+14.0	+14.6	+14.5	+11.5	+ 7.0	+ 6.4
APRIL	+ 5.8	+ 5.8	+ 5.5	+ 5.5	+ 6.0	+ 6.2	+ 7.0	+ 8.0	+ 5.8	+ 3.8	+ 3.2
MAY	+ 5.9	+ 6.2	+ 7.5	+ 8.8	+10.3	+12.0	+13.6	+14.2	+11.7	+ 8.6	+ 6.0
JUNE	+ 5.2	+ 4.5	+ 4.8	+ 6.0	+ 7.0	+ 8.4	+10.0	+10.0	+ 9.2	+ 5.9	+ 3.5
JULY	+ 5.9	+ 6.5	+ 6.5	+ 7.0	+ 7.8	+ 8.5	+ 8.8	+ 8.2	+ 8.7	+ 6.6	+ 4.5
AUGUST	+ 6.2	+ 6.2	+ 6.7	+ 7.0	+ 7.4	+ 8.7	+10.0	+10.8	+11.3	+ 7.9	+ 5.9
SEPTEMBER	+ 6.5	+ 6.8	+ 7.2	+ 8.1	+ 8.9	+ 9.2	+11.0	+11.1	+10.0	+ 9.7	+ 8.1
OCTOBER	+ 6.4	+ 6.4	+ 7.8	+ 7.5	+ 9.3	+10.6	+13.7	+13.7	+11.6	+ 7.0	+ 4.9
NOVEMBER	+ 6.2	+ 7.6	+ 8.8	+10.0	+11.7	+11.0	+11.7	+12.0	+11.8	+ 7.7	+ 5.3
DECEMBER	+ 9.1	+ 8.7	+ 9.1	+10.8	+13.0	+15.4	+18.2	+19.6	+18.3	+13.0	+10.0
MAXIMUM	+ 9.8	+11.4	+12.3	+12.2	+13.6	+15.4	+18.2	+19.6	+18.3	+13.0	+10.0
ANNUAL	+ 6.9	+ 7.1	+ 7.8	+ 8.4	+ 9.7	+10.8	+12.1	+12.3	+11.0	+ 7.8	+ 5.8
**50% QSS	26.4	30.6	34.7	38.8	42.9	47.0	47.0	47.0	47.0	47.0	41.8
75% QSS	33.1	37.9	42.6	47.4	52.2	57.0	57.0	57.0	57.0	57.0	50.5
90% QSS	40.2	45.8	51.3	56.9	62.4	68.0	68.0	68.0	68.0	68.0	60.3
95% QSS	45.0	51.0	57.0	63.0	69.0	75.0	75.0	75.0	75.0	75.0	66.7
99% QSS	58.4	66.1	73.8	81.5	89.3	97.0	97.0	97.0	97.0	97.0	87.5

*Reference 17   **Reference 6   + Denotes Right Crosswind
− Denotes Left Crosswind

TABLE 13

SA-204/LM-1 STAGE SEPARATION SEQUENCE OF EVENTS

S-IB STAGE EVENT	TIME OF OCCURRENCE (SECONDS)*	S-IVB STAGE EVENT
IECO	T - 4.379	
OECO	T - 1.379	
H-1 90% Decayed (Engines No. 2 and No. 4, Fuel)	T - 1.034	
H-1 90% Decayed (Engines No. 1 and No. 3, LOX)	T - 0.877	
	T - 0.279	Ullage Ignition
	T - 0.202	Ullage 90% Buildup
Fire Separation Devices	T - 0.079	
Separation Structure Severed	T	Separation Structure Severed
Retro Ignition	T + 0.004	
Retro 10% Buildup	T + 0.046	
First Motion (Nominal)	T + 0.047	
Retro 90% Buildup	T + 0.078	
	T + 0.121	S-IVB Roll Control and J-2 Gimbal Activation
Ungimballed J-2 Bell Clears Top of Interstage (Nominal)	T + 0.916	
H-1 100% Decayed	T + 1.056	
Ungimballed J-2 Bell Clears Top of Interstage (One Retro Out)	T + 1.068	
3.048 Met. Longitudinal Clearance Between J-2 Bell and Top of Interstage (Nominal)	T + 1.128	

(continued next page)

TABLE 13 (continued)

SA-204/LM-1 STAGE SEPARATION SEQUENCE OF EVENTS

S-IB STAGE EVENT	TIME OF OCCURRENCE (SECONDS)*	S-IVB STAGE EVENT
3.048 Met. Longitudinal Clearance Between J-2 Bell and Top of Interstage (One Retro Out)	T + 1.320	
	T + 1.321	J-2 Engine Start Command
Begin Retro Decay	T + 1.504	
Retro 100% Decayed	T + 2.254	
	T + 3.178	J-2 10% Buildup
	T + 3.321	Begin Ullage Decay
	T + 4.621	J-2 90% Buildup
	T + 7.721	Ullage 100% Decayed
	T + 16.979	IGM Activation

*Note: T represents nominal SA-204/LM-1
flight time of separation signal
plus .079 sec. bias for simulation
purposes.

TABLE 14

SA-204/LM-1 POST SEPARATION S-IVB PEAK DYNAMIC RESPONSES TOLERANCES

GROUP	ITEM	DEVIATION
S-IB Stage Non-Propulsion	Thrust Misalignment (Pitch) Thrust Misalignment (Yaw) Thrust Misalignment (Roll) Center of Gravity Offset (Z)	±1.75 Degrees (NOT Composite) ±1.75 Degrees (NOT Composite) ±1.75 Degrees (NOT Composite) ±0.05 Meters
Environment	Right Cross Wind Left Cross Wind	95% January Monthly 95% January Monthly
S-IB Stage Propulsion	Propellant Mass Thrust and Flow Rate Isp and Flow Rate	±0.35% LOX ±1.5% ±0.9 Seconds
S-IVB Stage Non-Propulsion	Center of Gravity Offset (Z) Center of Gravity Offset (X) Thrust Misalignment (Pitch) Thrust Misalignment (Yaw)	±0.05 Meters ±0.05 Meters ±1.24 Degrees ±1.24 Degrees

TABLE 15

STAGE SEPARATION TOLERANCES CONSIDERED IN THE SA-204/LM-1
SINGLE RETRO OUT COLLISION ANALYSIS

ITEM	DEVIATION
Retro Thrust Variation (NOT Composite)	±13.28%
Retro Thrust Misalignment (NOT Composite)	± .50 Degrees
S-IB Lateral CG Offset	± 1.1 Inches

TABLE 16

SA-204/LM-1 SINGLE RETRO ROCKET FAILURE STAGING ANALYSIS

Retro Failures Are Simulated During an Otherwise Nominal Separation

Retro Failed	Lateral Clearance Assuming Fully Seated Residual S-IB Propellants* (Meters)	Lateral Clearance Assuming 732 Kgm. of Residual S-IB Propellants Become Unseated* (Meters)
No. 1	0.192	0.225
No. 2	0.185	0.217
No. 3	0.126	0.158
No. 4	0.133	0.166

*Lateral clearance of the undeflected J-2 bell bottom (at Interstage Exit Plane) with the S-IB Interstage.

GOVERNMENT FURNISHED DOCUMENTATION

DELIVERABLE ITEM NO.

GFDA NO.	DATE MSFC APPROVAL	DESCRIPTION OF GFD REQ'D	IDENTIFICATION OF GFD
04A00003	1-2-68	Control System Specifications	R-ASTR-F-66-237
04A00003	1-2-68	Prescribed Wind Data	a) TM X-53328 b) R-AERO-Y-118-66
04A00003	1-2-68	Launch Vehicle Liftoff Tolerances	R-AERO-FF-96-67
04A00003	1-2-68	Launch Vehicle Preliminary Operational Trajectory	TN-AP-67-255
04A00003	1-2-68	Launch Vehicle Boost Tolerances	R-AERO-FF-96-67
04A00003	1-2-68	Structural Flight Limits	R-P&VE-SLL-67-33

REFERENCES

1. CCSD TN-AP-67-212, "SA-204/LM-1 Launch Vehicle Operational Flight Trajectory," dated 28 April 1967.

2. MSFC Dwg. 75M-16406, "Launch Equipment Installation S-IB LC-37B AS-203," dated 15 April 1966.

3. MSFC Dwg. 75M-07285, "Swing Arm #4 Saturn IB Complex 37," dated 28 August 1963.

4. MSFC Dwg. 75M-00600, "Complex 37B Firing Accessories Saturn IB," dated 15 February 1962.

5. MSFC R-AERO-AD-66-42, "Saturn IB/LEM, AS-206, Aerodynamic Static Stability Characteristics," dated 14 October 1966.

6. NASA TM X-53328, "Terrestrial Environment (Climatic) Criteria Guidelines for Use in Space Development, 1966 Revision," dated 1 May 1966.

7. CCSD TB-AE-65-239, "Saturn IB Liftoff Motion Parametric Analysis," dated 5 August 1965.

8. MSFC R-AERO-DCC-15-64, "Saturn IB Liftoff Tower Clearance Study," dated 9 September 1964.

9. MSFC Letter, R-AERO-FF-96-67.

10. MSFC R-AERO-AD-66-58, "Saturn IB/LEM AS-206, Aerodynamic Static Stability Characteristics," dated 6 October 1966.

11. CCSD TB-AP-66-72, "Range Safety Aerodynamics Characteristics of the Saturn IB/LEM AS-206 Space Vehicle," dated 6 December 1966.

12. CCSD TB-AP-66-57, "Axial Force Characteristics of the Saturn IB/LEM, AS-206 Vehicle," dated 4 October 1966.

13. MSFC R-ASTR-F-66-237, "Control Gains and Shaping Networks for Saturn AS-208, S-IB and S-IVB Stages," dated 8 December 1966.

14. MSFC R-ASTR-NFM-128-65, "The Linear Equations and Nonlinear Models for Saturn IB Thrust Vector Control System," dated 18 March 1965.

15. MSFC R-ASTR-NG- 4-66, "Control System Information for SA-203," dated 19 May 1966.

16. MSFC R-P&VE-SLI-67-33, "Structural Limits for the SA-204/LM-1 Saturn IB Vehicle," preliminary information, in process of being published.

REFERENCES (continued)

17. MSFC R-AERO-Y-118-66, Admendment #1, "Addendum to Cape Kennedy Wind Component Statistics 0-60 KM. Altitude, for All Flight Azimuths for Monthly and Annual Reference Periods," dated 5 December 1966.

18. MSFC R-AERO-DCC-12-66, "Chi-freeze Values for Single Engine Out on AS-204," dated 1 July 1966.

19. CCSD TB-AE-65-313, "Saturn IB Preliminary Engine Out Controllability Study," dated 7 December 1965.

20. CCSD BB 3.6.1-1-101, "Saturn IB Vehicle Thrust Vector Control (TVC) System Mathematical Model and Load Analysis," dated 31 March 1967.

21. CCSD TN-AP-66-46, "AS-202 Launch Vehicle Dynamics Analyses."

22. NASA TM X-53042, "A Technique for Including the Effects of Vehicle Parameter Variations in Wind Response Studies," dated 1 May 1964.

23. MSFC Dwg. 1B31436, "Frame Installation Forward Interface, Aft Interstage."

24. MSFC Dwg. 1B32282, "Inboard Cap, Forward Closing Frame, Aft Interstage."

25. MSFC Dwg. 40M33604C, "Interface Control Document Definition of Saturn SA-204 Flight Sequence Program," dated 13 December 1965 (Original), dated 22 March 1967 (Revision C).

26. Thiokol TEMS-17, "Model Specification Rocket Motor, Solid Propellant, Recruit, Thiokol Chemical Corporation, Model No. TE-M-29-5," dated 31 May 1966.

27. Thiokol SP-544A, "Model Specification Motor, Rocket, Solid Propellant," dated 23 February 1966.

28. MSFC R-P&VE-PPF-66-M-82, "Data for Use in S-IB-203 and Sub Vehicle Specifications and Future Separation Studies," dated 21 June 1966.

29. CCSD TB-AP-66-68, "Aerodynamics of the Saturn IB/LEM, AS-206 Vehicle during First Stage Separation and Second Stage Flight," dated 28 November 1966.

30. CCSD TN-AP-66-156, "AS-206A Launch Vehicle Operational Flight Trajectory Dispersion Analysis," dated 29 December 1966.

31. MSFC R-AERO-DCC-16-64, "Saturn IB Separation-Clearance Phase," dated 8 July 1964.

32. MSFC R-P&VE-VAW-66-30, "SA-203 Center of Gravity and Moment of Inertia Three Sigma Deviations for Separation Studies," dated 29 March 1966.

REFERENCES (continued)

33. Government Furnished Documentation Agreement No. 04A00003

DISTRIBUTION

Marshall Space Flight Center

Mr. Mann	I-I/IB-E	(1)
Mr. McNair	R-AERO-P	(101) and (1) Reproducible